AN ABSTRACT OF THE DISSERTATION OF

Medagama Liyanage Amila Udayanga Liyanage for the degree of Doctor of Philosophy in Chemistry presented on June 9, 2015.

Title: Synthesis of Intercalation Compounds and Nanocomposites of Inorganic Layered Hosts.

Abstract approved:

Michael M. Lerner

Novel synthetic strategies are developed to prepare new intercalation compounds and nanocomposites with several layered hosts ($NiPS_3$, Na-montmorillonite, MoS_2 and MoO_3). In these products, alkali metals are ionic intercalates and linear polymers, dendrimers or amines act as co-intercalates. In addition to new synthetic approaches, new structures are identified and characterized.

A template synthesis method to prepare $NiPS_3$/polymer nanocomposites is reported for the first time. Polymers studied were polyethylene oxide (PEO), polyethylenimine (PEI), polyvinyl alcohol (PVA) and polyvinylpyrrolidone (PVP). $NiPS_3$/PEO nanocomposites prepared by this template method contain polymer monolayers (Δd = 0.42 nm) between host layers, in contrast to the polymer bilayers reported in previous reports using a topotactic method. Packing fraction calculations reveals that the interlayer space is denser for template synthesized $NiPS_3$/PEO than for the topotactically-derived MPS_3/PEO nanocomposites (M = Ni, Fe, Cd, and Mn).

$NiPS_3$/PEI, $NiPS_3$/PVA and $NiPS_3$/PVP nanocomposites were prepared for the first time and also have polymer monolayers between host layers (Δd = 0.41, 0.42 and 1.56 nm, respectively). The monomer unit / $NiPS_3$ formula ratio is ~ 1 for PEO, PEI and PVA nanocomposites and ~ 0.5 for PVP nanocomposites. More dilute conditions, more polar solvents, and longer aging times increase the crystallite size of the obtained products. Reaction progress studies indicate that the $P_2S_6^{4-}$ and Ni^{2+} concentrations in the reaction mixture govern nanocomposite nucleation and growth.

Intercalated nanocomposites with lower generation (G0.0−2.0) polyamidoamine (PAMAM) dendrimers and Na-montmorillonite (Na-MMT) are synthesized using an exfoliation–adsorption method. This is the first report of the G0.0 and G1.0 PAMAM/Na-MMT nanocomposites and of a structurally-ordered G2.0 PAMAM/Na-MMT nanocomposite. The structures obtained depend on the PAMAM generation and the starting reactant ratio. The spherical PAMAM in aqueous medium transforms to a highly flattened conformation after incorporation between the host layers. G0.0 PAMAM forms only monolayer galleries (Δd = 0.42 nm), while G2.0 PAMAM forms monolayers, bilayers (Δd = 0.84 nm), and mixed phase structures at lower, higher, and intermediate, organic content, respectively, and exhibits an interesting monolayer to bilayer transition. G1.0 PAMAM shows intermediate behavior, with a monolayer to mixed-phase transition observed at the reactant ratios studied. This is the first report of a monolayer arrangement for PAMAM/clay nanocomposites. The maximum organic contents of G0.0 PAMAM monolayer and G2.0 PAMAM bilayer nanocomposites are ∼7% and ∼14% respectively, and these materials have ~2 times lower packing fractions (0.31−0.32)

than for linear polymer intercalate nanocomposites of Na-MMT. Under acidic conditions all these nanocomposites form only monolayer galleries, which is ascribed to the stronger electrostatic attraction between negatively charged MMT layers and protonated PAMAM. Acidic conditions also slow the rate of formation of the nanocomposites and generate more ordered products. The Na^+ ions in the Na-MMT structure play a significant role in PAMAM/Na-MMT nanocomposite formation. Both Na-MMT and PAMAM structural units are preserved in the nanocomposites obtained.

Electride solutions obtained by dissolution of Na(m) in ethylenediamine (en) are used for the first time to generate MoS_2 intercalation compounds with Na and en as intercalate and cointercalate, respectively. Two new phases, labeled α and β, have $\Delta d = 0.35$ and 0.57 nm, respectively; the different gallery dimensions are ascribed to parallel *vs.* perpendicular orientations of en in the galleries. The β phase structure has not been reported previously in any MS_2 intercalation compounds. The intercalation reaction proceeds *via* the formation of a metastable kinetic product, the β phase, and the subsequent generation of the thermodynamically stable α phase. Lower electride concentrations, lower reaction temperatures and shorter reaction times favor production of the β phase. The products obtained have compositions of $Na_{0.2–0.3}MoS_2 \cdot 0.3–0.4en$ with a larger packing fraction than the structurally analogous A-en-GICs (A = alkali metal, GIC = Graphite intercalation compound). The electrochemical reduction of MoS_2 in en/$NaPF_6$ does not result in these intercalation reactions.

The incorporation of dendrimers into MoO_3 is reported for the first time. PAMAM/MoO_3 nanocomposites are synthesized using an exfoliation - adsorption method. G0.0 PAMAM only forms monolayers (Δd = ~ 0.5 nm) between MoO_3 layers and G2.0 PAMAM forms both monolayer and bilayers (Δd = ~ 0.7-0.8 nm). In addition to these two structures, a third unknown phase is observed with a much larger gallery expansion (Δd = ~ 1.4 nm). These nanocomposites have a comparable structures, compositions (12-14% organic component for G0.0 monolayer and 22-25% for G2.0 bilayer) and packing fractions (0.5-0.7 for monolayer and 0.7-0.9 for bilayer) to those in the previously reported linear polymer/MoO_3 nanocomposites.

In the above studies, analyses by powder X-ray diffraction (PXRD) are supported by compositional data from thermogravimetric analyses (TGA) and structural optimization (Gaussian). Additionally, the product morphologies, surface properties and constituents are evaluated using scanning electron microscopy (SEM), energy-dispersive X-ray spectroscopy (EDS), and Fourier transform infrared (FTIR) and Raman spectroscopies. UV-visible spectroscopy (UV-vis) is used to monitor reaction progress. Capillary zone electrophoresis (CZE) is used to study compositions and reaction progress.

Synthesis of Intercalation Compounds and Nanocomposites of Inorganic Layered Hosts

by
Medagama Liyanage Amila Udayanga Liyanage

A DISSERTATION

submitted to

Oregon State University

in partial fulfillment of
the requirements for the
degree of

Doctor of Philosophy

Presented June 9, 2015
Commencement June 2016

Doctor of Philosophy dissertation of Medagama Liyanage Amila Udayanga Liyanage presented on June 9, 2015

APPROVED:

Major Professor, representing Chemistry

Chair of the Department of Chemistry

Dean of the Graduate School

I understand that my dissertation will become part of the permanent collection of Oregon State University libraries. My signature below authorizes release of my dissertation to any reader upon request.

Medagama Liyanage Amila Udayanga Liyanage, Author

ACKNOWLEDGEMENTS

First of all, I would like to express my sincere gratitude to my advisor, Prof. Michael M. Lerner for the guidance, encouragement and resources provided throughout my studies at Oregon State University.

I am grateful to Profs. Douglas A. Keszler, MAS Subramanian, Vincent T. Remcho, and Chih-hung (Alex) Chang for serving on my graduate committee and for allowing me to use their laboratory facilities and instruments whenever needed.

I would also like to acknowledge the nice company and discussions of Dr. Bahar Özmen-Monkul, Dr. Tosapol Maluangnont, Dr. Esther Ikhuoria, Dr. Weekit Sirisaksoontorn, Hanyang Zhang, and Xiaochao Liu who are the past and present members of Lerner group.

I take this opportunity to thank Dr. Christine Pastorek for assisting and allowing me to use instruments in teaching labs. My gratitude goes to Dr. Adeniyi Adenuga, Dr. Sean Muir and Changqing Pan (OSU Chemical Engineering) for their assistance in various experiments.

Thank goes to the members of Subramanian and Remcho research groups, Cindy, Paula, Luanne, Talley, Kristi, Todd, Greg, Jenna, Dan, Mark, Teresa (OSU Electron Microscopy Facility) and Nick (OSU Chemical Engineering) for being helpful at various research, administrative, and teaching environments. Also, I would like to thank all the instructors and lab coordinators of General Chemistry Sequence and Integrated Lab program.

I thank OSU Chemistry for the financial support provided throughout my graduate studies and especially for Whiteley Fellowship in Materials Sciences for Summer 2014, Travel awards in Summer 2011 and Summer 2014, and TA award for Winter 2015. Also, I would like to thank College of Science for the Travel award (COSSTA) in Summer 2014.

I thank all my teachers who enlightened me with their wisdom.

Special thanks to my friends and fellow graduate students; Weekit, Adeniyi, and Mohamad Nazari, and the small Sri Lankan community in Corvallis for making the life in Corvallis eventful and joyful.

Finally, and most importantly, I would like to thank my family. I thank my loving parents, father Karunarathne Liyanage and mother Sunila Vithanage for raising me up to who I am today. Your endless love, guidance and dedication made me come this far. I wish to thank my little sister Achala Liyanage, my grandmother Alice Ranathunga and my lovely wife Sulochana Wasala for the love and support given throughout this journey.

CONTRIBUTION OF AUTHORS

Prof. Michael M. Lerner has contributed to the design and writing of each manuscript. Dr. Esther U. Ikhuoria assisted in sample preparation in Chapter 3. Dr. Adeniyi A. Adenuga, and Prof. Vincent T. Remcho assisted in capillary zone electrophoresis experiments in Chapter 3. Dr. Esther U. Ikhuoria contributed in sample preparation and analysis in Appendix A.

TABLE OF CONTENTS

TABLE OF CONTENTS (Continued)

TABLE OF CONTENTS (Continued)

LIST OF FIGURES

LIST OF FIGURES (Continued)

LIST OF FIGURES (Continued)

LIST OF TABLES

LIST OF APPENDIX FIGURES

LIST OF APPENDIX TABLES

CHAPTER 1

INTRODUCTION

1.1 INTERCALATION CHEMISTRY

The term intercalation is derived from the Latin verb “intercalate”, which refers to the insertion of an additional day in special years to synchronize the calendar with the solar year.[1] In 1959, Rüdorff applied this term to all chemical derivatives of graphite, indicating that atoms or ions have been inserted, or intercalated, with a lattice expansion perpendicular to the nearly unchanged graphite layers.[2] The terms “inclusion”, “interstitial”, and “intercalation” compounds were used interchangeably in the early days of this chemistry. Lerf has more recently distinguished clearly the differences among these terms and redefined intercalation compounds as described below.[1,3]

Solids that form intercalation compounds contain stable structural elements like chains, layered sheets or three dimensional frameworks (with a network of channels or unidirectional channels)[1,4] (Table 1.1). If the 1D or 2D structural elements are electrically neutral, such as in graphite or MoS_2, they are bound by weak van der Waals forces. Neutral framework structures, such as aluminophosphates,[5] contain empty 1D channels or interconnected cavities. If these structural elements carry an electrical charge, these are compensated by small counter ions contained between them or occupying their channels and cavities. Most such compounds have many empty lattice sites, or can be expanded to generate sites, that can be occupied by

additional atoms or molecules. Therefore the mobility of the interstitial atoms can be very high if their interaction with the host structure is not too strong. This allows many intercalation reactions to be carried out at or near ambient temperature, which permits the preparation of metastable products that cannot be obtained by traditional high temperature solid state reactions. In summary, intercalation is the reversible uptake of atoms, ions, molecular cations, or molecules, generally at moderate temperatures, and with conservation of structural elements in the host lattice. However, the term intercalation refers to topology, and does not describe the nature of the chemical reaction underlying this process.[1]

Table 1.1 Representative host lattices for intercalation[1,4,5]

Three-dimensional structures	Zeolites • $M_x^+(Al_xSi_{2-x}O_2)\cdot nH_2O$ Aluminophosphates • $Al_2O_3\cdot P_2O_5\cdot nH_2O$
Two-dimensional structures	Clays and layered silicates • Montmorillonite $Na_x(Al_{2-x}Mg_x)Si_4O_{10}(OH)_2\cdot mH_2O$ Graphite Metal dichalcogenides • MX_2 (M = Sn, Ti, Zr, Hf, V, Nb, Ta, Mo, W; X = S, Se, Te) Metal phosphorus trichalcogenides • MPX_3 (M = Mg, V, Mn, Fe, Co, Ni, Zn, Cd, In; X = S, Se) Metal oxides • Molybdenum trioxide MoO_3 • Vanadium pentoxide V_2O_5 • Transition metal dioxides $M^IM^{III}O_2$ (M^I=alkali metal; M^{III}=Ti, V, Cr, Mn, Fe, Co, Ni)

One-dimensional structures	Carbon nanotubes MX_3 (M = Ti, Zr, Hf, Nb, Ta; X = S, Se)

Framework structures can intercalate species (molecules or ions) that can be accommodated within their channels or cavities. On the other hand, 1D and 2D lattices can expand in two or one dimensions, and are therefore relatively unrestricted by intercalate size. This expansion potential allows the intercalation of a large variety of intercalate species including atoms, ions, small molecules, organic cations, metal complexes and polymers.[1] From here onwards, this dissertation will focus only on the intercalation compounds with layered host materials.

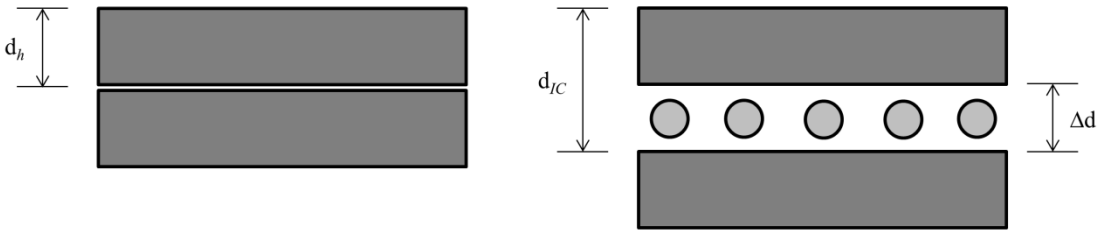

Figure 1.1 Structure of a typical layered host and intercalation compound

The repeat distance in the stacking direction for layered structures is defined as the interlayer distance (d_h); in many cases this is the same as the layer thickness (Figure 1.1). As an example sodium montmorillonite sheet thickness and d_h are the same which is 0.96 nm.[6] In the case of graphite which has an AB stacking arrangement, the repeat distance is 2 × sheet thickness (0.335 nm for graphite).[7] The incorporation/uptake of intercalate species to form galleries expands the lattice along this direction; the new repeat distance is defined as d_{IC}. The difference between the

interlayer repeat distance of the intercalation compound and the host, d_{IC}-d_h, can be called the interlayer expansion (Δd), or gallery height, and reflects the steric requirements of the intercalate. Powder X-ray diffraction technique can be used to determine d_h and d_{IC} for both the layered host and intercalation compounds that are produced. On the molecular scale, interlayer expansions can be very small (< 0.1 nm for some Li^+ intercalation compounds) to very large (> 5 nm),[8] depending on the nature of the intercalate species, their arrangement in the galleries, and in some cases on the synthetic methods and post-reaction processing employed.

When the intercalate species are oligomers, polymers, or dendrimers, the resulting intercalation compounds are often called nanocomposites, as both organic and inorganic components co-exist alternatively with domains (in at least one dimension) in the nanometer scale.[1] These nanocomposites have properties markedly differ from those of their components or micro- or macro-scaled composites with similar compositions. As an example, nylon-6-based montmorillonite nanocomposites have been shown to achieve a ~2 times higher Young's modulus with respect to the commercial nylon-6.[9] In another study, a poly(ethylene oxide)/Li-montmorillonite nanocomposite was shown to enhance the stability of the ionic conductivity when compared to a PEO/$LiBF_4$ polymer-salt complex.[10]

In most intercalation compounds, intercalate species are present between all the host layers. In some cases, especially in graphite intercalation chemistry, some of the layers do not separate to admit intercalate, and ordered sequences can form comprising intercalate galleries and more than one host layer. This phenomenon is referred to as staging. Stage 1, 2, and 3 intercalation compounds indicates that one,

two and three host layers, respectively, are separated by the expanded galleries in an ordered sequence. Daumas and Herold introduced a more realistic model to describe this staging phenomenon in terms of intercalate domains (Figure 1.2). There are also examples where disordered or random sequences of intercalate and host layers can arise, this is termed interstratification and is common in clay chemistry.[1,3]

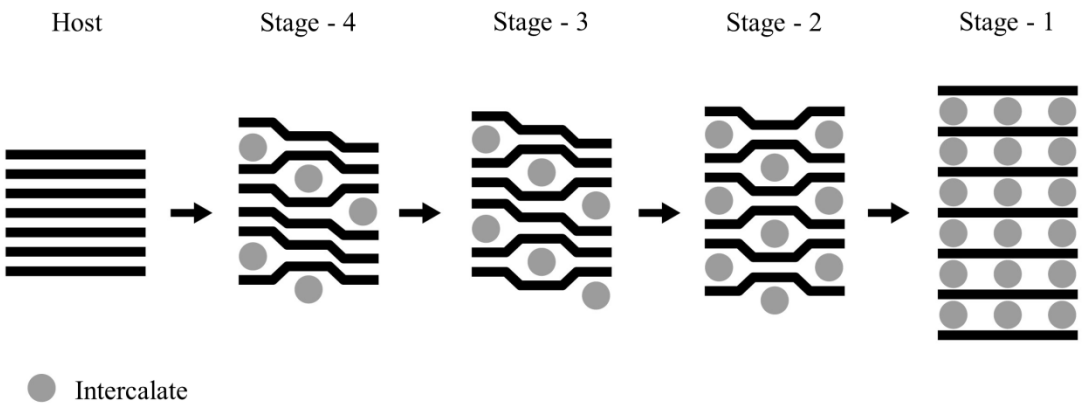

Figure 1.2 Daumas-Herold models for staging in graphite intercalation chemistry

Intercalate species are observed with a variety of arrangements within the expanded galleries (Figure 1.3). Most common are monolayers or bilayers, although trilayers and other organizations are also known. If the intercalate is anisotropic, it may be oriented with longer axis “parallel” to the host layers, i.e. in a manner leading to a minimal gallery height. Often the intercalates are charged and contain more and less polar surfaces - the charged or polar ends will typically orient towards opposite charges on the host, with nonpolar ends directed towards the gallery center. The paraffinic structure arises when two intercalate layers are present to compensate the charges of the host layers. These bilayers can be arranged with the intercalates

oriented at an angle to the host surfaces, where 90^{o} is defined as the orientation perpendicular to the host layer.[11,12]

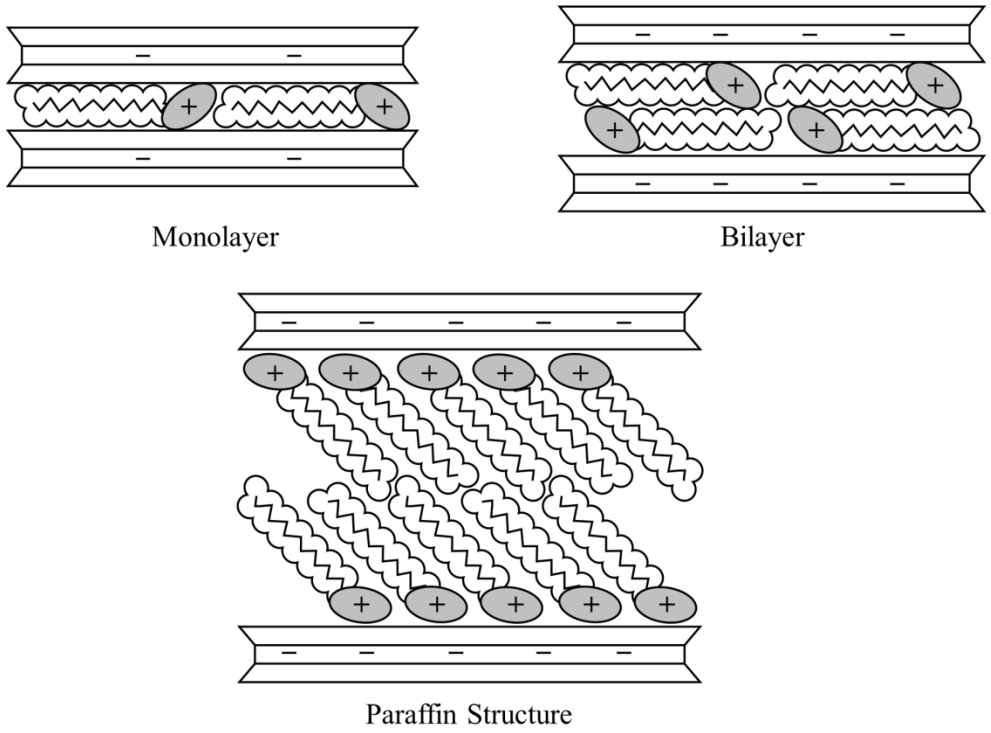

Figure 1.3 Some intercalate arrangements within galleries

One characteristic property of the expanded galleries is a packing density or packing fraction, which can be defined as the ratio of the volume occupied by intercalates to the total expanded volume. The expanded volume in intercalation compounds can be obtained from the known host layer structure and the interlayer expansion (Δd). The packing density can then be calculated if the product composition and molecular dimensions are known or can be estimated. The size, shape and degree of free rotational motion of the intercalate species can all play a role in the intercalate orientation, arrangement, and packing density. The host sheet charge density and charge distribution is often a dominant factor, as this determines the

required surface density of the intercalate counter charges in the galleries. This latter property varies widely in different hosts, and may depend on synthetic conditions. If the intercalate species are small and have a higher charge density, they tend to form monolayers. On the other hand, larger intercalate species may form bilayers because the ratio of charge to available host surface (or footprint) is too small to allow charge compensation for the host in a monolayer arrangement. Therefore, bilayer, pseudo-trilayers, or paraffinic structures may be observed.[1]

In clays such as Na-montmorillonite, the host is electronically insulating and the sheet charge density and distribution are less dependent on chemical potential. This is in marked contrast to graphite or many metal dichalcogenides, which are electronically conductive and redox active, with variable sheet charge densities and distributions.[1] Next, we will focus on a selected set of host materials, and the reported syntheses and structures of their intercalation compounds and nanocomposites.

1.2 METAL PHOSPHOROUS TRISULFIDES (MPS_3)

Metal phosphorous trisulfides (MPS_3) form a broad and varied class of compounds that exhibit several related structure types. $FePS_3$ is often used as a representative structure. $FePS_3$ is monoclinic and deviates slightly from hexagonal symmetry (Figure 1.4). The structure can be described by analogy to the layered $CdCl_2$ structure. In $FePS_3$, the S atoms form an essentially cubic close packed array. Alternate layers of octahedral sites within this array are vacant, the remaining octahedral sites are filled by metal (M) and phosphorous atom pairs (P_2). The formula can be rewritten as $M_{2/3}(P_2)_{1/3}S_2$, to highlight the analogy to transition metal

disulfides (MS_2). In one direction, the MPS_3 layers (d_h = 0.65 nm) are held together by van der Waals forces, which can separate to admit intercalate guests. These compounds can also be visualized as salts of divalent metal cations with hexathiohypodiphosphate anions ($P_2S_6^{4-}$). X-ray data indicated that MPS_3 compounds with M = Mg, V, Mn, Co, Ni, Pd, Zn and Cd have structures very similar to $FePS_3$.[13-15]

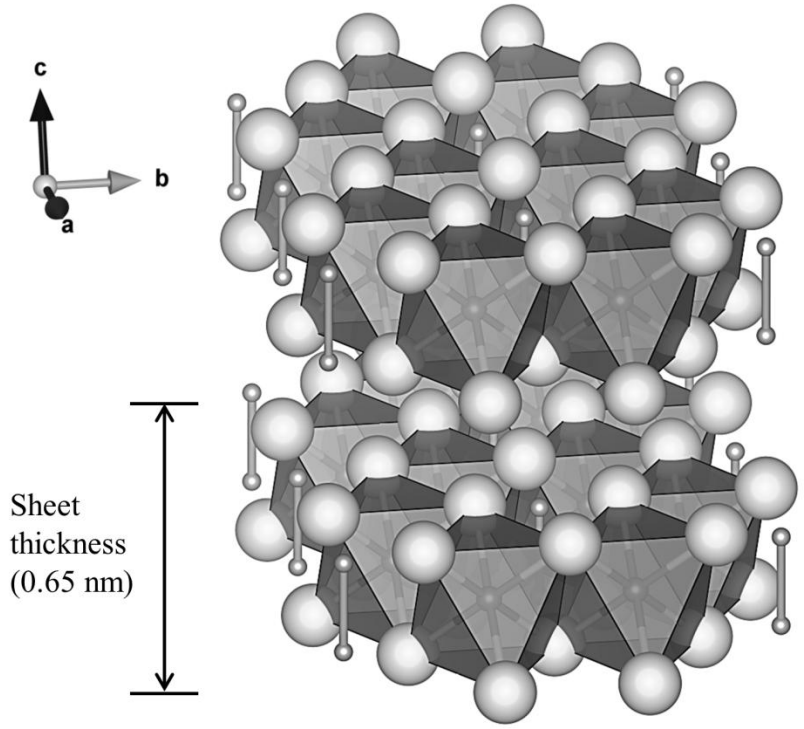

Figure 1.4 The $FePS_3$ structure (octahedral units - FeS_6, connected small spheres - P_2)

MPS_3 compounds can be prepared by several methods, including the direct heating of stoichiometric quantities of the elements (or metal sulfides) in an evacuated silica tube,[13-15] or the reaction of aqueous solutions of the divalent cations with aqueous $P_2S_6^{4-}$ anions.[16-18]

Several MPS_3 hosts directly react with n-alkylamines to form intercalation compounds. This chemistry has been studied extensively with $MgPS_3$, $MnPS_3$ and $ZnPS_3$. The interlayer distances obtained are invariant to the carbon number of the n-alkylamine, with d_{IC} = 1.05 and Δd = 0.40 nm. The observed expansion can be attributed to the van der Waals radius of a methyl group. From these observations it is evident that the amine carbon chains are arranged parallel to the host layers. Based on the interlayer expansions reported for n-alkylamine intercalates of $MgPS_3$ and $ZnPS_3$, bilayer of amines are obtained arranged perpendicular to the host layers.[13,15,19]

Alkali metal cations can intercalate into MPS_3 hosts by either chemical or electrochemical reduction. The chemical approach uses a reactive organoalkali metal compound like n-butyllithium, or sodium or potassium naphthalenide, at mild temperatures (20-70 °C). However, not all MPS_3 hosts react similarly with n-butyllithium. Complete occupancy of the vacant octahedral sites would lead to $Li_{1.5}MPS_3$. When the lithium content exceeds $Li_{1.2}NiPS_3$, X-ray diffraction data indicate that the $NiPS_3$ host lattice is degraded irreversibly with the formation of Li_2S. $FePS_3$ and some other $MPSe_3$ compounds react with lower degrees of lithiation, and $CdPS_3$, $ZnPS_3$ and $MnPS_3$ do not react at all under these conditions. Another interesting observation is that no interlayer expansion occurs upon Li^+ intercalation. For this same reason, the reaction can be difficult to monitor using powder X-ray diffraction alone.[13,15]

Li_xNiPS_3 is hygroscopic and reacts with atmospheric moisture, resulting in a new intercalation phase with an interlayer expansion of 0.58 nm. This increased expansion is attributed to the uptake of a bilayer of water molecules that solvate the

intercalate Li^+ ions. Other alkali metal intercalation compounds with MPS_3 show a similar water uptake.[13]

Lithium intercalation into MPS_3 has also been achieved electrochemically, for example with $NiPS_3$ as the cathode and Li(m) as the anode of an electrochemical cell containing a Li salt electrolyte dissolved in an aprotic solvent. When the cell is connected, Li(m) is spontaneously oxidized and $NiPS_3$ reduced. Two different Li_xNiPS_3 phases (with x = 0-0.5 or x = 0.5-1.5) were obtained with this approach. For $x < 1.5$, the intercalation reaction is electrochemically reversible, whereas lithiation to $x > 1.5$ results in irreversible decomposition of the host lattice. The reaction rates depend in part on the electrolyte employed. LeMehaute[20] reported different discharge curves obtained in dimethoxyethane-based electrolytes due to the co-intercalation of solvent molecules along with Li^+. Although many MPS_3 hosts have been tested, only $NiPS_3$ and $FePS_3$ have been found to undergo substantial electrochemical intercalation. $CdPS_3$, $MnPS_3$ and $ZnPS_3$ are less reactive or unreactive under similar conditions. This has been explained in terms of the electronic band structure. $ZnPS_3$ and $CdPS_3$ contain d^{10} ions; because the 4s and 4p molecular orbitals levels are too high in energy (~12eV) with respect to e_g sub band, these compounds do not undergo reductive intercalation.[13,15]

$MnPS_3$ also reacts with aqueous salt solutions to form intercalation compounds of general composition $Mn_{1-x}PS_3A_{2x}(H_2O)_y$. These compositions result from the abstraction of Mn^{2+} from the host structure, generating new cation vacancies and a negative layer charge, rather than by the reduction of the transition metal cations. To compensate this host layer charge, guest cations must intercalate between

host layers. A wide range of cations, including K^+ and alkylammonium ions, have been intercalated in this manner. Other relatively ionic hosts such as $ZnPS_3$ and $CdPS_3$, with M^{2+} ions less stabilized by ligand field, show similar behavior. The more covalent hosts $NiPS_3$ have greater ligand field stabilization and do not show this layer metal abstraction behavior; $FePS_3$ is in this class and rarely show this chemistry.[13,15] These reactions and the intercalation compounds produced have been explored for applications in ion exchange and as precursors to new materials. For example, the intercalate cations and/or solvent co-intercalates can be exchanged; $Mn_{1-x}PS_3A_{2x}(H_2O)_y$ (A = Na, K) reacts in a solution of polyethylene oxide (PEO) to generate new polymer nanocomposites.[21]

MPS_3 compounds are mostly broad band semiconductors with bandgaps from 1.5-3.5 eV. The electrochemically active $NiPS_3$ (1.6 eV) and $FePS_3$ (1.5 eV) have smaller band gaps. The optical properties and dc conductivities of these hosts can change markedly upon intercalation. As an example, Brec *et al*. found that the electronic resistivities of $FePS_3$ and $NiPS_3$ decreased gradually or rapidly, respectively, when reacted with n-butyllithium. They suggested that reduction inserts electrons to delocalized conduction bands resulting in enhanced conductivity, also leading to free carrier absorption and increased reflectivity. The increased conductivities also allow these materials to function efficiently as cathodes in electrochemical cells. Chemical intercalation has little effect on the magnetic properties of $FePS_3$, but decreases the overall susceptibility with increasing Li content in $NiPS_3$. It was proposed that the populated band was not associated with either metal 3d orbitals or P orbitals, but derives instead from S or metal 4s orbitals.[13]

Lagadic *et al*. first reported the synthesis of nanocomposites containing PEO and MPS_3 (M = Mn, Cd) *via* the reaction of an aqueous polymer solution with $M_{1-x}PS_3A_{2x}(H_2O)_y$ (A = Na, K). The products obtained showed Δd ~ 0.8–0.9 nm, attributed to the intercalation of bilayers of zig-zag-like PEO chains which also coordinate alkali metal ions.[21] Jeevanandam *et al*. prepared PEO/A_xCdPS_3 nanocomposites in a methanolic solution at 55 ^oC.[22] Manriquez *et al*. reported PEO/ Li_xMPS_3 (M = Ni, Fe) using a similar method, and proposed a polymer helical conformation.[23] Manova *et al*. reported the intercalation of polyethylene glycol into Na_xNiPS_3 by reaction in a methanolic aqueous solution, with Δd ~0.8 nm.[24] Other polymers that have been reported to form nanocomposites with MPS_3 include linear polyethylenimine (LPEI) and polyvinylpyrrolidone (PVP). LPEI was reported by Oriakhi *et al*. to form nanocomposites with polymer monolayers (Δd = 0.4 nm) *via* the reaction of $K_x(H_2O)_yM_{1-x/2}PS_3$ (M = Mn, Cd) and polymers in aqueous solution.[25] The PVP-containing nanocomposite was reported by Yang *et al*. *via* reaction of a potassium-intercalated MPS_3 (M = Mn, Cd) and an aqueous PVP solution. The reported Δd ~ 2.3 nm was much greater than that observed for the PEO nanocomposites.[26]

A solvent-free, melt intercalation approach to obtain PEO/MPS_3 nanocomposites (M = Mn, Cd) was first reported by Sukpirom *et al*. With this method, $K_xM_{1-x/2}PS_3\cdot\delta H_2O$ was shown to directly intercalate PEO at 125 °C. The nanocomposite basal repeat distances were increased by ~ 0.8 nm, attributed to the presence of PEO bilayers within the intercalate galleries.[27]

These synthetic approaches involve either topotactic reactions or an exfoliation/reassembly processes. Some potential limitations of these approaches can include the need for higher temperatures (i.e. melt intercalation) or the use of highly-reactive organoalkali reductants (such as butyllithium). A new low-temperature approach utilizing templated synthesis to obtain polymer $NiPS_3$ nanocomposites (Figure 1.5) will be discussed in Chapter 2.

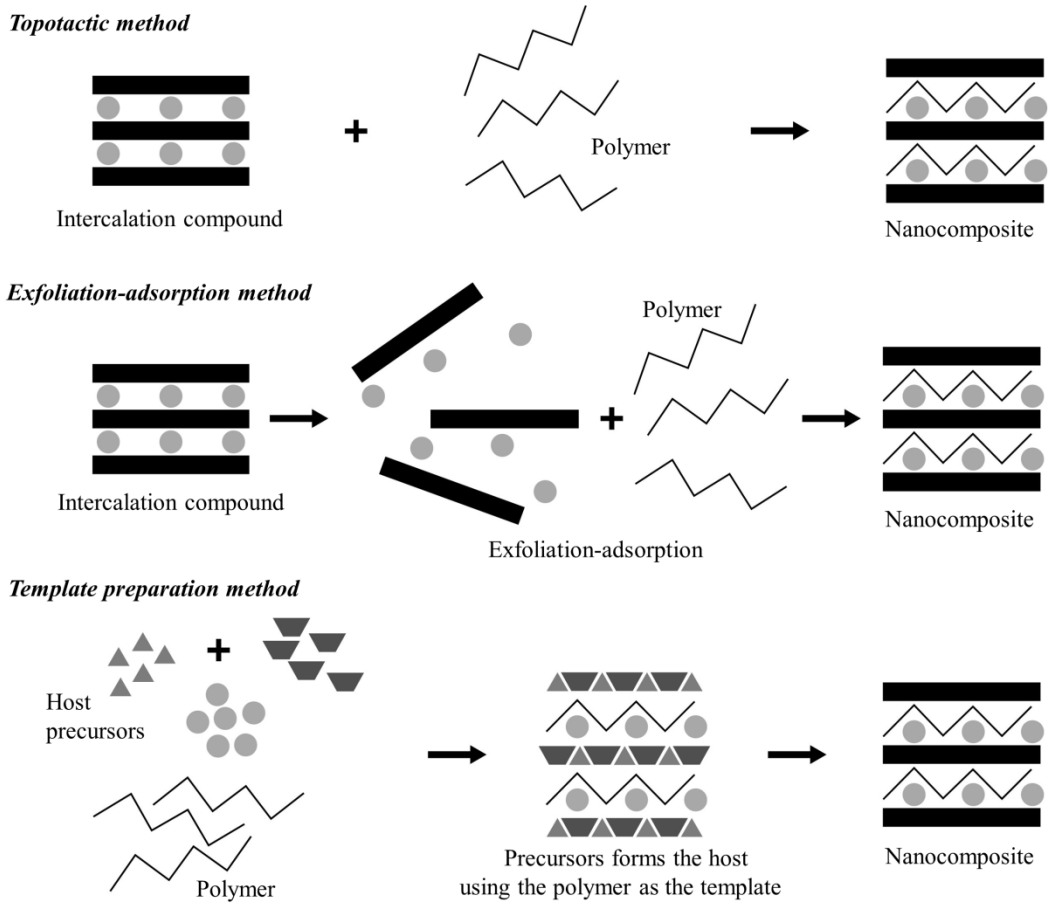

Figure 1.5 Topotactic, exfoliation-adsorption *vs* template preparation method

1.3 SODIUM MONTMORILLONITE

Montmorillonites belong to the structural family known as the 2 : 1 phyllosilicates. Their crystal lattice consists of two-dimensional layers where a central octahedral sheet of alumina or magnesia is encased by silica tetrahedra, with oxygen ions of the octahedral sheet shared with SiO_4 units (Figure 1.6). The layer thickness/interlayer distance is ~ 1 nm. Substitution within the layers (for example, Al^{3+} replaced by Mg^{2+}) generates negative charges that are counterbalanced by alkali or alkaline earth cations, situated in the interlayer volume. Sodium montmorillonite (Na-MMT), has the formula $Na_x(Al_{4-x}Mg_x)Si_8O_{20}(OH)_4$ with a stacking repeat distance of 0.96 nm for the anhydrous structure. The layer charge is not constant - it varies from layer to layer, and derived values must be considered as an average value over the whole crystal. The cation exchange capacity (CEC) is usually a good qualitative or quantitative measure of the average sheet surface charge densities. Smectite clays such as montmorillonite have a moderately negative surface charge, and a CEC of 60-120 mEq/ 100 g.[12,13,28]

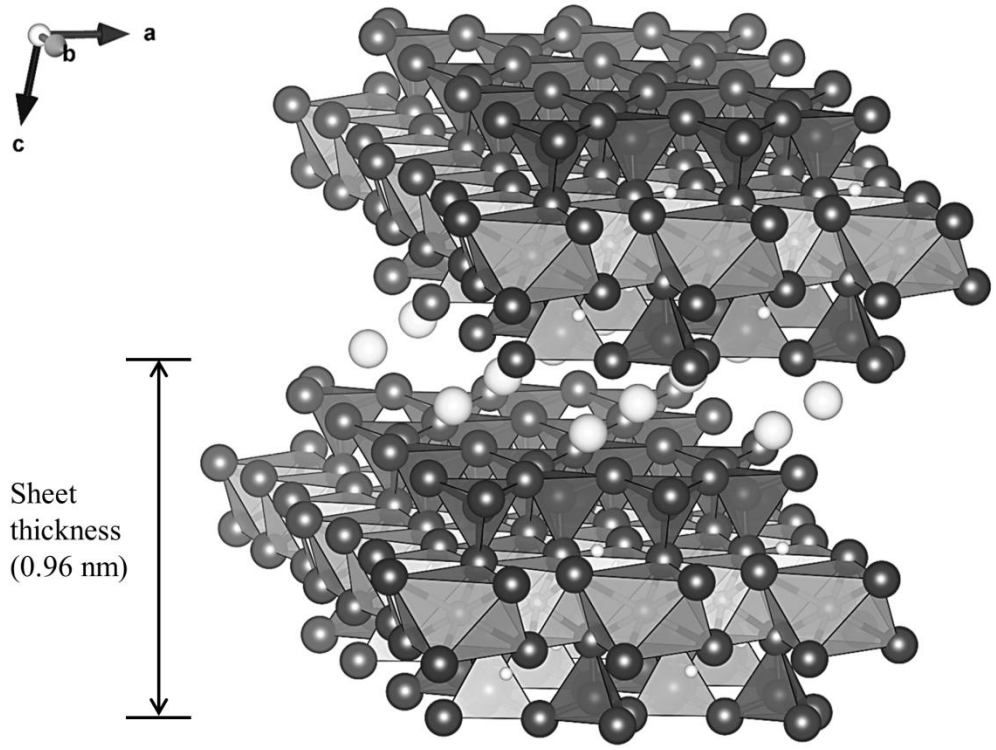

Figure 1.6 Structure of anhydrous Na-montmorillonite (octahedral sheets – SiO_6 and some AlO_6, tetrahedral sheets – AlO_4, large white spheres – Na, small white spheres – H)

The exchange of Na^+ cations with other metal cations, or with organic cations, usually results in larger interlayer distances (1.2 - 2.3 nm). Alternately, the co-intercalation of solvent can also cause considerable gallery expansion. For example, Na-montmorillonite in the hydrated form $Na_{0.5}(Al_{3.5}Mg_{0.5})Si_8O_{20}(OH)_4 \cdot 3.5H_2O$ has a Δd = 1.24 nm.[13] Ion exchange or co-intercalation of molecules, surfactants, or polymers between the layers, can result in an ordered expansion of the layers, or in delamination of the sheets to form a colloidal suspension.

In order to render these hydrophilic phyllosilicates more organophilic, the hydrated cations of the interlayer can be exchanged with cationic surfactants such as alkylammonium or alkylphosphonium. These modified organoclays have lower surface energies and are more compatible with non-polar organic intercalates.[11]

Intercalation of larger molecules like polyethylene glycol (PEG) and polymers such as polyethylene oxide (PEO) can be achieved for both hydrophilic and organophillic montmorillonites. Polymer-clay nanocomposites combine constituents in at least one nanoscale dimension, typically on the order of 1 to 10 nm. Because of this nanostructure, polymer-clay nanocomposites can possess unique properties. As reported in the literature, polymer-clay nanocomposites can show enhanced mechanical and thermal properties, gas permeability resistance, and fire retardancy.[11]

Nanocomposites can be produced by an in-situ polymerization, by solid phase melt blending, or by reaction in solution phase (exfoliation/reassembly). The synthetic method employed, as well as other material processing such as annealing time, can have a significant impact on the product structure and properties. The dimensions and microstructures of the dispersed phase significantly influence the properties of polymer composites. When registry between the host layers is maintained, the material is described as an intercalation compound. When this registry is lost, and the clay layers are more randomly distributed throughout the polymer matrix, the system is described as an exfoliated or delaminated nanocomposite. If the clay is not dispersed, it is simply a microfiller. Polymer composite materials are used widely as structural materials in diverse applications

such as transport (vehicles), construction, electronics and consumer products such as packaging and sporting goods.[11]

The melt intercalation process was first reported relatively recently, in 1993, by Vaia *et al*.[29] A thermoplastic polymer is mechanically mixed with an organophilic clay at elevated temperatures. The polymer chains intercalate between the individual silicate layers of the clay. The proposed driving force is the enthalpic contribution from polymer/organoclay interactions.[11]

In solution phase syntheses, both the clay (hydrophilic or organophilic), and the polymer, are dissolved in water or a polar organic solvent. The entropy gain due to solvent desorption drives the polymer chains to diffuse between the clay layers, compensating for any decrease in chain conformational entropy. Solvent evaporation leads to the desired nanocomposites product.[11]

In situ polymerization is an earlier strategy used to synthesize polymer-clay nanocomposites. This is similar to the solution method indicated above, with the solvent replaced by a polar monomer solution. Once the organoclay is swollen by the monomer, a curing agent is added and, in favorable cases, complete exfoliation occurs. According to previous studies, polymerization is believed to be the indirect driving force of the exfoliation. The clay, due to its high surface energy, attracts polar monomer molecules into the clay galleries until equilibrium is reached. The polymerization reaction lowers the intercalate polarity and therefore displaces the equilibrium. This allows new polar species to diffuse between the layers, and this

process progressively exfoliates the clay. Therefore, the nature of the curing agent as well as the curing conditions can each play a role in the exfoliation process.[11]

Nanocomposites comprising polyethylene oxide and Na-montmorillonite can form polymer monolayer or bilayer galleries, with Δd = 0.41 or 0.81 nm, respectively.[6] Polyethylene imine nanocomposites are only reported to form intercalate monolayers with Δd = 0.42 nm.[25] Ca-montmorillonite forms nanocomposites with polyvinyl alcohol and the interlayer expansion ranged 0.59-0.74 nm, depending on processing conditions.[30] There are a limited number of reports related to the intercalation and formation of nanocomposites of montmorillonite with dendrimers. Those structures include hyperbranched polymers,[31, 32] higher-generation polyamidoamines,[33] dendrons,[34] or dendritic quaternary ammoniums[26]. Intercalation of these species was found to result in very large gallery expansions (~ 3 nm),[26,31,34] or pure and mixed phase nanocomposites,[26,31,33,34] and or in some cases result in exfoliated nanocomposites.[31] Ratanarat *et al*. reported that generation 2.0 (G2.0) polyamidoamine (PAMAM) forms an exfoliated nanocomposite with Na-montmorillonite.[35] Alongi *et al*. reported the synthesis of nanomposites containing higher generation (G4.0−7.0) PAMAM with Na-montmorillonite (Δd = 0.78−0.97 nm).[33]

Nanocomposites can show dramatic property changes with respect to their native constitutents, or even to micro/macrocomposites of similar composition. The thermal stability of a polymer-layered-silicate nanocomposite of poly(methylmethacrylate) (PMMA) and montmorillonite clay increases by 40-50 °C.[36] The nanocomposited forms of both linear and cross-linked PMMA in

montmorillonite are more stable by 40–50 °C than the native polymers.[36] This increased stability is ascribed to both the structure change and to the restricted thermal motion of the PMMA intercalates in the nanocomposite galleries. Aside from thermal stability, reduced gas & liquid permeability, increased flame retardancy and increased optical clarity have all been reported for polymer montmorillonite nanocomposites.[11]

Adding to previous reports on the formation of some dendrimer-montmorillonite nanocomposites, in Chapter 3 this dissertation will report the formation and characterization of new lower generation polyamidoamine dendrimer Na-montmorillonite nanocomposites. The materials contain a flattened PAMAM monolayer or bilayer arrangement within galleries, and a monolayer to bilayer transition with increasing dendrimer content.

1.4 TRANSITION METAL DICHALCOGENIDES (MX_2)

Many transition metal dichalcogenides (MX_2) are layered structures consisting of metal cations bound between hexagonal planes of chalcogenide anions. The transition metal cations may have either trigonal prismatic or octahedral coordination. The large number of relative dispositions of chalcogenide planes leads to a wide variety of MX_2 structures and polytypes. Some commonly observed arrangements are represented by 1T-TiS_2 with an $(AbC)_n$ stacking repeat, 2H-TaS_2 with an $(AbACbC)_n$ stacking repeat, and 2H-MoS_2 with an $(AbABcB)_n$ stacking repeat. 1T-TiS_2 has octahedral coordination, whereas 2H-TaS_2 and 2H-MoS_2 have trigonal prismatic coordination around transition metal cations. Typically the sheet thickness for MS_2 hosts is ~ 0.6 nm (Figure 1.7).[13,37,38]

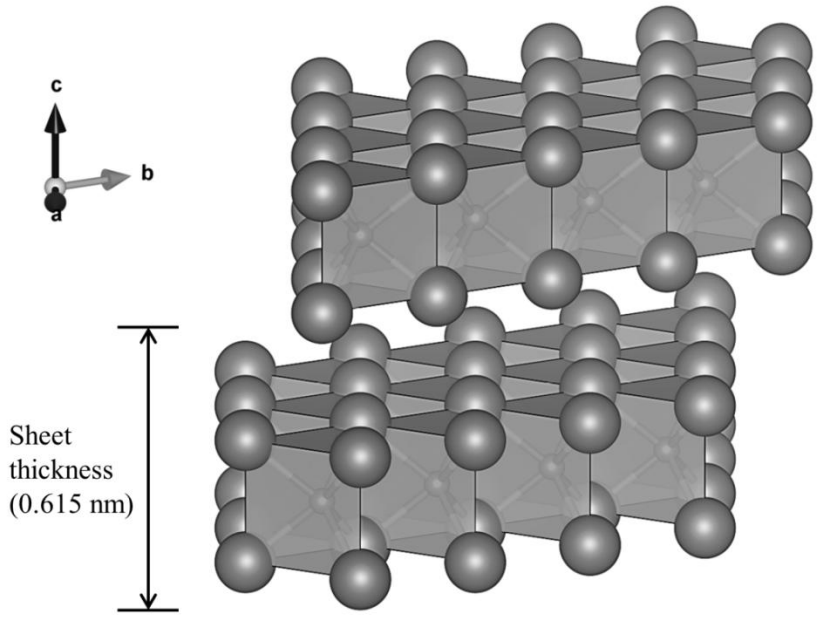

Figure 1.7 The layered structure of 2H-MoS_2 (containing trigonal prismatic MoS_6 sheets)

These layered materials have been investigated intensively as intercalation hosts. Known intercalates include the alkali metal cations, alkylammonium cations, ammonia, amines, water and other solvents. Alkali metal intercalation compounds can be obtained directly by high temperature solid state synthesis, either by the reaction of an MX_2 host with an alkali metal, or by the direct reaction of the A, M and X constituent elements.[13, 37] Another widely-used technique is the intercalation of the MX_2 host using a liquid-phase reductant like butyllithium or sodium naphthalide dissolved in suitable organic solvents, or with alkali metals dissolved in liquid ammonia.[2,13,39-41] Another common synthetic approach involves the electrochemical reduction of the MX_2 host in a suitable electrolyte.[42,43]

For the MX_2 host structures with more readily reduced transition metal cations, reductive intercalation can be accomplished using ammonia, amines or aqueous solutions. This redox process need not involve any other reductant. In many cases, additional neutral solvent co-intercalates along with cations.[13]

Alkali metal intercalation of MS_2 was first observed in 1959, when Rudorff reported a wide range of A_xMX_2 intercalation compounds prepared from MoS_2, $MoSe_2$, WS_2, WSe_2, ReS_2, TiS_2, and $TiSe_2$.[2,39] Rouxel and coworkers also extensively studied the intercalation of the group 4 transition metal MX_2 compounds.[37] Whittingham *et al*. studied the lithium intercalation of MX_2, and Schollhorn *et al*. reported several different syntheses and exchange reactions for MX_2 intercalation compounds.[13,44]

Rudorff reported the formation of $Li_{0.8}MoS_2 \cdot 0.8NH_3$, $Na_{0.6}MoS_2$, $K_{0.6}MoS_2$ and $Cs_{0.5}MoS_2$ compounds with interlayer expansions of 0.335, 0.135, 0.195 and 0.274 nm, respectively.[39] The much larger expansion seen in $Li_{0.8}MoS_2 \cdot 0.8NH_3$ arises from the presence of NH_3 co-intercalate. Schollhorn and Weiss reported that these intercalation compounds absorb water with a further increase in Δd of 0.29–0.70 nm, depending on the reaction conditions.[44]

A series of alkali metal and alkaline earth intercalation compounds of MoS_2 were synthesized in anhydrous NH_3(l), with the observed Δd values ranging from 0.14 to 0.37 nm.[40,41] The same method was utilized to prepare intercalation compounds for TaS_2, with the resulting products Na_xTaS_2 and K_xTaS_2 giving Δd of 0.11 and 0.21 nm, respectively.[45]

Some organic and inorganic bases react to form intercalation compounds with groups 4 and 5 MX_2 hosts, with Δd ranging from 0.30 nm (for smaller molecules like NH_3) to 5.23 nm (for octadecylamine), with compositions reflecting the uptake of 0.1 to 1.0 guests per MX_2 unit.[37] Schollhorn and Zagefka have suggested that in these reactions the metals are reduced and amine molecules are protonated and intercalate as ammonium cations; the interaction between the host and guest has been ascribed to either charge transfer or a redox reaction.[46] The correlation of reactivities to redox potentials supports the latter interpretation. For example, the Group 6 chalcogenides hosts are less easily reduced and do not react to form intercalation compounds with organic bases.[13,37]

Some MX_2 hosts react in strong aqueous base to intercalate hydrated alkali metal cations, e.g. $Na_{0.3}TaS_2 \cdot \delta H_2O$.[37,47] These complex intercalates undergo facile exchange in aqueous salt solutions.[44] The water co-intercalate can be displaced in polar inorganic or organic solvents (i.e. alcohols, ethers, amines, sulfoxides, etc).[44] The product compositions, including both the contents of intercalate cations and of cointercalates, depend on the degree of reduction, conditions of exposure to the exchange solutions, and post-reaction processing.

Ethylenediamine (en) and trimethylenediamine (tn) react directly with TiS_2, NbS_2, and TaS_2 to form intercalation compounds with Δd = 0.34–0.41 nm. These gallery dimensions indicate that the amine intercalates form monolayers with long molecular axes oriented parallel to the host layers.[48-50] These products show a compositional range that depends on the host and the sample processing conditions, with intercalate to MX_2 ratios of 0.17–0.39 for en and 0.15–0.33 for tn. Secondary amines, such as diethylamine, dibutylamine, and dipentylamine react with exfoliated MoS_2, generating $Li_{0.1}MoS_2 \cdot \delta$dialkylamine, with ranges of δ = 0.11–0.42 and Δd = 0.37–0.45 nm, depending on the dialkylamine cointercalate.[51]

Recently, electride solutions in liquid amines have been used to synthesize graphite intercalation compounds.[7,52-54] In Chapter 4, the use of amine electride chemistry to synthesize intercalation compounds of MoS_2 will be described in detail.

1.5 MOLYBDENUM(VI) OXIDE (MoO_3)

The binary molybdenum(VI) oxide (MoO_3), has a layer structure consisting of distorted MoO_6 octahedra that share edges and vertices to form sheets (Figure 1.8). The sheet thickness for MoO_3 is 0.69 nm, and the material is a well-known host for intercalation chemistry.[13]

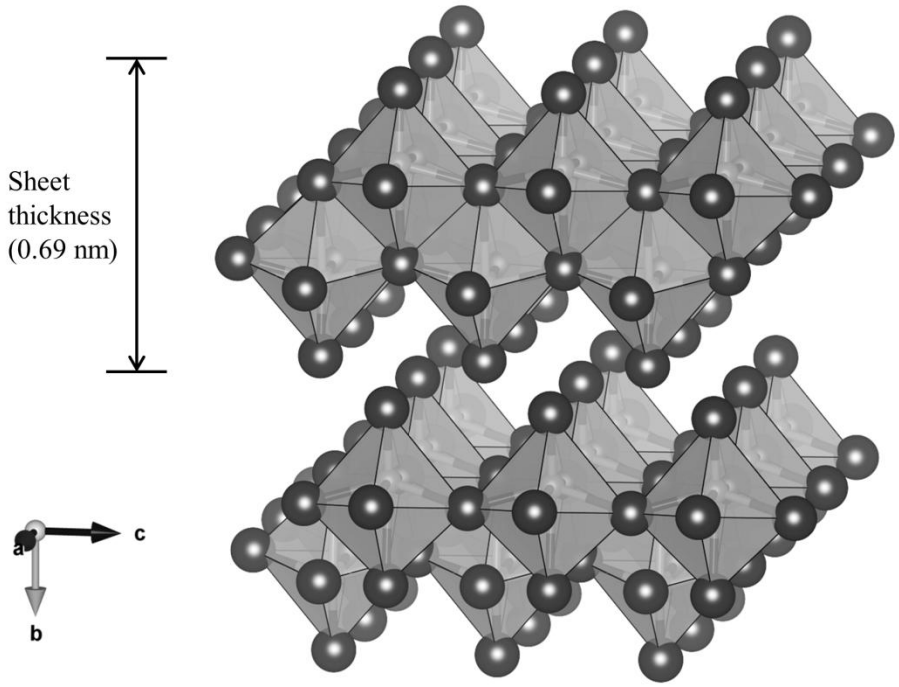

Figure 1.8 Structure of MoO_3, showing the sheets containing edge-sharing MoO_6 octrahedra.

Various techniques have been employed to synthesize intercalation compounds of MoO_3. Reaction with an n-butyllithium/hexane solution gives Li_xMoO_3. Product homogeneity is facilitated by subsequent equilibration of the product in a non-aqueous electrolyte containing lithium ions.[13]

Li(s)|Li^+(nonaqueous solvent)|MoO_3 electrochemical cells with non-aqueous electrolytes have an open-circuit voltage of ~ 2.8 V and have been utilized to intercalate lithium into MoO_3. Typical electrolytes are $LiClO_4$ or LiI dissolved in organic solvents like dimethylsulfoxide (DMSO) or propylene carbonate (PC).[55] The extent of these reactions can often be monitored coulometrically, and the products obtained have the general formula of Li_xMoO_3 and Δd ~ 0.1 nm. The charge/discharge reaction is reversible up to x = 1.5.[13]

The intercalation of MoO_3 by hydrogen is perhaps the most extensively investigated. Chemical reduction of MoO_3 in aqueous acid was first shown by Glemser *et al.* to form a series of compounds that could be formulated as H_xMoO_3.[13, 56-58] The vigorous reduction of MoO_3 by Zn/HCl produces H_2MoO_3.[59] Intermediate phases in the $0 < x < 2$ range are obtained by the reaction of H_2MoO_3 with MoO_3 in sealed tubes at < 100 °C.[59] Four distinct and highly colored hydrogen bronze phases are observed: blue orthorhombic ($0.23 < x < 0.40$), blue monoclinic ($0.85 < x < 1.04$), red monoclinic ($1.55 < x < 1.72$), and green monoclinic ($x = 1.99$).[59] These hydrogen intercalation compounds are acidic and will react with Lewis bases (L) to form intercalation compounds of general composition $L_yH_xMoO_3$.[13,55]

Stoichiometric MoO_3 is a white insulator; reductive intercalation, even at low levels, results in both a large increase in electronic conductivity and a dramatic color change to metallic blue-black. The intercalation compounds are often rapidly re-oxidized when exposed to air.[13]

The cathodic reduction of MoO_3 in aqueous solutions (typically mineral acids)[55] results in protonation to form H_xMoO_3; whereas the use of aqueous electrolytes containing alkali metal or transition metal ions leads to metallic blue hydrated phases $A_x^+(H_2O)_y[MoO_3]^{x-}$. For example, MoO_3 is reduced in $Na_2S_2O_4$(aq) to form $Na_x(H_2O)_yMoO_3$. Both intercalate ions and co-intercalate solvent are often readily exchanged by reaction with aqueous or polar organic solutions (e.g. DMSO). Observed interlayer expansions are ~ 0.28 nm with large monovalent cations (Rb^+, Cs^+), ~ 0.46 nm with small monovalent cations (Li^+, Na^+, K^+, NH_4^+) and ~ 0.71 nm for divalent cations.[13,55]

The reaction of $Li_x(H_2O)_yMoO_3$ with aqueous polymer solutions can result in exchange of water for a polymer co-intercalate.[25] Previous studies have reported the intercalation of polyethylene oxide (PEO),[27,60] linear polyethylenimine (LPEI),[25] polyaniline (PANI),[61] polyvinylpyrrolidone (PVP) and polyacrylamide (PAM),[62] using this method or melt intercalation method.[27] The interlayer expansions vary from 0.47 - 0.83 nm, depending on the polymer and how it is arranged in the galleries (for example, to form mono or bilayers).[25,61,63]

Dendrimers are branched polymers which can similarly exchange into the galleries. There have been no previous reports on the intercalation of dendrimers into MoO_3. The synthesis and characterization of dendrimer-MoO_3 nanocomposites are discussed in Appendix A.

1.6 SUMMARY

The further development of intercalation chemistry holds numerous possibilities and potential impacts. The discovery of new synthetic routes, new compounds, and new nanocomposites, may all solve important technological problems. The next three chapters and Appendix A of this dissertation will describe some novel experimental techniques to synthesize intercalation compounds and the characterization of the new materials thereby obtained.

1.7 REFERENCES

1. A. Lerf, in *Handbook of nanostructured materials and nanotechnology*, ed. H. S. Nalwa, Academic Press, San Diego, 2000, vol. 5, ch. 1, pp. 1-166.

2. W. Rüdorff and H. H. Sick, *Angew. Chem.*, 1959, 71, 127.

3. A. Lerf, *Dalton Trans.*, 2014, 43, 10276-10291.

4. A. J. Jacobson and L. F. Nazar, Intercalation Chemistry, *Encyclopedia of Inorganic and Bioinorganic Chemistry*, John Wiley & Sons, 2011.

5. S. T. Wilson, B. M. Lok, C. A. Messina, T. R. Cannan and E. M. Flanigen, *J. Am. Chem. Soc.*, 1982, 104, 1146-1147.

6. J. H. Wu and M. M. Lerner, *Chem. Mater.*, 1993, 5, 835-838.

7. T. Maluangnont, K. Gotoh, K. Fujiwara and M. M. Lerner, Carbon, 2011, 49, 1040-1042.

8. F. R. Gamble, J. H. Osiecki, M. Cais, R. Pisharody, F. J. Disalvo and T. H. Geballe, *Science*, 1971, 174, 493-497.

9. L. M. Liu, Z. N. Qi and X. G. Zhu, *J. Appl. Polym. Sci.*, 1999, 71, 1133-1138.

10. E. P. Giannelis, *Adv. Mater.*, 1996, 8, 29-35.

11. S. Pavlidou and C. D. Papaspyrides, *Prog. Polym. Sci.*, 2008, 33, 1119-1198.

12. M. Alexandre and P. Dubois, *Mater. Sci. Eng. R*, 2000, 28, 1-63.

13. *Intercalation Chemistry*, ed. M. S. Whittingham and A. J. Jacobson, Academic Press, New York, NY, 1982.

14. G. Ouvrard, R. Brec and J. Rouxel, *Mater. Res. Bull.*, 1985, 20, 1181-1189.

15. R. Brec, *Solid State Ionics*, 1986, 22, 3-30.

16. P. J. S. Foot and B. A. Nevett, *Chem. Commun.*, 1987, 380-381.

17. E. Prouzet, G. Ouvrard, R. Brec and P. Seguineau, *Solid State Ionics*, 1988, 31, 79-90.

18. H. Loboue, C. Guillot-Deudon, A. F. Popa, A. Lafond, B. Rebours, C. Pichon, T. Cseri, G. Berhault and C. Geantet, *Catal. Today*, 2008, 130, 63-68.

19. S. Yamanaka, H. Kobayashi and M. Tanaka, *Chem. Lett.*, 1976, 329-332.

20. A. Lemehaute, *C. R. Acad. Sci.*, 1978, 287, 309-311.

21. I. Lagadic, A. Leaustic and R. Clement, *Chem. Comm.*, 1992, 1396-1397.

22. P. Jeevanandam and S. Vasudevan, *Chem. Mater*., 1998, 10, 1276-1285.

23. V. Manriquez, P. Barahona, D. Ruiz and R. E. Avila, *Mater. Res. Bull.*, 2005, 40, 475-483.

24. E. Manova, C. Severac, A. Andreev and R. Clement, *J. Catal.*, 1997, 169, 503-509.

25. C. O. Oriakhi, R. L. Nafshun and M. M. Lerner, *Mater. Res. Bull.*, 1996, 31, 1513-1520.

26. F. Chen, H. Xiong, J. T. Yang, W. W. Cai and M. Q. Zhong, *e-Polym.*, 2012, No. 016.

27. N. Sukpirom, C. O. Oriakhi and M. M. Lerner, *Mater. Res. Bull.*, 2000, 35, 325-331.

28. S. S. Ray and M. Okamoto, *Prog. Polym. Sci.*, 2003, 28, 1539.

29. R. A. Vaia and E. P. Giannelis, *Macromolecules*, 1997, 30, 8000-8009.

30. K. A. Carrado, P. Thiyagarajan and D. L. Elder, *Clays Clay Miner.*, 1996, 44, 506-514.

31. S. He and J. Lin, *Appl. Mech. Mater.*, 2012, 108, 91-94.

32. M. Rodlert, C. J. G. Plummer, L. Garamszegi, Y. Leterrier, H. J. M. Grunbauer and J. A. E. Manson, *Polymer*, 2004, 45, 949-960.

33. J. Alongi, O. Monticelli, S. Russo and G. Camino, *J. Nanostruct. Polym. Nanocompos.*, 2006, 2, 127-133.

34. T.-Y. Juang, Y.-C. Chen, C.-C. Tsai, S. A. Dai, T.-M. Wu and R.-J. Jeng, *Appl. Clay Sci.*, 2010, 48, 103-110.

35. K. Ratanarat, M. Nithitanakul, D. C. Martin and R. Magaraphan, *Rev. Adv. Mater. Sci.*, 2003, 5, 187-192.

36. J. W. Gilman, *Appl. Clay Sci.*, 1999, 15, 31-49.

37. *Intercalated layered materials*, ed., F. A. Lévy, D. Reidel Publishing, Dordrecht, Holland, 1979.

38. E. Benavente, M. A. Santa Ana, F. Mendizabal and G. Gonzalez, *Coord. Chem. Rev.*, 2002, 224, 87-109.

39. W. Rüdorff, *Chimia*, 1965, 19.

40. R. B. Somoano, V. Hadek and A. Rembaum, *J. Chem. Phys.*, 1973, 58, 697-701.

41. R. B. Somoano, V. Hadek, A. Rembaum, S. Samson and J. A. Woollam, *J. Chem. Phys.*, 1975, 62, 1068-1073.

42. M. A. Santa Ana, V. Sanchez and G. Gonzalez, *Electrochim. Acta*, 1995, 40, 1773-1775.

43. M. S. Whittingham, *J. Electroanal. Chem.*, 1981, 118, 229-239.

44. R. Schöllhorn and A. Weiss, *J. Less-Common Met.*, 1974, 36, 229-236.

45. O. Matsumoto, E. Yamada, Y. Kanzaki and M. Konuma, *J. Phys. Chem. Solids*, 1978, 39, 191-192.

46. R. Schollhorn and H. D. Zagefka, *Angew. Chem. Int. Ed.*, 1977, 16, 199-200.

47. M. S. Whittingham, *Mater. Res. Bull.*, 1974, 9, 1681-1690.

48. H. Ogata, H. Fujimori, S. Miyajima, K. Kobashi, T. Chiba, R. E. Taylor and K. Endo, *J. Phys. Chem. Solids*, 1997, 58, 701-710.

49. E. Figueroa, J. W. Brill and J. P. Selegue, *J. Phys. Chem. Solids*, 1996, 57, 1123-1127.

50. H. Boller and H. Blaha, *J. Solid State Chem.*, 1982, 45, 119-126.

51. V. Sanchez, E. Benavente, M. A. Santa Ana and G. Gonzalez, *Chem. Mater.*, 1999, 11, 2296-2298.

52. T. Maluangnont, G. T. Bui, B. A. Huntington and M. M. Lerner, *Chem. Mater.*, 2011, 23, 1091-1095.

53. T. Maluangnont, M. M. Lerner and K. Gotoh, *Inorg. Chem.*, 2011, 50, 11676-11682.

54. T. Maluangnont, W. Sirisaksoontorn and M. M. Lerner, *Carbon*, 2012, 50, 597-602.

55. R. Schollhorn, R. Kuhlmann and J. O. Besenhard, *Mater. Res. Bull.*, 1976, 11, 83-90.

56. O. Glemser and G. Lutz, *Z. Anorg. Allg. Chem.*, 1951, 264, 17.

57. O. Glemser and G. Lutz, *Z. Anorg. Allg. Chem.*, 1952, 269, 93.

58. O. Glemser, G. Lutz and G. Meyer, *Z. Anorg. Allg. Chem.*, 1956, 285, 173.

59. J. J. Birtill and P. G. Dickens, *Mater. Res. Bull.*, 1978, 13, 311-316.

60. Y. S. Hu, W. Chen, Q. Xu and R. Z. Yuan, *J. Mater. Sci. Technol.*, 2001, 17, S124-S126.

61. O. Y. Posudievsky, S. A. Biskulova and V. D. Pokhodenko, *J. Mater. Chem.*, 2002, 12, 1446-1449.

62. L. Wang, J. Schindler, C. R. Kannewurf and M. G. Kanatzidis, *J. Mater. Chem.*, 1997, 7, 1277-1283.

63. L. F. Nazar, H. Wu and W. P. Power, *J. Mater. Chem.*, 1995, 5, 1985-1993.

CHAPTER 2

TEMPLATE PREPARATION OF $NiPS_3$ POLYMER NANOCOMPOSITES

Amila Udayanga Liyanage, and Michael M. Lerner

Department of Chemistry

Oregon State University

Corvallis, OR 97331-4003, USA

RSC Adv., 2012, 2, 474-479.

2.1 ABSTRACT

A template synthesis method can be used to prepare $NiPS_3$ nanocomposites with polyethylene oxide (PEO), polyethylenimine (PEI), polyvinyl alcohol (PVA) and polyvinylpyrrolidone (PVP). Nanocomposites of $NiPS_3$/PEI, $NiPS_3$/PVA and $NiPS_3$/PVP have not been previously reported. The resulting materials are characterized by powder X-ray diffraction (PXRD), thermogravimetric analysis (TGA), scanning electron microscope (SEM) and energy-dispersive X-ray spectroscopy (EDS). Reaction progress was monitored using UV-visible spectroscopy. Template synthesized $NiPS_3$/PEO nanocomposites show only polymer zig-zag monolayers, in contrast to the bilayers obtained using the topotactic method, and can generate denser interlayers than those obtained by topotactic methods. The crystallite sizes increase for more dilute conditions, a more polar solvent, and longer aging time. $P_2S_6^{4-}$ and Ni^{2+} concentrations govern nanocomposite nucleation and growth, respectively.

2.2 INTRODUCTION

MPS_3 and materials containing MPS_3 layers show interesting properties for nonlinear optics,[1,2] magnetic[3,4] or photomagnetic devices,[5] catalysis,[6] and energy storage in secondary batteries.[7] For the latter example, $NiPS_3$ shows an electrochemical reduction that proceeds in several stages at potentials from 2.7 to 1.8 V up to a Li/Ni ratio of ~7.5. The reduction occurs quasi-reversibly over the range $0 \leq$ Li/Ni ≤ 3 range, providing a high theoretical capacity as a secondary cathode.[7]

Xiao *et al.* reported that MoS_2 shows a significantly higher reversible capacity after an exfoliation process. Furthermore, the formation of a nanocomposite with polyethylene oxide (PEO) allows both higher capacities and improved charge/discharge cycling.[8] Since MS_2 and MPS_3 are both layered materials with intercalation chemistries, the preparation and electrochemical characterization of PEO/$NiPS_3$ nanocomposites are therefore of interest.

The synthesis and structures of MPS_3 nanocomposites with different polymers has been studied by several groups. In all cases, a topotactic method has been employed, starting with a compound containing alkali metal cations between MPS_3 layers. This intercalation compound may be obtained directly at high temperature,[9] or by introduction of alkali metal cations into the MPS_3 host *via* ion exchange[10] or reduction of the M(II) cations in the host layers.[6] The alkali metal cations likely enable nanocomposite formation by coordinating to polymer functional groups, as has been observed with many other layered hosts.[11]

Lagadic *et al.* first reported the synthesis of nanocomposites of PEO and MPS_3 (M = Mn, Cd) by reacting an aqueous polymer solution with $M_{1-x}PS_3A_{2x}(H_2O)_y$ (A = Na, K). The products obtained showed gallery expansions of ≈ 0.8-0.9 nm, consistent with the intercalation of bilayers of zig-zag-like PEO chains that coordinate to alkali metal ions.[10] Jeevanandam *et al.* subsequently prepared PEO/$CdPS_3$ nanocomposites in a methanolic solution at 55 °C.[12] Manriquez *et al.* reported the preparation of PEO nanocomposites from Li_xMPS_3 (M = Ni, Fe) using a similar approach. However, in this case the authors proposed a polymer helical conformation.[9]

Manova *et al.* reported the intercalation of polyethylene glycol into a Na_xNiPS_3 by reaction in a methanolic aqueous solution, with a gallery expansion of ≈0.8 nm.[6]

Other polymers that are known to form nanocomposites with MPS_3 layers include linear polyethylenimine, LPEI, and polyvinylpyrrolidone, PVP. The former was reported by Oriakhi *et al.* to form nanocomposites with polymer monolayers (expansion of 0.4 nm) *via* the reaction of $K_x(H_2O)_yM_{1-x/2}PS_3$ (M = Mn, Cd) and polymer in aqueous solution;[13] the latter was reported by Yang *et al. via* reaction of a potassium intercalated intermediate MPS_3 (M = Mn, Cd) and an aqueous PVP solution. The interlayer expansion in that case was ≈ 2.3 nm, much greater than that for PEO.[14]

A solvent-free, melt intercalation approach to obtain PEO/MPS_3 nanocomposites (M = Mn, Cd) was reported by Sukpirom *et al*. With this method,

$K_xM_{1-x/2}PS_3 \cdot \delta H_2O$ was shown to directly intercalate PEO at 125 °C. The nanocomposite basal repeat distances were increased by ≈ 0.8 nm, again ascribed to the presence of PEO bilayers.[15]

MPS_3 compounds are normally prepared by combining the elements or simple precursors at elevated temperature.[16,17] However, the synthesis of highly disordered or amorphous $NiPS_3$ at ambient temperature has been reported by reaction of Ni^{2+} salts with alkali metal hexathiohypodiphosphate ($Na_4P_2S_6.6H_2O$ or $Li_4P_2S_6.6H_2O$) in aqueous solution.[18-20] In the following study, we describe the first template approach to MPS_3 compounds, where layered nanocomposites are obtained directly using a one-pot reaction with solution-phase precursors at ambient temperature.

2.3 EXPERIMENTAL

2.3.1 REAGENTS AND ANALYTICAL METHODS

Li_2S (99.9%, Cerac), P (99%, Johnson Matthey), S (99.9%, Mallinckrodt), $Ni(NO_3)_2 \cdot 6H_2O$ (Aldrich), PEO (Aldrich, M_w=100,000), linear polyethylenimine (Alfa Aeser, M_w=25,000), polyvinyl alcohol, 80% hydrolyzed (Aldrich, M_w=9-10,000) and polyvinylpyrrolidone (Alfa Aeser, M_w=8,000) were purchased and used without further purification.

Powder XRD (PXRD) patterns from 3-60° 2θ were obtained on a Rigaku Miniflex II diffractometer, using Ni-filtered Cu-K_α radiation at a scan rate of 3° min^{-1} and step size of 0.020° 2θ. A modified Scherrer equation[21] was used to determine crystallite size (L) for the prepared nanocomposites:

$$L_{hkl} = \frac{0.9\lambda}{cos\ \theta_{hkl}\,[\Delta^2(2\theta_{hkl}) - \Delta^2(2\theta_{hkl})_{std}]^{1/2}} \quad (1)$$

where λ = 0.15406 nm, $\Delta(2\theta_{hkl})$ = full width at half maximum (in radians) and θ_{hkl} = diffraction angle. A Si(m) powder standard was employed for these measurements. Thermogravimetric (TGA) analyses were performed under Ar flow (20 mL min^{-1}) using a Shimadzu TGA-50 analyzer, from ambient to 500 °C at 5 °C min^{-1}. An Agilent 8453 UV-visible spectrophotometer was used for UV analyses. Background subtractions were carried out for all the UV-visible measurements. Scanning electron micrographs (SEMs) were obtained using an FEI Quanta 600F FEG SEM. Energy-dispersive X-ray spectroscopy (EDS) was used as a semi-quantitative elemental analysis method.

Van der Waals volumes of C_2H_4O oligomers (C = 2-40) were calculated based on Bondi radii using a method termed Atomic and Bond Contributions of van der Waals volume (VABC).[22]

2.3.2 SYNTHESES

$Li_4P_2S_6$ was synthesized as a white powder according to a published procedure.[23] Li_2S, P and S were combined in 1 : 1 : 2 mole ratio and sealed in a quartz tube under an inert atmosphere. The mixture was heated to 900 °C at 100 °C h^{-1}, maintained at 900 °C for 0.5 h, rapidly cooled to 450 °C and held at 450 °C for 24 h. Highly disordered or amorphous $NiPS_3$ was synthesized *via* a process previously reported by Prouzet *et al.*[19] An aqueous solution of $Ni(NO_3)_2 \cdot 6H_2O$ (0.31 g, 5.00 mL) was added dropwise to an aqueous solution of $Li_4P_2S_6$ (0.10 g, 5.00 mL) and stirred

vigorously for 24 h. The reddish precipitate was centrifuged for 15 min, triple washed with deionized (DI), and then dried under vacuum at room temperature.

To prepare the nanocomposites, $Ni(NO_3)_2 \cdot 6H_2O$ (0.31 g) and PEO (0.01-0.05 g) were dissolved in 5-500 mL of DI water and then slowly added to a solution $Li_4P_2S_6$ (0.1 g) dissolved in DI water (5.00-500.0 mL) and stirred vigorously for 24 h. Depending on the solvent volume, the precipitation time varied from few minutes to 12 days. After aging (1-7 days) the resulting brown precipitate was centrifuged for 15 min and washed three times with a copious amount of DI water. The solid product was dried under vacuum at 60 °C for 18 h. Where noted, some reactions substituted water with 10% ethanol as the solvent.

Samples are identified below based on starting g/g PEO/$Li_4P_2S_6$ ratio (*R*) and total solvent volume (*V*). For example, the product of $Ni(NO_3)_2 \cdot 6H_2O$ (0.31 g) and PEO (0.05 g) dissolved in 5 mL of DI water with 5 mL of aqueous $Li_4P_2S_6$ (0.1 g) solution is labeled R0.5V10.

The same procedures were used to synthesize other polymer/$NiPS_3$ nanocomposites with linear polyethylenimine (LPEI), polyvinyl alcohol (PVA) and polyinylpyrrolidone (PVP).

2.4 RESULTS AND DISCUSSION

PXRD patterns (Figure 2.1) show that polymer nanocomposite structures are obtained by the template method. The basal repeat distance increases from 0.64 nm in a-$NiPS_3$ to 1.06 nm for all the PEO nanocomposites. This expansion of 0.42 nm along the stacking direction indicates the presence of PEO monolayers incorporated between $NiPS_3$ layers.

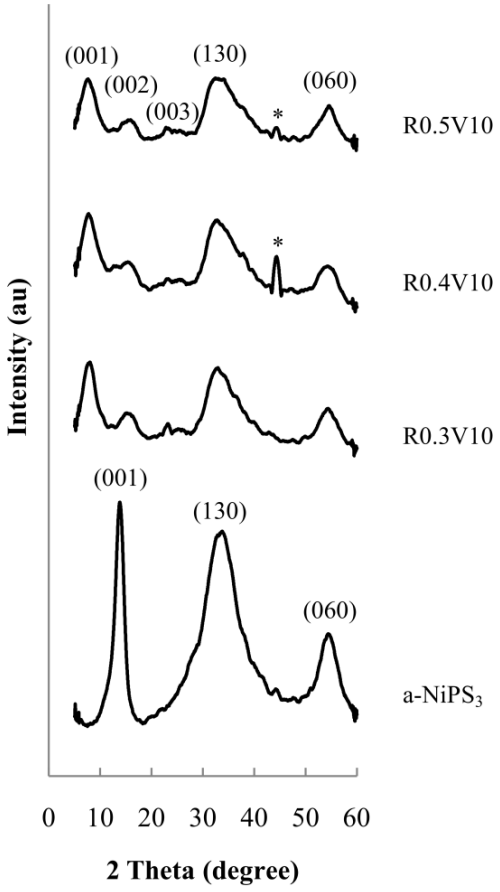

Figure 2.1 PXRD patterns for PEO/$NiPS_3$ nanocomposites obtained by the template method. a-$NiPS_3$ obtained by the same approach without PEO is shown for comparison. (*Al holder)

Figure 2.2 shows a typical microstructure of the prepared PEO/$NiPS_3$ nanocomposites, in this case for sample R0.5V10. The nanocomposites show an expanded layered morphology with most particle dimensions above 10 μm. For samples with R = 0.5, *i.e.* with a high polymer content, SEM images also reveal the presence of surface adsorbed polymer and show charging effects during imaging, indicating the presence of non-conducting polymer on surfaces. TGA data (see below) support the presence of surface-adsorbed PEO.

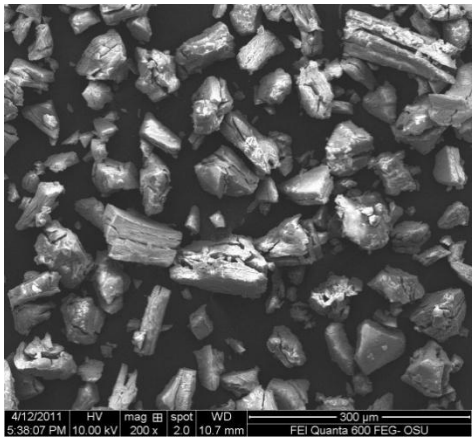

Figure 2.2 SEM image for a PEO/$NiPS_3$ nanocomposite (sample R0.5V10).

EDS data indicates the presence of Ni, P, S, C and O in the nanocomposite samples with an Ni : P : S ratio of 1 : 1 : 2.7. This supports the formation of host $NiPS_3$ structure from the precursors. Some sample degradation during analysis may account for the less than nominal sulfur content.

Figure 2.3 shows thermal analysis data of the obtained products. The DTG loss peak at 100–150 °C is ascribed to volatilization of intercalated water, and the loss peak around 250 °C to PEO decomposition and volatilization. From the mass losses, the relative contents of these components can be determined. For the R0.5V10

sample, some new features are observed. The water loss region occurs over a broad range starting at lower temperature, a shoulder appears on the low temperature side of the main PEO loss peak, and a high temperature loss is observed at 350 °C. The low temperature shoulder on the main PEO loss peak, and the high temperature loss, are ascribed to the presence of surface-adsorbed or bulk PEO. The separation of thermal loss events allows quantification of PEO intercalate *vs.* surface PEO. Water content was close to 1 mol/formula unit of $NiPS_3$, but this composition was highly dependent on sample history and environmental conditions (humidity and temperature).

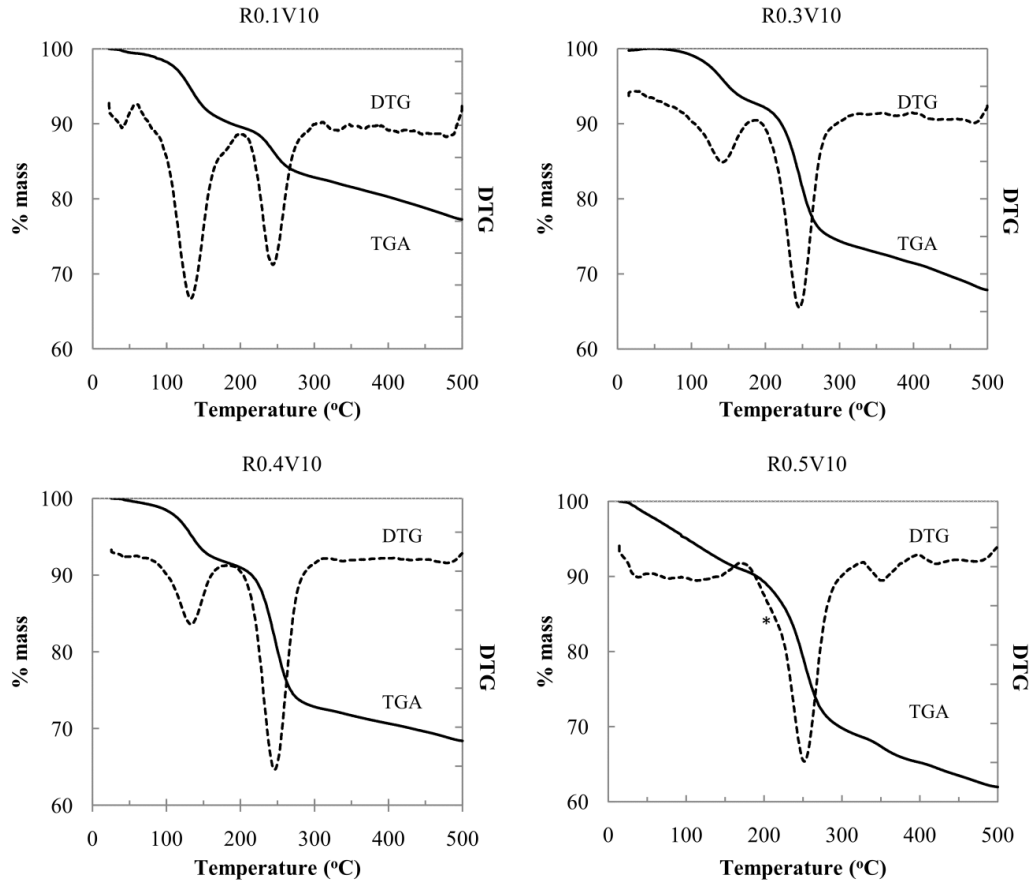

Figure 2.3 TGA of nanocomposites with different PEO compositions (* loss shoulder ascribed to surface PEO) DTG indicates the first derivative of TGA curves.

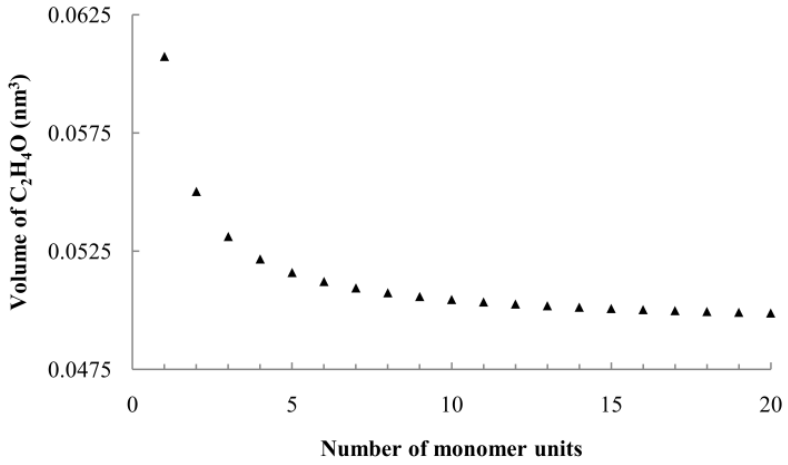

Figure 2.4 Calculated C_2H_4O unit volumes from VABC.

The packing fractions, *i.e.* fraction of volume in the expanded galleries occupied by intercalates, were derived from the known host MPS_3 cell dimensions, the gallery expansion determined by PXRD, the product stoichiometries and intercalate volumes. The PEO monomer unit volume was estimated by calculating the C_2H_4O monomer unit volume for increasing oligomer sizes until a stable volume of 0.050 nm^3 was observed. (Figure 2.4) As an example, for sample R0.1V10, the packing fraction, was calculated as:

$$Packing\ fraction = [(Z * 0.34 * 0.050\ nm^3)/(a * b *\ \Delta d)] = 0.28 \qquad (2)$$

where a = 0.5812 nm and b = 1.0070 nm are $NiPS_3$ unit cell parameters,[16] Δd = gallery expansion = 0.42 nm, and Z = $NiPS_3$ units per unit cell = 4. Water content was highly variable, as noted above, and may be on particle surfaces or intercalated, and thus was not considered in these packing fractions. The calculated PEO packing fractions are shown in Table 2.1. Intercalate PEO content and packing fractions

increase with higher PEO/$Li_4P_2S_6$ up to R = 0.3. At higher ratios, the additional PEO does not intercalate, although some remains as surface-adsorbed polymer.

Table 2.1 Compositional data from thermal analyses and calculated packing fractions for PEO/$NiPS_3$ nanocomposites

Sample	Reacted (PEO)/$NiPS_3$ (mol/mol)	Product (PEO)/$NiPS_3$ (mol/mol)			H_2O/$NiPS_3$ (mol/mol)	Packing fraction
		Total	Intercalated	Surface		
R0.1V10	0.34	0.34	0.34	-	1.29	0.28
R0.2V10	0.68	0.69	0.69	-	1.21	0.56
R0.3V10	1.01	1.02	1.02	-	1.01	0.83
R0.4V10	1.35	1.03	1.03	-	1.17	0.84
R0.5V10	1.69	1.30	1.01	0.29	1.34	0.82

As determined from diffraction peak widths, crystallite sizes for the nanocomposites, which are the products of 0.3 g/g PEO/$Li_4P_2S_6$ reaction mixtures, increases from 2.6 nm to 4.2 nm upon a 20-fold decrease in the reaction concentrations as shown in Table 2.2. A further dilution of 5 × results in a crystallite size increase to 4.5 nm. Aggregation times were also greatly increased in the more dilute solutions.

Table 2.2 Effect of synthetic conditions on crystallite size

Sample	Aggregation time (days)	Solvent	Aging time (days)	L (nm)
R0.3V10	0.004	DI water	1	2.6
R0.3V200	4-5	DI water	1	4.2
R0.3V1000	11-12	DI water	1	4.5
R0.3V1000	11-12	DI water	4	4.7
R0.3V1000	11-12	DI water	7	5.2
R0.3V1000	5-6	10% ethanol	1	4.2

The use of an ethanolic solvent also decreases the aggregation time with respect to the aqueous reaction mixtures, and results a smaller crystallite size. For an R0.3V1000 sample prepared using 10% ethanol, the crystallite size decreased from 4.5 nm (in DI water) to 4.2 nm. Crystallite size increased from 4.5 to 5.2 when the aging time was increased from 1 to 7 days, suggesting that exchange between solution and precipitate continues after aggregate formation.

Nanocomposites of PEI/$NiPS_3$, PVA/$NiPS_3$ and PVP/$NiPS_3$ have not been previously reported, but can be prepared by this template method. Table 2.3 shows the structural and compositional data for these new nanocomposites, obtained as for PEO/$NiPS_3$.

Table 2.3 Structural and compositional data for new polymer/$NiPS_3$ nanocomposites

Nanocomposite	d (nm)	Δd (nm)	Polymer/ $NiPS_3$ ratio (mol/mol)
PEO/$NiPS_3$	1.06	0.42	1.0
PEI/$NiPS_3$	1.05	0.41	1.0
PVA/$NiPS_3$	1.06	0.42	0.9
PVP/$NiPS_3$	2.20	1.56	0.5

In previous reports, PEO/MPS_3 (M = Mn, Cd) nanocomposites have shown interlayer expansions of 0.8-0.9 nm, corresponding to the presence of PEO bilayers between host sheets. For these nanocomposites the polymer/MPS_3 ratio is 1.9-2.1 which supports the zig-zag bilayer arrangement.[10] Alternately, Manriquez *et al.* describe a single helical PEO arrangement in MPS_3 nanocomposites (M = Ni, Fe) with an interlayer expansion of ≈ 0.8 nm.[9] All these compounds were synthesized using a topotactic method. The current template method results in only single PEO zig-zag polymer layers. However, these layers are more densely packed, as is indicated by the derived packing fractions shown in Table 2.4. Topotactic methods are kinetically limited by the slow diffusion of polymers,[24] which may impede development of densely packed intercalate layers. With a template method, denser polymer layers can form before the host layer structure fully develops.

Table 2.4 Comparison of packing fractions of known PEO/MPS_3 nanocomposites. The packing fractions were derived from compositional and structural data in the references indicated

Nanocomposite	Method of synthesis	Alkali ion	Packing fraction	Reference
PEO/$NiPS_3$	Topotactic	Li^+	0.27	9
PEO/$FePS_3$		Li^+	0.40	9
PEO/$CdPS_3$		Li^+, Na^+	0.58, 0.72	12
PEO/$CdPS_3$		Cs^+, K^+	0.62, 0.69	12
PEO/$CdPS_3$		K^+	0.61	10
PEO/$MnPS_3$		Na^+, K^+	0.73, 0.77	10
PEO/$NiPS_3$	Template	Li^+	0.84	this work

The PEI/$NiPS_3$ nanocomposites obtained show a similar interlayer expansion to that from the topotactic preparation (0.41 nm *vs.* 0.4 nm for PEI/MPS_3 (M = Mn, Cd) reported by Oriakhi *et al.*),[13] corresponding to a PEI monolayer. PVA/$NiPS_3$ shows a similar interlayer expansion of 0.42 nm. The template synthesis of $NiPS_3$/PVP gives a much smaller expansion of 1.46 nm than for the topotactic method.[14]

In order to evaluate the growth mechanism for these template reactions, the evolution of UV-visible absorption spectra were recorded under different reaction conditions. As shown in Figure 2.5, a new absorbance at 330 nm indicates the formation of the nanocomposite. This absorbance can be ascribed to Ni coordination

by sulfide in $P_2S_6^{4-}$ (Ni-dithiolene complexes show a prominent absorbance in this region).[25,26]

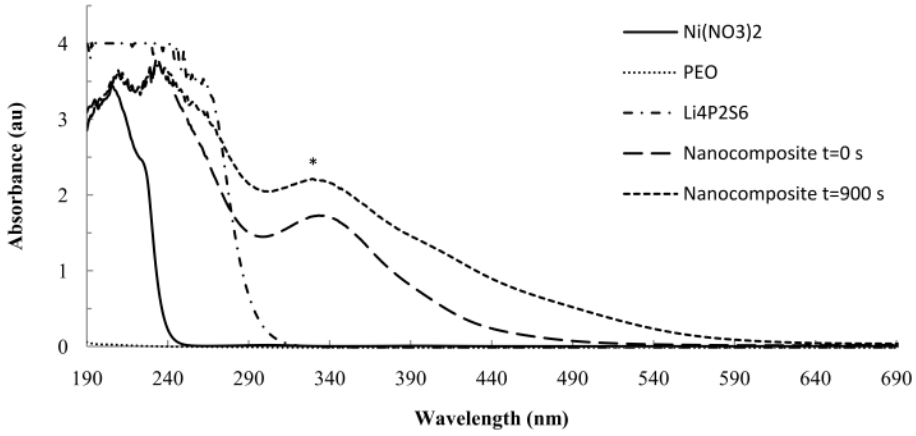

Figure 2.5 UV-visible spectra of some reactants and products of the template reactions. The absorbance at 330 nm (*) is used to monitor nanocomposite formation.

In the first set of experiments, the concentrations of Ni^{2+} and PEO were varied while maintaining a constant $P_2S_6^{4-}$ concentration and a constant Ni^{2+}/PEO ratio of 1 : 1. The initial absorbances at 330 nm under these conditions remain unchanged (Figure 2.6, compare the y-intercept of the three plots), indicating that nanocomposite nucleation is independent of PEO and Ni^{2+} concentration. These initial values are all obtained within 15 s of solution mixing.

The growth in the absorbance peak (from about 1.75 to 2.25 (Figure 2.6, curve for 2 mM)), indicates that the rate of nucleation (as indicated by the initial values) are significantly greater than the rate of nanocomposite growth. The growth rate, however, is strongly dependent on Ni^{2+} concentration.

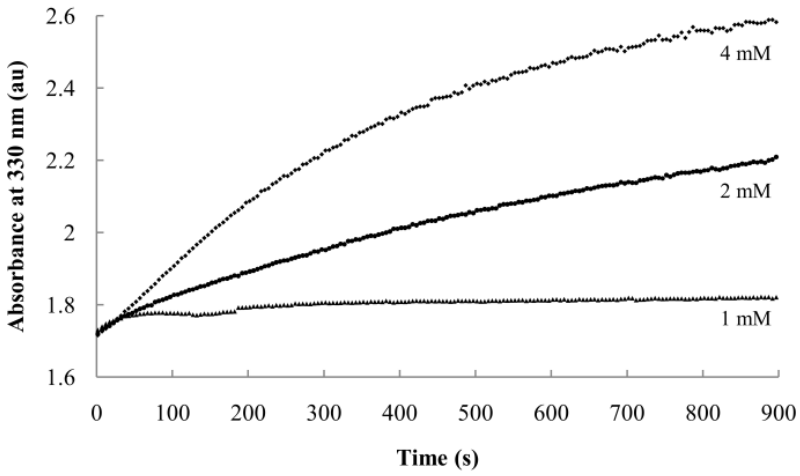

Figure 2.6 Effect of Ni^{2+} and PEO concentrations on the rate of nanocomposite formation. Curves are obtained using the indicated Ni^{2+} concentrations.

In contrast, the initial absorbances vary significantly for reactions using three different concentrations of $P_2S_6^{4-}$ with a constant Ni^{2+} and PEO concentrations and Ni^{2+}/PEO = 1. (Figure 2.7) This confirms the role of $P_2S_6^{4-}$ in nucleation. The growth curves are parallel under these conditions, indicating that nanocomposite growth is not significantly affected by $P_2S_6^{4-}$ concentration in this range.

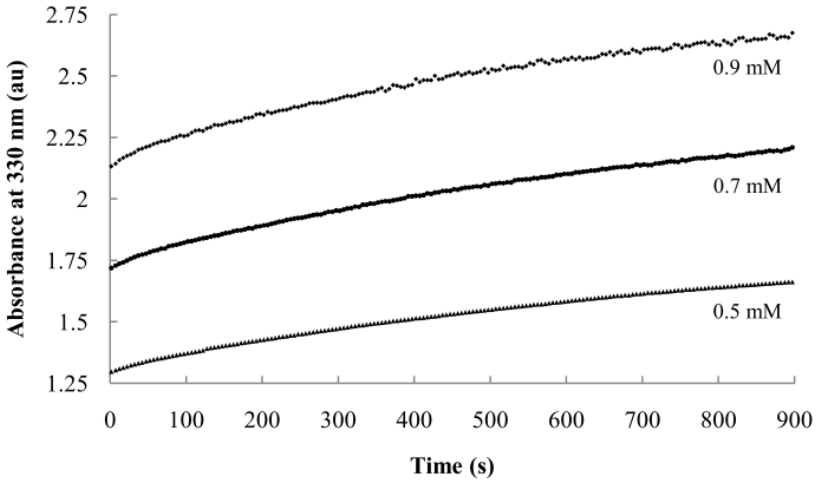

Figure 2.7 Effect of $P_4S_6^{4-}$ concentration on the rate of nanocomposite formation. Curves are obtained using the indicated $P_4S_6^{4-}$ concentrations.

2.5 CONCLUSIONS

A template synthesis method can be used to synthesize $NiPS_3$ nanocomposites. The obtained $NiPS_3$/PEO nanocomposites show polymer zig-zag monolayers at all combination ratios, in contrast to PEO nanocomposites derived from a topotactic method, and the packing fractions are greater. The product crystallite size increases with higher solvent volume, use of polar solvent and higher aging time. $P_2S_6^{4-}$ and Ni^{2+} concentrations govern nanocomposite nucleation and growth, respectively. Nanocomposites of $NiPS_3$/PEI, $NiPS_3$/PVA and $NiPS_3$/PVP are reported for the first time using this template method.

2.6 REFERENCES

1. T. Coradin, R. Clement, P. G. Lacroix and K. Nakatani, *Chem. Mater.*, 1996, 8, 2153.

2. I. Lagadic, P. G. Lacroix and R. Clement, *Chem. Mater.*, 1997, 9, 2004.

3. X. Chen, Z. Li, H. Zhou, T. Wang, J. Qin and M. Inokuchi, *Polymer*, 2007, 48, 3256.

4. R. Clement, J. J. Girerd and I. Morgensternbadarau, *Inorg. Chem.*, 1980, 19, 2852.

5. S. Benard, A. Leaustic, E. Riviere, P. Yu and R. Clement, *Chem. Mater.*, 2001, 13, 3709.

6. E. Manova, C. Severac, A. Andreev and R. Clement, *J. Catal.*, 1997, 169, 503.

7. Y. V. Kuzminskii, B. M. Voronin, I. M. Petrushina, N. N. Redin and G. P. Prikhodko, *J. Power Sources*, 1995, 55, 1.

8. J. Xiao, D. Choi, L. Cosimbescu, P. Koech, J. Liu and J. P. Lemmon, *Chem. Mater.*, 2010, 22, 4522.

9. V. Manriquez, P. Barahona, D. Ruiz and R. E. Avila, *Mater. Res. Bull.*, 2005, 40, 475.

10. I. Lagadic, A. Leaustic and R. Clement, *J. Chem. Soc. Chem. Commun.*, 1992, 1396.

11. M. M. Lerner and C. O. Oriakhi, *Handbook of Nanophase Materials*, ed. A. N. Goldstein, Dekker, New York, N.Y, 1997, 199-219.

12. P. Jeevanandam and S. Vasudevan, *Chem. Mater.*, 1998, 10, 1276.

13. C. O. Oriakhi, R. L. Nafshun and M. M. Lerner, *Mater. Res. Bull.*, 1996, 31, 1513.

14. D. Yang and R. F. Frindt, *J. Mater. Res.*, 2000, 15, 2408.

15. N. Sukpirom, C. O. Oriakhi and M. M. Lerner, *Mater. Res. Bull.*, 2000, 35, 325.

16. G. Ouvrard, R. Brec and J. Rouxel, *Mater. Res. Bull.*, 1985, 20, 1181.

17. R. Brec, *Solid State Ionics*, 1986, 22, 3.

18. P. J. S. Foot and B. A. Nevett, *J. Chem. Soc. Chem. Commun.*, 1987, 380.

19. E. Prouzet, G. Ouvrard, R. Brec and P. Seguineau, *Solid State Ionics*, 1988, 31, 79.

20. H. Loboue, C. Guillot-Deudon, A. F. Popa, A. Lafond, B. Rebours, C. Pichon, T. Cseri, G. Berhault and C. Geantet, *Catal. Today*, 2008, 130, 63.

21. P. Fragnaud, E. Prouzet and R. Brec, *J. Mater. Res.*, 1992, 7, 1839.

22. Y. H. Zhao, M. H. Abraham and A. M. Zissimos, *J. Org. Chem.*, 2003, 68, 7368.

23. R. Mercier, J. P. Malugani, B. Fahys, J. Douglade and G. Robert, *J. Solid State Chem.*, 1982, 43, 151.

24. C. O. Oriakhi, I. V. Farr and M. M. Lerner, *J. Mater. Chem.*, 1996, 6, 103.

25. J. F. Bai, J. L. Zuo, W. L. Tan, W. Ji, Z. Shen, H. K. Fun, K. Chinnakali, I. A. Razak, X. Z. You and C. M. Che, *J. Mater. Chem.*, 1999, 9, 2419.

26. Y. Ji, J. L. Zuo, L. X. Chen, Y. Q. Tian, Y. L. Song, Y. Z. Li and X. Z. You, *J. Phys. Chem. Solids*, 2005, 66, 207.

CHAPTER 3

SYNTHESIS AND CHARACTERIZATION OF LOW-GENERATION POLYAMIDOAMINE (PAMAM) DENDRIMER – SODIUM MONTMORILLONITE (Na-MMT) CLAY NANOCOMPOSITES

Amila U. Liyanage, Esther U. Ikhuoria,[a] Adeniyi A. Adenuga,

Vincent T. Remcho, and Michael M. Lerner

Department of Chemistry

Oregon State University

Corvallis, OR 97331-4003, USA

[a] Fulbright visiting scholar, Oregon State University, 2011/2012. Permanent address: Department of Chemistry, University of Benin, Benin City, Nigeria.

Inorg. Chem., 2013, 52 (8), 4603–4610.

3.1 ABSTRACT

Polymer-inorganic nanocomposites are a recently developed class of materials which have altered physical or chemical properties with respect to the pure polymer, inorganic host, or their micro- and macro composites. Lower generation (G0.0-2.0) polyamidoamine (PAMAM) dendrimer/Sodium montmorillonite (Na-MMT) nanocomposites were synthesized in a solution-phase exfoliation adsorption reaction. These are the first reports of the G0.0/ and G1.0/Na-MMT nanocomposites, and of a structurally-ordered G2.0/Na-MMT. The materials were characterized using powder X-ray diffraction (PXRD), thermogravimetric analysis (TGA) and Fourier transform infrared spectroscopy (FTIR). PAMAM characteristics at acidic and basic aqueous media were studied using capillary zone electrophoresis (CZE). Pseudospherical PAMAM dendrimers in aqueous medium attain a highly flattened conformation within the confined space between MMT sheets upon nanocomposite formation. The nanocomposite structure depends on the PAMAM generation and the starting dendrimer/organic composition. G0.0 always forms monolayer structures (Δd = 0.42 nm), while G2.0 forms monolayer structure, mixed phase and bilayer structures (Δd = 0.84 nm) at lower, intermediate, and higher organic content respectively, showing an interesting monolayer to bilayer transition. G1.0 showed an intermediate behavior, with monolayer to mixed-phase transition at the reactant ratios studied. This monolayer arrangement of PAMAM/clay nanocomposites is reported for the first time. Maximum organic contents of G0.0 monolayer and G2.0 bilayer nanocomposites were ~7% and ~14%, respectively. Gallery expansions were similar to those observed with linear polymer intercalates, but the packing fractions (0.31-

0.32) were 2-3 times lower. At acidic pH, the nanocomposites forming only monolayer structures are obtained, indicating a stronger electrostatic attraction between MMT and protonated PAMAM, and these nanocomposites formed more slowly and were more ordered. Na^+ ions play a significant role in nanocomposite formation. At high pH, PAMAMs show high mobility, zeta potential, and surface charge densities due to Na^+ complexation in solution. FTIR data indicates that both Na-MMT and PAMAM structural units are preserved in the nanocomposites obtained.

3.2 INTRODUCTION

Polymer-inorganic nanocomposites are a recently developed class of materials with at least one dimension of the phase combination in the nanometer range. Depending on the overall dimensionality, there are several types of nanocomposites; a prominent example is where two-dimensional (layered) inorganic structures incorporate or are dispersed into polymers.[1] In these polymer-containing layered nancomposites, some polymers studied include poly(ethylene oxide) (PEO),[2-4] linear polyethylenimine (LPEI),[4,5] polyvinyl alcohol (PVOH),[4,6] poly(vinyl pyrrolidone) (PVPyr),[4] and polyaniline (PANI)[7] polymers; the inorganic structures include clays,[2,3] transition metal oxides, sulfides, selenides[3,5,7] or phosphorous trisulfides[4,5] and layered double hydroxides.[8] Depending on the nature and relative composition of these constituents and also on the preparative method employed, the nanocomposites may form as intercalation compounds (ordered) or as exfoliated (amorphous) structures.[9] Some preparative methods include exfoliation-adsorption,[2,3] in situ intercalative polymerization,[10] melt intercalation,[11,12] and template synthesis.[4] A major reason for the growing interest in these nanocomposite materials is their remarkably changed mechanical, thermal, optical or physicochemical properties with respect to the constituent phases or conventional microcomposites.[1] Specific improvement for applied materials include increased moduli, tensile stress, thermal stability and flame retardancy, decreased gas permeability, and enhanced thermal stability of the ionic conductivity.[1,13]

Sodium montmorillonite, $Na_x(Al_{4-x}Mg_x)Si_8O_{20}(OH)_4$ (Na-MMT), is a smectite belonging to the structural family known as 2:1 phyllosilicates, which has layers with

central alumina or magnesia octahedra bound and covered by silica surfaces.[1,13] These anionic sheets are stacked with monovalent cation (Na^+) residing in between them. The stacking repeat for the anhydrous structure is 0.96 nm; ion exchange or co-intercalation of molecules, surfactants, or polymers between the layers can result in expansion of the layer repeat or delamination of the sheets into solution.[5,14,15]

Dendrimers are monodisperse macromolecules with a regular and highly branched three-dimensional architecture, which consists of three basic components; an initiator core, interior zones comprising cascading tiers of branches with radial connectivity to the initiator core, and an exterior surface with terminal groups.[16,17] Higher generation dendrimers add to the interior zone tiers. Polyamidoamines (PAMAMs) are the first synthetic dendrimers, with potential applications in drug or gene delivery, sensors, and nanoparticle synthesis.[18-21] Although dendrimers can have functional groups similar to those in linear polymers, the net connectivity contrasts with that of linear polymers and provides an opportunity to evaluate the effect of organic component on nanocomposite structure and the gallery composition of intercalated nanocomposites.

Previous studies have reported nanocomposites combining hyperbranched polymers,[22,23] higher-generation PAMAMs,[24] dendrons,[25] or dendritic quaternary ammoniums[26] with smectite clays including montmorillonite,[22-26] or kaolinite.[27] Those reports indicated very large gallery expansions,[22,25,26] both pure and mixed-phase intercalated nanocomposites,[22,24-26] and exfoliated nanocomposites.[22]

Ratanarat *et al.*[15] have reported the only lower generation PAMAM/Na-MMT nanocomposite, an exfoliated nanocomposite of generation 2.0 (G2.0) PAMAM and Na-MMT. Alongi *et al.*[24] have reported the synthesis of higher generation (G4.0-7.0) PAMAM/Na-MMT nanocomposites. Here we report the first systematic compositional study on the synthesis and characterization of lower generation PAMAM/Na-MMT nanocomposites and clarify the adsorbed monolayer/bilayer arrangements that occur in dendrimer nanocomposite galleries.

3.3 EXPERIMENTAL

3.3.1 REAGENTS

Polyamidoamine (PAMAM) aqueous solutions (~16% w/w, Dendritech), sodium montmorillonite (Na-MMT) (SWy-2, Clay Minerals Society), HCl (36.5-38.0%, EMD), H_3PO_4 (85%, Mallinckrodt), Na_2HPO_4 (ACS grade, Mallinckrodt Baker), NaOH (ACS grade, Mallinckrodt), NaCl (ACS grade, Mallinckrodt), Montmorillonite K 10 (Sigma-Aldrich), and $AgNO_3$ (ACS grade, Alfa Aesar) were purchased and used without further purification.

3.3.2 SYNTHESES

Aqueous solutions of PAMAM (0.01-0.08 g, 10.00 mL, pH 11-12) were added dropwise to aqueous suspensions of Na-MMT (0.1000 g, 10.00 mL, pH 5-6). Cloudy or powder-like white particles were visible within a few seconds to several minutes of combining the reactants. The suspensions had a pH = 10-11 and were stirred vigorously overnight at room temperature. The white precipitate was collected after centrifugation for 10 minutes, washed twice with deionized (DI) water, and then

dried under vacuum at 60 °C for 18 h. Some reactions were performed at ambient temperature, some at 60 °C.

In another set of nanocomposite syntheses, the PAMAM aqueous solutions were adjusted to pH = 2-3 using 1M HCl prior to addition of the Na-MMT suspension. Higher temperatures (50, 80 °C) were also utilized for some of these syntheses. These obtained products were washed repeatedly until no precipitate formed on reaction with dilute $AgNO_3$ (aq).

Samples are labeled below based on the reacted g/g PAMAM/Na-MMT ratios and PAMAM generation. For example, the sample obtained by reaction of 0.010 g of generation 0.0 PAMAM with 0.1000 g of suspended Na-MMT is labeled "0.1G(0.0)". For reactions carried out at temperatures other than ambient temperature and pHs other than pH=10-11, the temperature (in °C) and pH are also indicated, for example "0.6G(2.0)-50-2".

3.3.3 ANALYTICAL METHODS

Powder XRD (PXRD) patterns from 2° to 15° 2θ were obtained on a Rigaku Miniflex II diffractometer, using Ni-filtered Cu Kα radiation at a scan rate of 1^{o} min^{-1} and step size of 0.020° 2θ. A modified Scherrer equation[4] was used to determine crystallite size (L) for the prepared nanocomposites:

$$L_{hkl} = \frac{0.9\lambda}{\cos\theta_{hkl}\,[\Delta^2(2\theta_{hkl}) - \Delta^2(2\theta_{hkl})_{std}\,]^{1/2}} \qquad (1)$$

where λ = 0.15418 nm, $\Delta(2\theta_{hkl})$ = full width at half-maximum (in radians), and θ_{hkl} = diffraction angle. A Si(m) powder standard was employed for these measurements.

Thermogravimetric (TGA) analyses were performed under Ar flow (20 mL/min) using a Shimadzu TGA-50 analyzer. Approximately 10-15 mg of sample was placed into an open platinum pan and heated from ambient to 600 °C at 5 °C/min.

Capillary zone electrophoresis was performed to determine migration times using an HP ^{3D}CE instrument equipped with a UV detector, using a 75 μm inner diameter, 58.5 cm long fused silica capillary (50.0 cm to the detection window). New capillaries were sequentially conditioned by flushing with methanol (30 min), water (Milli-Q) (5 min), 1.0 M NaOH (30 min), water (5 min), and finally the background electrolyte (BGE) for 30 min. As preconditioning, the capillary was flushed with 0.1 M NaOH (3 min), water (1 min), and BGE (4 min). As postconditioning, the capillary was flushed with water (1 min). Background electrolytes used were 100 mM H_3PO_4, pH adjusted to 2.7, and 50 mM Na_2HPO_4, pH adjusted to 10.9 with NaOH. Ionic strengths of BGEs were adjusted to ~0.16 mol L^{-1} using NaCl. Samples were prepared by freshly dissolving in H_3PO_4 or Na_2HPO_4, and the sample was adjusted to the pH and the ionic strength of BGE, using NaOH and NaCl, respectively. Migrations were accomplished at applied voltages of +15 kV (pH 2.7) and +18 kV (pH 10.9). The capillary was thermostatted at 25 °C (pH 2.7) or 30 °C (pH 10.9). Solutions were injected hydrodynamically at 50 mbar for 5 s. Direct detection was employed at a wavelength of 210 nm.

The dimensionless mobility (μ_0') of the dendrimers was calculated using

$$\grave{\mu_0} = \frac{\mu_0 3\eta e}{2\xi\xi_0 kT} = \frac{IL}{Vt_m}\frac{3\eta e}{2\xi\xi_0 kT} \qquad (2)$$

where l is the effective length, L is the total length, V is the voltage, t_m is the migration time, μ_0 is the electrophoretic mobility, ξ is the dielectric constant of water (80.5), ξ_0 is the dielectric permittivity of the vacuum, k is the Boltzmann constant, T is the temperature in kelvin, η is the viscosity and e is charge of the electron. Dimensionless zeta potentials and charge distribution functions (I_0) were obtained using numerical solutions published by Wiersema *et al.*[28] and Loeb *et al.*[29] Zeta potential (ζ) and surface charge densities (σ) were calculated according to the following empirical formulas:[30]

$$\zeta = \zeta' \frac{kT}{e} \qquad (3)$$

$$\sigma = 5.8718\,(I)^{1/2}\, I_0 \times 10^{-2}\ \mathrm{C/m^2} \qquad (4)$$

IR spectra were taken using a Nicolet iS10 FT-IR spectrometer with an ATR sample cell, using background corrections for air and collection geometry. Aqueous PAMAM solutions were preconcentrated at 80 °C before collecting spectra. Diamond and Ge ATR cells were used for liquid and solid samples, respectively.

Van der Waals volumes of PAMAM dendrimers (G 0.0, 1.0, and 2.0) were calculated based on Bondi radii using a method termed "Atomic and Bond Contributions of van der Waals volume" (VABC).[31] Packing fractions were calculated[4] using

$$\text{Packing fraction} = [(Z\ n\ V_{vdw}) / (a\ b\ \Delta d)] \qquad (5)$$

where a = 0.517 and b = 0.894 nm are Na-MMT unit cell parameters,[32] Δd = interlayer expansion = d_i - 0.96 nm, where d_i and 0.96 nm are interlayer repeat distances of the nanocomposite and anhydrous Na-MMT, respectively, Z = the number of Na-MMT formula units per cell = 1, n = the number of PAMAM molecules per Na-MMT formula unit, and V_{vdw} = van der Waals volume of the PAMAM molecule.

Energy optimization of the gas-phase highly flattened and pseudospherical G0.0 PAMAM molecules was performed using DFT B3LYP method with 6-31G(d) basis set using Gaussian 09W software.

3.4 RESULTS AND DISCUSSION

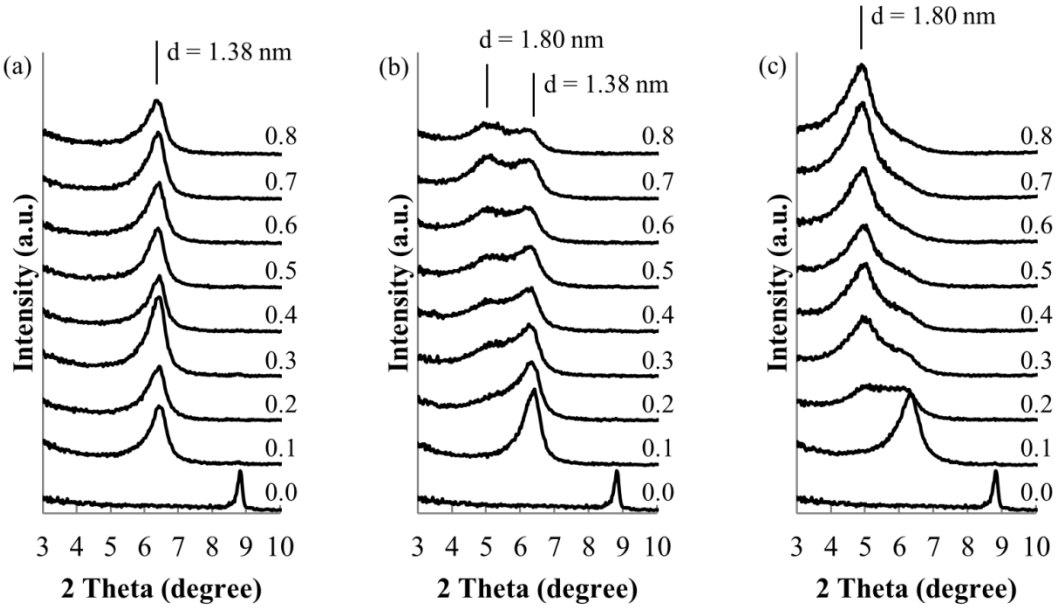

Figure 3.1 PXRD patterns for (a) G(0.0), (b) G(1.0), and (c) G(2.0) PAMAM/Na-MMT nanocomposites. The reactant ratios (g/g PAMAM/Na-MMT) are indicated.

As shown in Figure 3.1, G0.0 nanocomposites show interlayer repeat spacings (d) of 1.37-1.38 nm. Since the interlayer repeat distance of anhydrous Na-MMT is 0.96 nm, these spacings correspond to an interlayer expansion (Δd) of 0.41-0.42 nm. For G2.0 PAMAM, the nanocomposites obtained show a compositional effect with a more expanded phase, with Δd = 0.83-0.84 nm appearing only at compositions richer in dendrimer content. Except for 0.1G(1.0), which shows only the Δd = 0.42 nm phase, G(1.0) PAMAM nanocomposites show both these expanded phases, with the more expanded phase increasing in relative intensity at higher starting dendrimer compositions. These observations differ from Ratanarat *et al.*[15] report on exfoliated G2.0 PAMAM/Na-MMT nanocomposite. But the observed d values and the corresponding Δd calculated are comparable to those obtained by Alongi *et al.* with higher generation (G4.0-7.0) PAMAM and Na-MMT (d = 1.74-1.93 nm; Δd = 0.78-0.97 nm)[24] and Amin *et al.* with a hyperbranched polymer and Na-MMT (d = 1.397, 1.705 nm, Δd = 0.437, 0.745 nm).[33]

As will be discussed below, the two expanded phases obtained in our compositional studies contain galleries comprising ~0.4 nm thick PAMAM mono- or bilayers. The dendrimers are strongly adsorbed onto the clay surface and do not structurally resemble their solution-phase conformations.

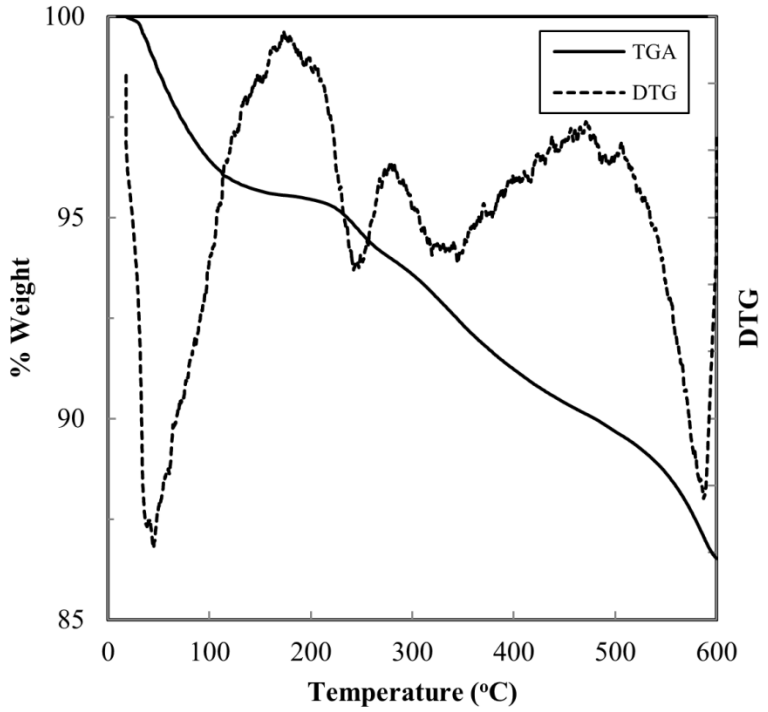

Figure 3.2 Mass loss and differential plots for 0.6G(1.0)-2 PAMAM/Na-MMT nanocomposite.

TGA data for these nanocomposites show four mass loss regions, also indicated by four peaks in the derivative (DTG) curves at <100, 210, 350 and >590 °C (Figure 3.2). These are attributed, respectively, to loss of intercalate water, a two-step degradation of PAMAM, and finally the degradation of the MMT sheet structure to liberate H_2O. Alongi *et al*.[24] observed a decomposition step around 200 °C that was ascribed to nonintercalated PAMAM. Since native PAMAM degrades in a single step around 300 °C, the lower temperature loss was attributed to a previously reported catalytic effect for organic decomposition on clays, for example, with quaternary ammonium/MMT intercalated composites.[34] Because the PAMAM content in our

products does not change significantly upon extended washing, and many different starting compositions resulted in similar mass losses, the presence of a significant fraction of nonintercalated PAMAM residue appears unlikely, and both mass loss steps at 210 and 350 °C are ascribed to the decomposition of intercalated PAMAM.

Table 3.1 compares interlayer distance (d), interlayer expansion (Δd), composition, packing fraction and crystallite size (L) of different nanocomposites obtained in this study.

Table 3.1 Structural and compositional data for PAMAM/Na-MMT nanocomposite products obtained using PXRD (d and Δd) and TGA (organic mass %), and derived packing fractions and crystallite sizes (L).

Sample	Reactant ratio (g/g PAMAM/Na-MMT)	Condition Temp./pH	Phase	d (nm)	Δd (nm)	Organic mass %	Packing fraction	L (nm)
0.1G(0.0)	0.1	RT/10-11	monolayer	1.38	0.42	5.6	0.23	129
0.2G(0.0)	0.2			1.37	0.41	6.5	0.28	126
0.3G(0.0)	0.3			1.38	0.42	6.6	0.28	128
0.4G(0.0)	0.4			1.37	0.41	6.6	0.28	130
0.5G(0.0)	0.5			1.38	0.42	7.2	0.30	128
0.6G(0.0)	0.6			1.37	0.41	7.4	0.31	126
0.7G(0.0)	0.7			1.38	0.42	7.3	0.31	125
0.8G(0.0)	0.8			1.38	0.42	7.5	0.31	122
0.1G(1.0)	0.1	RT/10-11	monolayer	1.38	0.42	5.6	0.23	127
0.2G(1.0)	0.2		mixed	1.39, 1.74	0.43, 0.78	8.2	n.a.	n.a.

0.3G(1.0)	0.3			1.42, 1.74	0.46, 0.78	9.1		
0.4G(1.0)	0.4			1.39, 1.78	0.43, 0.82	9.2		
0.5G(1.0)	0.5			1.40, 1.76	0.44, 0.80	10.2		
0.6G(1.0)	0.6			1.41, 1.75	0.45, 0.79	10.2		
0.7G(1.0)	0.7			1.72, 1.42	0.76, 0.46	10.7		
0.8G(1.0)	0.8			1.77, 1.41	0.81, 0.45	11.0		
0.1G(2.0)	0.1	RT/10-11	monolayer	1.39	0.43	5.3	0.21	115
0.2G(2.0)	0.2		mixed	1.77, 1.42	0.81, 0.46	10.4	n.a.	n.a.
0.3G(2.0)	0.3			1.80, 1.42	0.84, 0.46	11.7		
0.4G(2.0)	0.4			1.79, 1.42	0.83, 0.46	13.1		
0.5G(2.0)	0.5			1.79, 1.42	0.83, 0.46	13.8		
0.6G(2.0)	0.6		bilayer	1.80	0.84	14.1	0.32	116
0.7G(2.0)	0.7			1.80	0.84	13.9	0.31	108
0.8G(2.0)	0.8			1.80	0.84	14.5	0.33	103
0.6G(0.0)-2	0.6	RT/2-3	monolayer	1.36	0.40	6.6	0.29	141
0.6G(1.0)-2	0.6			1.36	0.40	6.6	0.29	145
0.6G(2.0)-50-2	0.6	50 °C/2-3		1.36	0.40	7.9	0.35	141
0.6G(2.0)-80-2	0.6	80 °C/2-3		1.36	0.40	7.1	0.31	144
0.3G(0.0)-60	0.3	60 °C/ 10-11	monolayer	1.37	0.41	6.2	0.26	133
0.3G(1.0)-60	0.3		mixed	1.40, 1.80	0.44, 0.84	8.5	n.a.	n.a.
0.3G(2.0)-60	0.3			1.81, 1.41	0.85, 0.45	11.4		

RT = ambient temperature, n.a. = not applicable

Depending on the relative charge densities of the clay host and guest, different intercalate arrangements can arise, including monolayers, lateral bilayers, pseudotrilayers, or an inclined paraffin-like structure.[1,35] Linear polymer/Na-MMT and linear alkyl ammonium/Na-MMT nanocomposites have shown monolayer intercalate structures that transition to bilayers with increasing intercalate content.[2,14] For all the obtained materials, only two interlayer expansions were observed, ~0.42 and ~0.84 nm, as shown in Figure 3.3 and Table 3.1. A plot of organic mass content for the G0.0 nanocomposites reaches a plateau at ~7% and that for G2.0 at ~14% (Table 3.1, Figure 3.4). Where two intercalated phases have both gallery dimensions and organic compositions in a 2:1 ratio, a monolayer/bilayer structure model is strongly indicated. Because only mixed phases and no intermediate values for interlayer expansion are observed, a monolayer to bilayer transition is observed with increasing PAMAM content for G1.0 and G2.0.

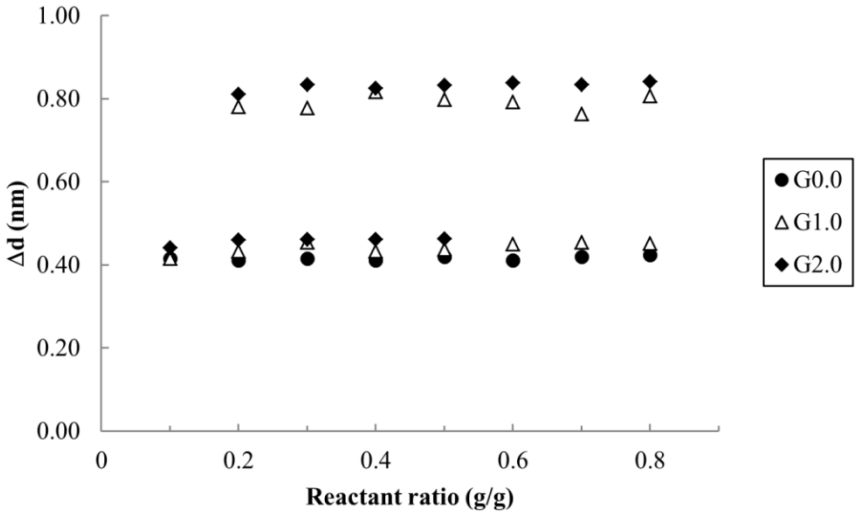

Figure 3.3 Interlayer expansion variation with reactant ratios, PAMAM/Na-MMT g/g, at room temperature and pH 10-11.

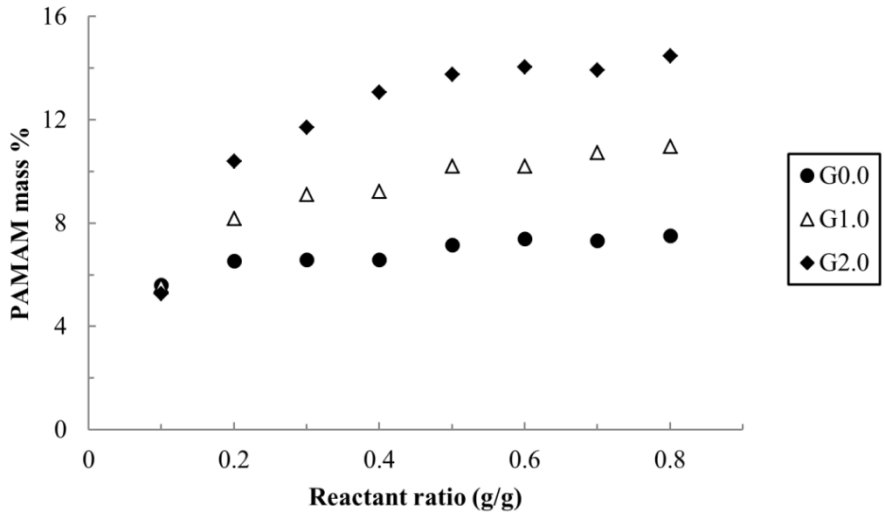

Figure 3.4 Dendrimer mass % variation with reactant ratios, PAMAM/Na-MMT g/g, at room temperature and pH 10-11.

The interlayer distances and interlayer expansion values for PAMAM/Na-MMT nanocomposites were also comparable with previously reported polymer/Na-MMT nanocomposites (Table 3.2), supporting the proposed monolayer and bilayer models. Although PVOH/Ca-MMT nanocomposites showed higher interlayer expansion values than with typical polymer monolayers, Carrodo *et al*.[6] note that extensive drying *in vacuo* at 65 °C also results in $\Delta d \approx 0.4$ nm.

Table 3.2 Compositional and packing data for polymer/A-MMT nanocomposites

Nanocomoposite	Phase	d_{001} (nm)	Δd (nm)	Organic mass %	Packing fraction*	Reference
PEO/Na-MMT	Monolayer	1.37	0.41	13*	0.67	2
PEO/Na-MMT	Bilayer	1.77	0.81	23	0.68	
PEI/Na-MMT	Monolayer	1.38	0.42	18	0.93	5
PVOH/Ca-MMT (heated)	-	1.70	0.74	10.3	0.24	6
PVOH/Ca-MMT	-	1.55	0.59	8	0.23	

* Calculated from the compositional and structural data provided in the references indicated.

These small dimensions require a highly flattened dendrimer conformation within the galleries. Compared with a solution diameter of >1.5 nm,[36,37] the maximum thickness for the dendrimers in the mono- and bilayers is ~0.4 nm for the nanocomposites we report. The strong adsorption of the dendrimers on the clay surfaces, coupled with the favorable lattice enthalpy for smaller expanions, result in minimum gallery expansions. The larger dendrimers show more favorability for the bilayer structure, most likely because their greater footprint in adsorbed form requires a larger intercalate volume for charge compensation of the anionic host.

Previous studies have shown altered PAMAM conformations due to interfacial or host-guest interactions. Lower generation (G0.0–G3.0) PAMAM dendrimers with an ethylenediamine core have an ellipsoidal shape, whereas the higher generation dendrimers (G4.0–G10.0) have a roughly spherical shape.[36,38] A significant flattening of dendrimers has been observed on mica,[39,40] Au,[41] and Pt[42]

substrates; Hierlemann *et al.* provided evidence for 0.5-0.8 nm thick G4.0 dendrimers on a Au surface.[41] Even the highly branched net PAMAM, at least for the lower generations, can compress into a highly flattened conformation with minimum dimension comparable to those observed in the mono- and bilayers obtained.

To further explore the feasibility for such highly flattened structures, a PAMAM G0.0 dendrimer was structurally optimized with flattened conformation of only 0.38 nm using Gaussian 09W (see Figure 3.5). While the flattened model may not correspond to the precise conformation of the dendrimer intercalates, the result does support the feasibility of such PAMAM conformations in the obtained nanocomposites. We calculate the flattened conformation energy of PAMAM G0.0 to be ~100-200 kcal/mol than the pseudospherical conformation. However, these are gas-phase calculations and do not account for the real synthetic conditions, where both solvation and clay surface interactions are important.

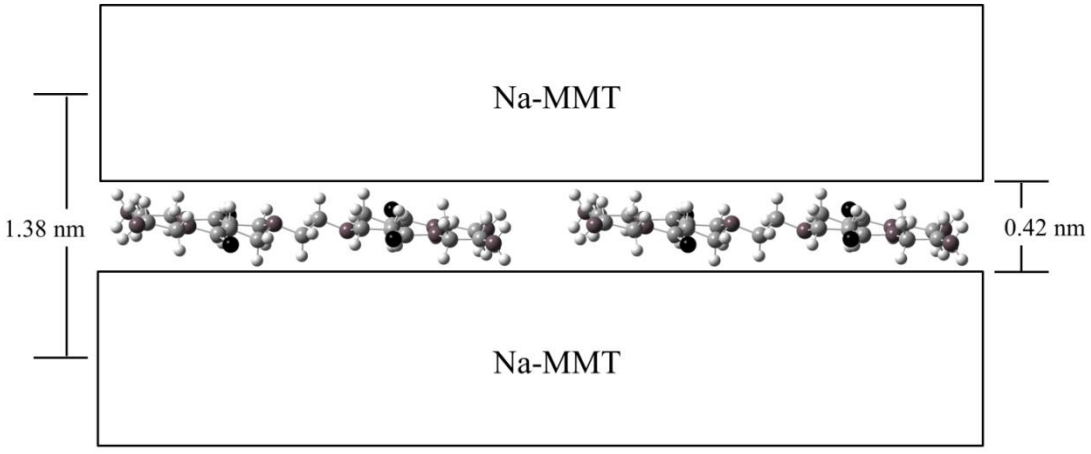

Figure 3.5 A structural model for the G0.0 monolayer nanocomposites. (H, white; O, black; C, light grey; N, dark grey).

Under acidic synthetic conditions (pH = 2-3), all the obtained nanocomposites show only intercalate monolayers. Figure 3.6 compares PXRD patterns obtained under acidic and basic conditions for the different PAMAM generations. As shown in Table 3.1, the interlayer expansion for acidic syntheses decreases slightly, by ~0.02 nm, while the crystallite domain size increases by ~10-15 nm. Under these acidic conditions, the terminal primary amines on PAMAM ($pK_a \approx 9\text{-}10$),[43-45] are protonated, and the cationic dendrimers must ion exchange with Na^+ ions in Na-MMT. The slightly smaller interlayer expansion suggests that the protonated PAMAM bonds strongly *via* electrostatic interaction with the anionic MMT sheets. A similar observation was reported by Alongi *et al.*[24] using protonated G4.0 PAMAM, where a smaller interlayer expansion occurs than for materials prepared at higher pH.

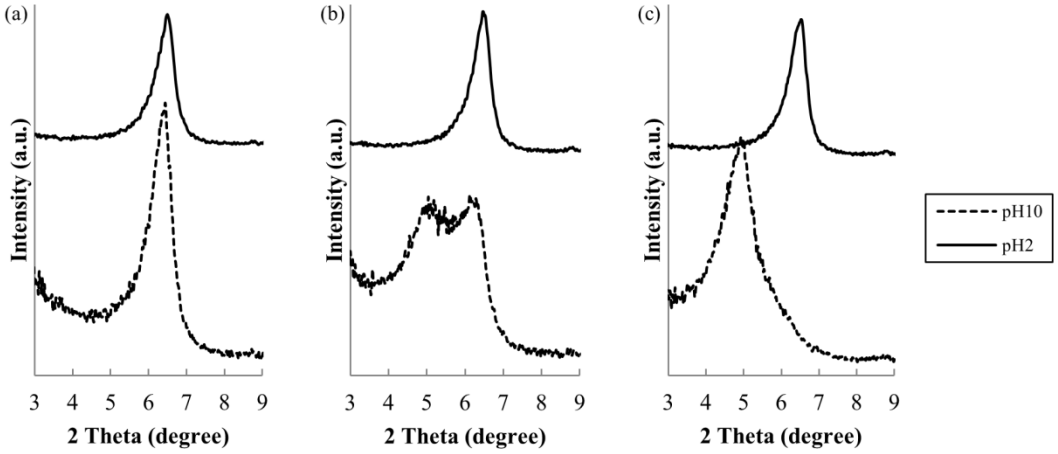

Figure 3.6 PXRD patterns of (a) G(0.0), (b) G(1.0), and (c) G(2.0)/Na-MMT nanocomposites synthesized in acidic (pH = 2-3) and basic (pH = 10-11) conditions. Reactant ratios for all the nanocomposites were 0.6 g/g PAMAM/Na-MMT.

The increase in crystallite size at lower pH can be attributed to the observed slower reaction rates. For example, under acidic conditions, a flocculate does not appear at ambient temperature with G2.0 PAMAM. At 50 °C, particles appear after reaction for 30 minutes, and at 80 °C they appear after 10 minutes. Elevated temperature also increases the nanocomposite yield, although the yield remains lower than that under basic conditions. The slower reaction kinetics may again be associated with an ion exchange process required for a positively charged dendrimer.

When reactions are performed where a protonated montmorillonite, K10 (H-MMT) is substituted for Na-MMT, no dendrimer intercalation is observed. This difference implicates Na^+ in the intercalation reaction, either *via* ion exchange or dendrimer complexation.

To study the effect of synthesis temperature, 0.3 g/g PAMAM/Na-MMT nanocomposites with all G0.0, G1.0, and G2.0 PAMAM were prepared at ambient temperature and at 60 °C. The obtained gallery dimensions (Table 3.1, Δd) and relative phase contents for mixed phases as indicated by PXRD reflection intensities (Figure B1, Appendix B) did not change significantly at higher temperature. However, the organic mass contents were lower at higher temperature (Table 3.1), which suggests that the higher rate of nanocomposite formation prevents efficient packing of the expanded galleries with PAMAM.

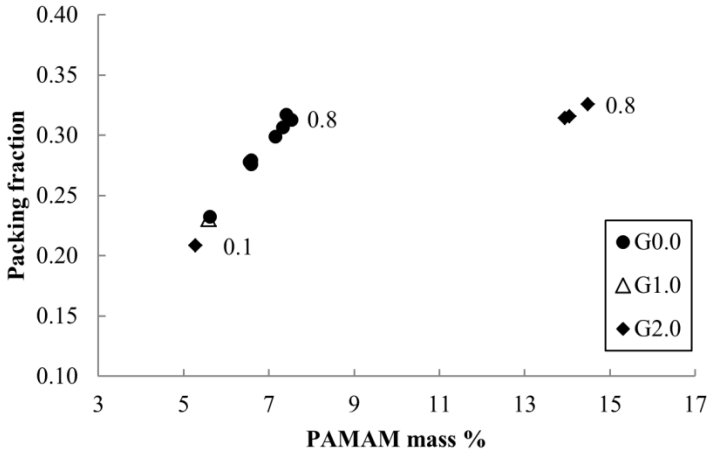

Figure 3.7 Packing fraction *vs* dendrimer mass % of nanocomposites synthesized at room temperature and pH 10-11. Labels show reactant ratios (g/g PAMAM/Na-MMT). Packing fractions were not calculated for mixed phases.

For G0.0 nanocomposites, an increase of PAMAM packing fraction was also observed at higher initial dendrimers ratios (Figure 3.7, left). G2.0 nanocomposites which formed with higher organic loading are more tightly clustered (Figure 3.7, right) indicating less effect of starting composition on product composition. It is very clear that there are two structures having similar packing fractions at full loading (0.31 for the monolayer, and 0.33 for the bilayer). H_2O may partially fill the available volume in the galleries; water content was not considered in the packing fraction calculation because the water contents are highly variable and depend in part on sample history. For comparison, packing fractions of ~0.67-0.68 can be deduced from reported data for PEO/Na-MMT mono- and bilayer intercalate structures[2] and of 0.93 for PEI/Na-MMT,[5] although a much lower value can be deduced from data reported for PVOH/Ca-MMT.[6] Linear polymers can yield packing fractions 2-3 times higher

than those observed for the PAMAM/Na-MMT nanocomposites. This difference may be due to inefficiencies in packing the flattened dendrimers but may also be an electrostatic effect related to the higher charge density of the dendrimers.

To help understand the mechanism of nanocomposite formation, capillary zone electrophoresis (CZE) was used to evaluate the nature of solvated PAMAM at pH conditions employed in these syntheses. Figure 3.8 shows electrograms of PAMAM at pH 2.7 and 10.9, with results summarized in Table 3.3. The positively charged PAMAM dendrimers migrate toward the cathode under a positive applied voltage. Migration times increase with increasing PAMAM generation, reflecting a decreased charge density for the higher generation dendrimers. Surface charge densities at pH 2.7 were estimated 0.10-0.19 C/m^2. Shi *et al.*[30] and Ebber *et al.*[46] also observed clear separation of PAMAM generations 2.0–5.0 at pH 2.5 and generations 1.0–5.0 at pH 2.7. Although these PAMAM generations have similar theoretical charge/mass ratios, Shi *et al.*[30] proposed a shielding model that retards migration for larger dendrimers.

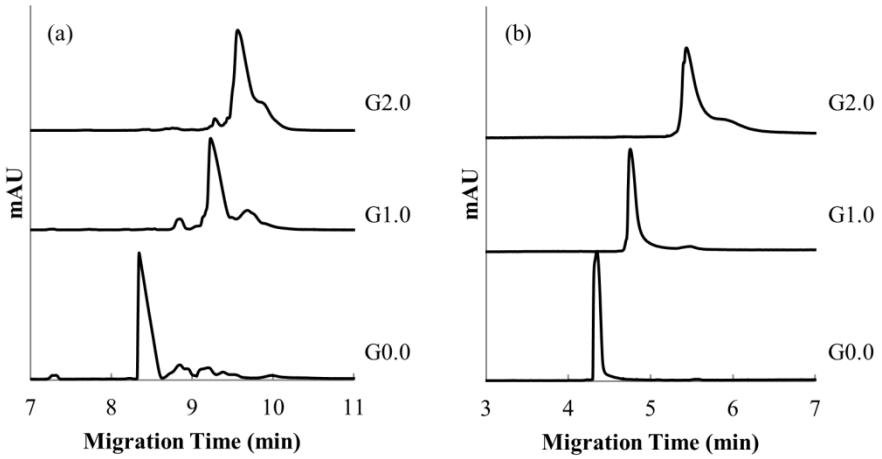

Figure 3.8 Capillary electrograms for different PAMAM generations at pH 2.7 (a) and 10.9 (b).

Table 3.3 Migration data from CZE and calculated charge data for PAMAM dendrimers.

	pH 2.7			pH 10.9		
	G(0.0)	G(1.0)	G(2.0)	G(0.0)	G(1.0)	G(2.0)
Hydrodynamic radius (nm)	0.75	1.10	1.45	0.75	1.10	1.45
Ionic strength (mol L^{-1})	0.16			0.16		
Average migration time (min)	8.41	9.22	9.66	4.36	4.67	5.45
Electrophoretic mobility (m^2/V.s)	3.87E-08	3.52E-08	3.37E-08	6.21E-08	5.80E-08	4.97E-08
Dimensionless mobility	2.82	2.57	2.46	4.46	4.17	3.57
Dimensionless zeta potential	3.45	2.94	2.72	10.41	8.80	5.97
Zeta potential (V)	0.089	0.076	0.070	0.269	0.227	0.154
Charge distribution function (I_0)	8.18	5.59	4.38	192.69	86.05	20.82
Surface charge density (C/m^2)	0.192	0.131	0.103	4.526	2.021	0.489

At pH 10.9, the PAMAM dendrimers (terminal primary amine $pK_a \approx 9\text{-}10$)[43-45] are not protonated. However, they may readily coordinate to Na^+ ions in the aqueous solution, forming positively charged complexes. The much faster migration shows that these complexes have higher charge densities than the protonated dendrimers, with calculated surface charges of 0.49-4.5 C/m^2. As in acidic solution, the dendrimers generations show differential shielding and can be separated by migration time.

The differential shielding effects observed for PAMAM generations involve CZE buffer anions, and this mechanism is not necessarily operative under reaction conditions. However, the much higher dendrimer surface charge densities observed in basic aqueous conditions correlates with the faster, higher-yield nanocomposite reactions observed above. On the other hand, more highly charged dendrimers should favor monolayer structures over bilayers, whereas the opposite case was observed. The explanation for this difference may be either that dendrimer complexation within clay galleries is not the same as in aqueous solution (due to the dramatic conformation change) or related to the reduced MMT surface charge under acidic conditions. The reported zeta potentials and surface charge densities *vs* pH indicate less negative zeta potential and surface charge density at lower pHs for Na-MMT,[47] bolstering the latter explanation.

Figure 3.9 and Table 3.4 compare the FTIR spectra and bond vibrations observed for Na-MMT, PAMAM G(0.0) and a 0.4 PAMAM G(0.0)/Na-MMT nanocomposite. Characteristic bands observed for pristine Na-MMT at 1120 cm^{-1} (Si-O bend), 1048 (Si–O stretch), and 920 (Al–OH stretch) were also present in the

nanocomposites without significant shifts, confirming that the aluminosilicate sheets do not change.[48,49] A sharp peak near 3600 cm^{-1} and a broad band at 3400 cm^{-1}, corresponding to O-H stretches, were each present in both Na-MMT and the nanocomposites. The former arises from intrasheet O-H[5,49] the latter from H_2O adsorbate or intercalate.[49] The latter band, along with the associated O-H bend at 1636 cm^{-1}, are reduced or absent after Na-MMT is heated at 80 °C for 24 h (Figure B2, Appendix B). Both O-H absorption intensities are significantly reduced in the nanocomposite, indicating that less water is present in the nanocomposite than in Na-MMT. The terminal amine groups of dehydrated PAMAM G0.0 produce strong N-H stretches at 3284 cm^{-1} (asymmetric) and 3068 (symmetric).[50,51] These absorption intensities increase for higher PAMAM generations, reflecting the larger number of terminal amine groups.[51] The nanocomposites present a band at 3290 cm^{-1} (Figure 3.9c). The G2.0/Na-MMT nanocomposite (Figure B3, Appendix B) shows this band at higher intensity. Characteristic PAMAM absorptions at 2930, 1645, and 1554 cm^{-1}, corresponding to a C-H stretch, amide I (primarily C=O) stretch, and amide II (a combination of N-H in-plane bend and C-N stretch), respectively, are also seen in both dehydrated PAMAM and the obtained nanocomposites.[50]

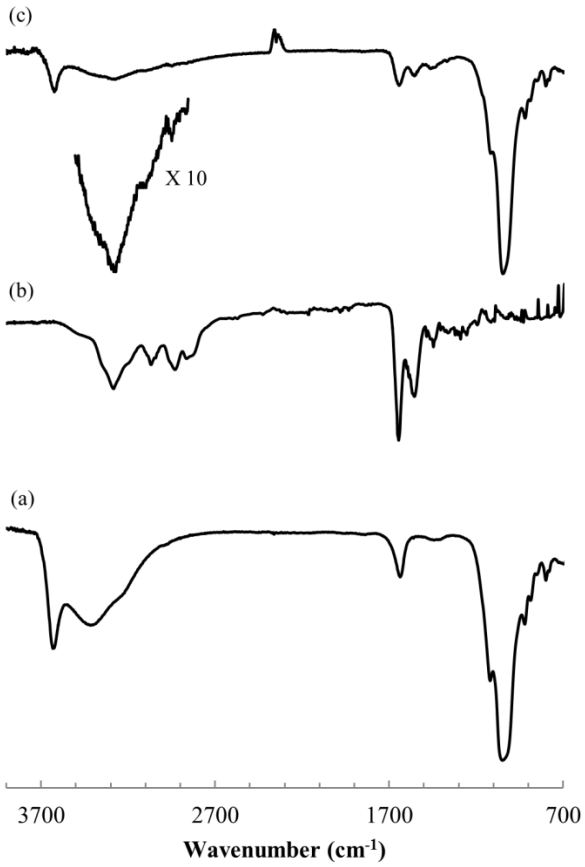

Figure 3.9 FTIR spectra of (a) NaMMT, (b) PAMAM G(0.0) and (c) 0.4 PAMAM G(0.0)/Na-MMT nanocomposite. The 2850-3500 cm^{-1} region of (c) is intensified x10 for clarity.

Table 3.4 Comparison of IR bond vibrations in reactants and nanocomposites.

Wavenumber (cm^{-1})	PAMAM	Na-MMT	Nanocomposites	Bond Vibration
3600		X	X	O-H str.
3300-3400 (b)		X	X	O-H str.
3300	X		X	N-H asymmetric str.
3000	X		X	N-H symmetric str.
2900	X		X	C-H str.
1640	X		X	Amide I (C=O str.)
1635		X		O-H bend.
1550	X		X	Amide II (N-H bend. + C-N str.)
1120		X	X	Si-O bend.
1045		X	X	Si-O str.
920		X	X	Al-OH str.

3.5 CONCLUSIONS

Lower generation (G0.0-2.0) PAMAM dendrimers form intercalated nanocomposites with Na-MMT. These are the first reports of the G0.0 and G1.0/Na-MMT nanocomposites and of a structurally ordered G2.0/Na-MMT. Compositional studies show clearly that the structures obtained depend on the generation of PAMAM and the starting organic composition. G0.0 always forms monolayer structures ($\Delta d = 0.42$ nm), while G2.0 also forms bilayer structures ($\Delta d = 0.84$ nm) at higher organic content, showing a marked monolayer to bilayer transition. G1.0 showed an intermediate behavior, with mixed-phase products obtained at the reactant ratios studied. This monolayer arrangement of PAMAM/clay nanocomposites is reported for the first time. Maximum organic contents of G0.0 monolayer and G2.0 bilayer nanocomposites were ~7% and ~14% respectively. Although gallery expansions were similar to those observed with linear polymer intercalates, packing fractions of 0.31-0.32 were 2-3 times lower. At acidic pH, the nanocomposites forming only monolayer structures are obtained, indicating a stronger electrostatic attraction between MMT and protonated PAMAM, and these nanocomposites formed more slowly and were more ordered. Na^+ ions play a significant role in nanocomposite formation. At high pH, PAMAMs show high mobility, zeta potential, and surface charge densities due to Na^+ complexation in solution. FTIR data indicates that both Na-MMT and PAMAM structural units are preserved in the nanocomposites obtained.

3.6 ASSOCIATED CONTENT

Supporting information available in the Appendix B. Comparison of PXRDs for room temperature and 60 ^{0}C syntheses, and FTIR spectra of dehydrated Na-MMT and 0.4G(2.0)/Na-MMT nanocomposite.

3.7 REFERENCES

1. M. Alexandre and P. Dubois, *Mater. Sci. Eng. R*, 2000, 28, 1-63.

2. J. H. Wu and M. M. Lerner, *Chem. Mater.*, 1993, 5, 835-838.

3. J. P. Lemmon, J. H. Wu, C. Oriakhi and M. M. Lerner, *Electrochim. Acta*, 1995, 40, 2245–2249.

4. A. U. Liyanage and M. M. Lerner, *RSC Adv.*, 2012, 2, 474-479.

5. C. O. Oriakhi, R. L. Nafshun and M. M. Lerner, *Mater. Res. Bull.*, 1996, 31, 1513-1520.

6. K. A. Carrado, P. Thiyagarajan and D. L. Elder, *Clays Clay Miner.*, 1996, 44, 506-514.

7. M. G. Kanatzidis, R. Bissessur, D. C. Degroot, J. L. Schindler and C. R. Kannewurf, *Chem. Mater.*, 1993, 5, 595–596.

8. C. O. Oriakhi, I. V. Farr and M. M. Lerner, *J. Mater. Chem.*, 1996, 6, 103-107.

9. E. P. Giannelis, *Adv. Mater.*, 1996, 8, 29-35.

10. P. B. Messersmith and E. P. Giannelis, *Chem. Mater.*, 1993, 5, 1064-1066.

11. N. Sukpirom, C. O. Oriakhi and M. M. Lerner, *Mater. Res. Bull.*, 2000, 35, 325-331.

12. J. C. Huang, Z. K. Zhu, J. Yin, X. F. Qian and Y. Y. Sun, *Polymer*, 2001, 42, 873-877.

13. S. S. Ray and M. Okamoto, *Prog. Polym. Sci.*, 2003, 28, 1539-1641.

14. J. L. Bonczek, W. G. Harris and P. Nkedi-Kizza, *Clays Clay Miner.*, 2002, 50, 11-17.

15. K. Ratanarat, M. Nithitanakul, D. C. Martin and R. Magaraphan, *Rev. Adv. Mater. Sci.*, 2003, 5, 187-192.

16. A. W. Bosman, H. M. Janssen and E. W. Meijer, *Chem. Rev.*, 1999, 99, 1665-1688.

17. D. A. Tomalia, A. M. Naylor and W. A. Goddard, *Angew. Chem. Int. Ed. Engl.*, 1990, 29, 138-175.

18. Y. Kim, A. M. Klutz and K. A. Jacobson, *Bioconjugate Chem.*, 2008, 19, 1660-1672.

19. M. X. Tang, C. T. Redemann and F. C. Szoka, *Bioconjugate Chem.*, 1996, 7, 703-714.

20. P. Singh, F. Moll, S. H. Lin, C. Ferzli, K. S. Yu, R. K. Koski, R. G. Saul and P. Cronin, *Clin. Chem.*, 1994, 40, 1845-1849.

21. M. Q. Zhao and R. M. Crooks, *Adv. Mater.*, 1999, 11, 217-220.

22. S. He and J. Lin, *Appl. Mech. Mater.*, 2012, 108, 91-94.

23. M. Rodlert, C. J. G. Plummer, L. Garamszegi, Y. Leterrier, H. J. M. Grunbauer and J. A. E. Manson, *Polymer*, 2004, 45, 949-960.

24. J. Alongi, O. Monticelli, S. Russo and G. Camino, *J. Nanostruct. Polym. Nanocompos.*, 2006, 2, 127-133.

25. T.-Y. Juang, Y.-C. Chen, C.-C. Tsai, S. A. Dai, T.-M. Wu and R.-J. Jeng, *Appl. Clay Sci.*, 2010, 48, 103-110.

26. F. Chen, H. Xiong, J. T. Yang, W. W. Cai and M. Q. Zhong, *e-Polym.*, 2012, No. 016.

27. M. H. A. Rehim, A. M. Youssef and H. A. Essawy, *Mater. Chem. Phys.*, 2010, 119, 546-552.

28. P. H. Wiersema, A. L. Loeb and J. T. Overbeek, *J. Colloid Interface Sci.*, 1966, 22, 78-99.

29. A. L. Loeb, J. T. G. Overbeek and P. H. Wiersema, *The Electrical Double Layer around a Spherical Colloid Particle;* MIT Press: Cambridge, MA, 1961.

30. X. Y. Shi, I. Banyai, W. G. Lesniak, M. T. Islam, I. Orszagh, P. Balogh, J. R. Baker and L. P. Balogh, *Electrophoresis*, 2005, 26, 2949-2959.

31. Y. H. Zhao, M. H. Abraham and A. M. Zissimos, *J. Org. Chem.*, 2003, 68, 7368-7373.

32. J. W. Anthony, R. A. Bideaux, K. W. Bladh and M. C. Nichols, *Handbook of Mineralogy;* Mineralogical Society of America: Chantilly, VA, 1990.

33. A. Amin, A. S. Taha and M. A. A. El-Ghaffar, *J. Appl. Polym. Sci.*, 2010, 118, 525-537.

34. W. Xie, Z. M. Gao, W. P. Pan, D. Hunter, A. Singh and R. Vaia, *Chem. Mater.*, 2001, 13, 2979-2990.

35. P. C. LeBaron, Z. Wang and T. J. Pinnavaia, *Appl. Clay Sci.*, 1999, 15, 11-29.

36. B. K. Nanjwade, H. M. Bechra, G. K. Derkar, F. V. Manvi and V. K. Nanjwade, *Eur. J. Pharm. Sci.*, 2009, 38, 185-196.

37. M. El-Sayed, M. F. Kiani, M. D. Naimark, A. H. Hikal and H. Ghandehari, *Pharm. Res.*, 2001, 18, 23-28.

38. Y. Y. Cheng, Z. H. Xu, M. L. Ma and T. W. Xu, *J. Pharm. Sci.*, 2008, 97, 123-143.

39. J. Li, L. T. Piehler, D. Qin, J. R. Baker, D. A. Tomalia and D. J. Meier, *Langmuir*, 2000, 16, 5613-5616.

40. T. A. Betley, M. M. B. Holl, B. G. Orr, D. R. Swanson, D. A. Tomalia and J. R. Baker, *Langmuir*, 2001, 17, 2768-2773.

41. A. Hierlemann, J. K. Campbell, L. A. Baker, R. M. Crooks and A. J. Ricco, *J. Am. Chem. Soc.*, 1998, 120, 5323-5324.

42. K. Takada, D. J. Diaz, H. D. Abruna, I. Cuadrado, C. Casado, B. Alonso, M. Moran and J. Losada, *J. Am. Chem. Soc.*, 1997, 119, 10763-10773.

43. M. Castagnola, C. Zuppi, D. V. Rossetti, F. Vincenzoni, A. Lupi, A. Vitali, E. Meucci and I. Messana, *Electrophoresis*, 2002, 23, 1769-1778.

44. H. M. Brothers, L. T. Piehler and D. A. Tomalia, *J. Chromatogr. A*, 1998, 814, 233-246.

45. D. Cakara, J. Kleimann and M. Borkovec, *Macromolecules*, 2003, 36, 4201-4207.

46. A. Ebber, M. Vaher, J. Peterson and M. Lopp, *J. Chromatogr. A*, 2002, 949, 351-358.

47. A. Delgado, F. Gonzalezcaballero and J. M. Bruque, *J. Colloid Interface Sci.*, 1986, 113, 203-211.

48. D. Lee, K. Char, S. W. Lee and Y. W. Park, *J. Mater. Chem.*, 2003, 13, 2942-2947.

49. O. M. Sadek and W. K. Mekhemer, *Thermochim. Acta*, 2001, 370, 57-63.

50. I. Grabchev, C. Petkov and V. Bojinov, *Dyes Pigm.*, 2004, 62, 229-234.

51. P. Punyacharoennon, S. Charuchinda and K. Srikulkit, *J. Appl. Polym. Sci.*, 2008, 110, 3336-3347.

CHAPTER 4

USE OF AMINE ELECTRIDE CHEMISTRY TO PREPARE MOLYBDENUM DISULFIDE INTERCALATION COMPOUNDS

Amila Udayanga Liyanage, and Michael M. Lerner

Department of Chemistry

Oregon State University

Corvallis, OR 97331-4003, USA

RSC Adv., 2014, 4, 47121-47128.

4.1 ABSTRACT

Electride solutions, formed by dissolution of Na(m) in ethylenediamine (en), are used to generate MoS_2 intercalation compounds. Two new intercalation compounds were obtained, labeled α and β phases, containing both Na and en as intercalate and cointercalate respectively. The intercalation reaction proceeds *via* formation of a kinetic product, the β phase, and subsequent generation of a stable thermodynamic product, the α phase. The β and α phases have interlayer distances, d_{IC}, of 1.19 and 0.97 nm, respectively, which are ascribed to a perpendicular or parallel orientation of en within the intercalate galleries. Product compositions, morphologies and spectrochemical features are obtained from thermogravimetry, SEM and Raman measurement. Electrochemical reduction of MoS_2 in an en-based electrolyte is investigated, but does not show the same intercalation reactions. The chemistry observed is compared with that previously reported for this and other MS_2 hosts, and with graphite intercalation.

4.2 INTRODUCTION

Many transition metal dichalcogenides (MX_2) are layered structures consisting of metal cations bound between hexagonal planes of chalcogenide anions.[1-3] The MX_2 layers can often be chemically[4-8] or electrochemically[9-11] reduced with concomitant intercalation of cationic guests, including the alkali metals,[4-6,8] alkaline earths,[7] or other molecular or complex cations.[1,10] The electrostatic attraction between the positive intercalates and the negative MX_2 layers stabilize these intercalation compounds.[1] In order to accommodate the cation guests, the MX_2 sheets separate, with the interlayer expansion, Δd, defined as:

$$\Delta d = d_{IC} - d_h \qquad (1)$$

where d_{IC} and d_h are the interlayer repeat distances observed for the intercalation compound and the MX_2 host, respectively (Figure 4.1). The many possible relative dispositions of chalcogenide planes leads to a rich variety of identified MX_2 structures and polytypes. The transition metal cations may have either trigonal prismatic or octahedral chalcogenide coordination. Some commonly observed arrangements are represented by 1T-TiS_2 with an $(AbC)_n$ stacking repeat, 2H-TaS_2 with an $(AbACbC)_n$ stacking repeat, and 2H-MoS_2 with an $(AbABcB)_n$ stacking repeat. 1T-TiS_2 has octahedral coordination, whereas 2H-TaS_2 and 2H-MoS_2 have trigonal prismatic coordination around transition metal cations.[1-3]

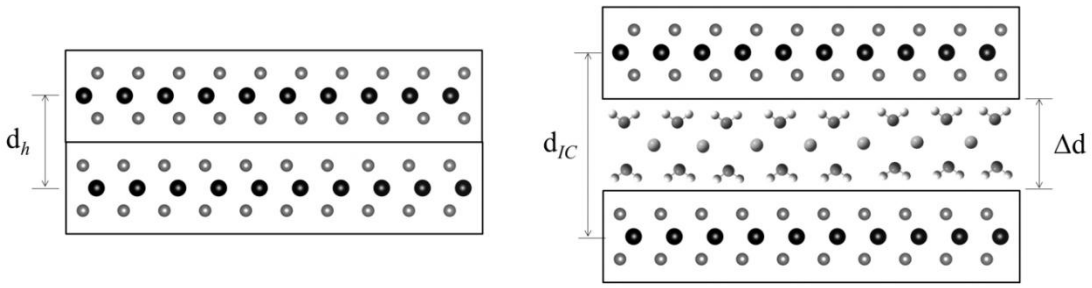

Figure 4.1 Schematic representations of MoS_2 and $Na_xMoS_2{\cdot}\delta H_2O$, where H_2O is a cointercalate.

MoS_2 is a rather chemically inert semiconductor, and is highly anisotropic, with an electrical resistivity 1000× greater in the direction perpendicular to the sheets. Important applications include use as a solid lubricant in both terrestrial and space environments (where graphite shows poor performance), as a catalyst in hydrodesulfurization and hydrogen evolution reactions, and as a photochemical catalyst in the oxidation of organics. MoS_2 holds promise for more efficient solar cells due to its resistance to photodegradation in water and photochemical activity over a wide frequency range.[3]

Intercalation by alkali metal cations and co-intercalates can change MoS_2 from a semiconductor to a metal.[3] For example, the band gap decreases and the electrical conductivity increases by formation of $Li_{0.1}MoS_2.\delta(PEO)$[12] and $Li_{0.1}MoS_2{\cdot}\delta$dialkylamine,[13] which both act as mixed electronic-ionic conductors. Intercalation chemistry may thereby enable tailored conductivities for specific materials applications. Some alkali metal or alkali earth metal intercalation

compounds with MoS_2 are superconducting, with transition temperatures typically ~7° K.[7,8]

Intercalation of promoter elements like Co or Ni has improved the catalytic activity of γ-Al_2O_3-supported MoS_2 in hydrodesulfurization.[3] Enhanced hydrogen evolution catalysis has been reported by use of metallic 1T-MoS_2 nanosheets obtained *via* chemical exfoliation of 2H-MoS_2 nanostructures grown directly on graphite.[14]

MoS_2 and its intercalation compounds may also be useful as electrodes in energy storage. Lemmon *et al.* have reported improved Li cycling stability and a significant increase in reversible capacity for the PEO/MoS_2 and PEO/MoS_2/graphene composites.[15,16] MoS_2, MoS_2/graphene composites and MoS_2 nanosheets have recently been explored for use in Na-ion batteries where cycling performance is highly correlated to the nanostructure.[17-19]

Several synthetic routes have been used to produce A_xMX_2 intercalation compounds where A is an alkali metal, including; (1) direct high temperature solid state synthesis by combining either the MX_2 host and an alkali metal or combining the A, M and X constituent elements,[1,2] (2) reaction of the MX_2 host with a reductant solution,[4-7] or (3) electrochemical reduction of the MX_2 host in a suitable electrolyte.[9,11] For some metal redox couples, such as Mo(IV)/Mo(III), the intercalation reaction requires powerful reductants such as an alkali metal dissolved in liquid ammonia.[4,5,8] This blue electride solution contains sodium ion complex cations and solvated electrons which are a powerful reductant:[20]

$$M(s) \xrightarrow{NH_3} [M(NH_3)_6]^+ (solv.) + e^- (solv.) \quad (2)$$

Other strong reductants that have been used to form A_xMX_2 include butyllithium or sodium naphthalide dissolved in suitable organic solvents.[1,6] For MX_2 hosts with more easily reduced metal cations, intercalation can be accomplished using ammonia,[2,21,22] amines[1,2,23-26] or aqueous solutions.[27]

In some cases, solvent (Sol.) cointercalation is observed (Figure 4.1), to generate compounds represented as $A_xMX_2 \cdot \delta Sol$. The driving force for such cointercalation is the retention of some solvation of the alkali metal intercalate.

Alkali metal intercalation of MS_2 was first reported in 1959.[4] Rüdorff has reported a wide range of A_xMX_2 intercalation compounds with the hosts including MoS_2, $MoSe_2$, WS_2, WSe_2, ReS_2, TiS_2, and $TiSe_2$.[4,5] Rouxel and coworkers have also extensively studied intercalation of the group 4 transition metal MX_2 compounds.[2] Whittingham *et al.* studied the lithium intercalation of MX_2s[6] and Schöllhorn *et al*. reported several different syntheses and exchange reactions for MX_2 intercalation compounds.[1,28]

Rüdorff reported formation of $Li_{0.8}MoS_2 \cdot 0.8NH_3$, $Na_{0.6}MoS_2$, $K_{0.6}MoS_2$ and $Cs_{0.5}MoS_2$ compounds with interlayer expansions (Δd, eqn (1)) of 0.335, 0.135, 0.195 and 0.274 nm, respectively.[5] Since the ionic radius of Li^+ is $\approx$ 0.076 nm,[29] the much larger expansion of $Li_{0.8}MoS_2 \cdot 0.8NH_3$ indicates the presence of NH_3 cointercalate. Schöllhorn and Weiss reported that these intercalation compounds can also absorb water to form hydrated cation complexes with an increase in Δd to 0.29–0.70 nm, depending on the reaction conditions.[28]

A series of alkali metal and alkaline earth intercalation compounds of MoS_2 were synthesized in NH_3(l), with the observed Δd values ranging from 0.14 to 0.37 nm.[7,8] The same method was utilized to synthesize intercalation compounds for TaS_2, with the resulting products Na_xTaS_2 and K_xTaS_2 giving Δd of 0.11 and 0.21 nm, respectively.[30]

Li_xTiS_2, Li_xMoS_2, and Li_xTaS_2 were obtained by reaction of the hosts with butyllithium in hexane, with Δd from 0.025–0.05 nm.[6]

Some organic and inorganic Lewis bases react to form intercalation compounds with groups 4 and 5 MX_2 hosts with Δd ranging from 0.30 nm (for smaller molecules like NH_3) to 5.23 nm (for octadecylamine), with compositions reflecting the uptake of 0.1 to 1.0 guests per MX_2 unit.[2] This interaction between the host and guest has been ascribed either to charge transfer[1] or to a redox reaction where the host is reduced and the cationic form of base, solvated by the neutral base, intercalate (i.e. NH_4^+ and NH_3 respectively). Group 6 chalcogenides hosts do not react to form intercalation compounds with organic bases in this manner.[1,2]

Some MX_2 hosts react in strong aqueous base to intercalate hydrated alkali metal cations, e.g. $Na_{0.3}TaS_2{\cdot}\delta H_2O$.[2,27] These complex intercalates undergo facile displacement by subsequent reaction with aqueous salt solutions.[28] Alternately, the water cointercalate can be displaced by reaction in polar inorganic or organic solvents.[28] The product compositions, including both the contents of intercalate cations and of cointercalates, depend on the degree of reduction, exposure to exchange solutions, and post-reaction processing.

Ethylenediamine (en) and trimethylenediamine (tn) react directly with TiS_2, NbS_2, and TaS_2 to form intercalation compounds with $\Delta d = 0.34–0.41$ nm. From the known intercalate dimensions, these gallery dimensions indicate that the amine intercalates must form monolayers with long molecular axes oriented parallel to the host layers.[24-26] These products show a range of compositions depending on the host and sample processing conditions, with intercalate to MX_2 ratios of 0.17–0.39 for en and 0.15–0.33 for tn. Secondary amines, such as diethylamine, dibutylamine, and dipentylamine react with exfoliated MoS_2, generating $Li_{0.1}MoS_2 \cdot \delta$dialkylamine, where δ = 0.11-0.42 and Δd = 0.374–0.445 nm, depending on the dialkylamine cointercalate.[13]

Our group has previously explored the use of electride solutions to prepare graphite intercalation compounds containing amines or diamine intercalates.[31-34] Stage 1 and 2 graphite intercalation compounds (GICs) were reported for syntheses using Li(m) or Na(m) dissolved in liquid en. When the intercalate is the $Li(en)^+$ complex, the intercalate guests show an orientation transition of perpendicular to parallel upon evacuation. With $Na(en)^+$, the complexes show only a parallel orientation.[33]

Since the reduction of graphite generally occurs at a lower potential than that for MoS_2, it is worthwhile to explore electride reactions for the intercalation of dichalcogenide hosts, especially since alkali metal-amine electride systems (other than with ammonia) have not previously been reported. In this work, we describe the first use of electride solutions to form MoS_2 intercalation compounds with amines, along with the product structures and compositions obtained. A novel intermediate

phase is found, and we propose a mechanism for the reaction. The results obtained are also analyzed in light of recent reports on electrochemical reduction of MoS_2.

4.3 EXPERIMENTAL

4.3.1 REAGENTS

Sodium metal (3-12 mm pieces in oil, 99.95%, Alfa Aeser), ethylenediamine (en) (99%, Alfa Aeser), molybdenum disulfide (MoS_2) (powder <2 micron, 99%, Aldrich), poly(ethylene-*co*-propylene-*co*-5-methylene-2-norbornene) (EPDM) (Aldrich), acetylene black (99.5+%, Alfa Aeser), cyclohexane (ACS grade, Alfa Aeser), sodium hexafluorophosphate ($NaPF_6$) (98%, Aldrich) and acetonitrile (HPLC grade, Fisher Scientific) were used as received.

4.3.2 CHEMICAL SYNTHESES

Synthesis and handling of the air-sensitive reagents were performed under an inert atmosphere (N_2) using either a drybox or septum-syringe techniques. In a typical reaction, Na metal (50 mg) was stirred overnight in ethylenediamine (3.0 mL) at 60 °C under an inert (N_2) atmosphere to form a blue-colored electride solution. MoS_2 (100 mg) was then added to the electride solution, and the reaction vigorously stirring at 60 °C for 48 h. Samples were centrifuged for 10 minutes and the solution phase was extracted by syringe. The solid products were placed under vacuum for 12 h at 60 °C.

As specified below, the above reaction conditions (time, temperature, reagent amounts and chemical addition sequence) were varied for some experiments.

Products obtained are labeled with reaction temperature and time. For example, the sample obtained by reaction at 60 °C for 24 h has been labeled “S-60C-24h”.

4.3.3 ELECTROCHEMICAL SYNTHESES

Galvanostatic reduction was performed in a 2-compartment cell with a fritted glass separator maintained under an inert (N_2) atmosphere at ambient temperature. Working electrodes were prepared by painting SS mesh (geometric area ~1 cm^2) with a cyclohexane slurry containing MoS_2 powder (80 mass pct.), acetylene black (15 mass pct.), and EPDM binder (5 mass pct.). The dried electrode mass was 18-20 mg. Counter and reference electrodes were SS mesh and SS wire. The electrolyte solution was 0.1 M $NaPF_6$ in ethylenediamine. Working electrodes were reduced at a constant current of 0.10 mA for 16–48 h, then immediately removed from the cell, rinsed briefly with 3–4 mL of acetonitrile, and dried overnight under vacuum at ambient temperature.

4.3.4 ANALYSES

Powder X-ray diffraction (XRD) data from 3–20° 2θ were collected on a Rigaku MiniFlex II diffractometer, using Ni-filtered Cu Kα radiation, at a scan rate of 3° min^{-1} and step size of 0.02°. Diffraction peak areas were obtained using MDI JADE 9.0 XRD analysis software. Thermogravimetric (TGA) analyses were performed using a Shimadzu TGA-50 analyzer under flowing Ar gas (20 mL min^{-1}) from ambient to 400 °C at a heating rate of 10 °C min^{-1} and under air from ambient to 900 °C at a heating rate of 10 °C min^{-1}. Scanning electron micrographs (SEM) were obtained using an FEI Quanta 600F scanning electron microscope equipped with a field emission gun and operated at 10 kV. Raman spectra were obtained from 60–

4000 cm^{-1} using a Witec Alpha 300 confocal Raman microscope with 514 nm laser source.

The van der Waals volume of en, V_{en} = 0.0651 nm^3 was calculated based on Bondi radii using a method termed "Atomic and Bond Contributions of van der Waals volume" (VABC).[35] Volume of Na^+, V_{Na} = 0.00445 nm^3 was calculated using the ionic radius of Na^+ (0.102 nm).[29] Packing fractions for MoS_2 intercalation compounds were calculated[36,37] as:

$$Packing\ fraction = 2\ (nV_{Na} + mV_{en})\ /\ \sqrt{3}a^2\Delta d \qquad (3)$$

where *n* and *m* are the molar ratios of Na : MoS_2 and en : MoS_2 respectively, and a = 0.3160 nm[1,2].

Energy optimization of the gas-phase en molecule was performed using the DFT B3LYP method with a 6-31G+(d,p) basis set and Gaussian 09W software.

4.4 RESULTS AND DISCUSSION

The powder XRD patterns obtained from reactions of MoS_2 with a sodium electride solution (Figures 4.2, and 4.3) shows host expansion to form new intercalation compounds. In Figure 4.2 (S-60C-48h), a single new phase is evident with interlayer distance, d_{IC} = 0.97 nm. The expansion relative to the host MoS_2 sheet thickness (d_{002} = 0.615 nm)[3] is Δd = 0.35 nm. Hereafter this new phase is labeled the α phase.

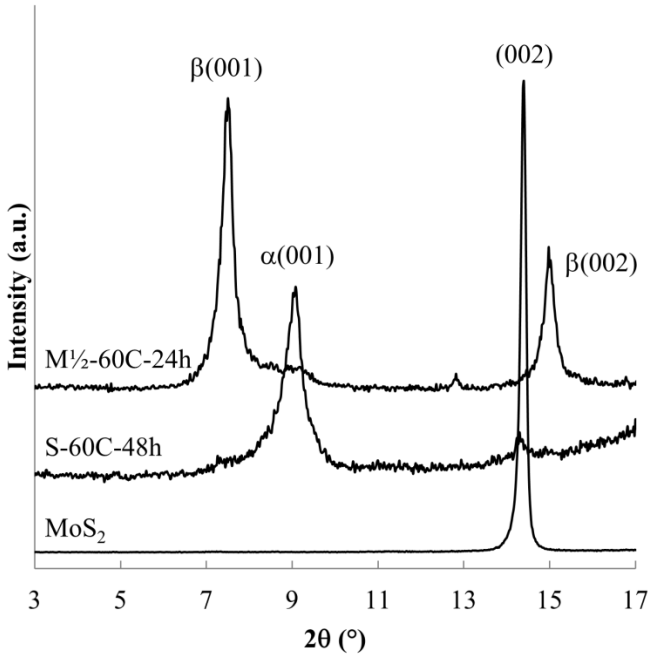

Figure 4.2 Powder XRD of MoS_2 and the intercalation compounds obtained after 48 h reaction at 60 °C (S-60C-48h) and after 24 h reaction at 60 °C using decreased Na mass (M½-60C-24h).

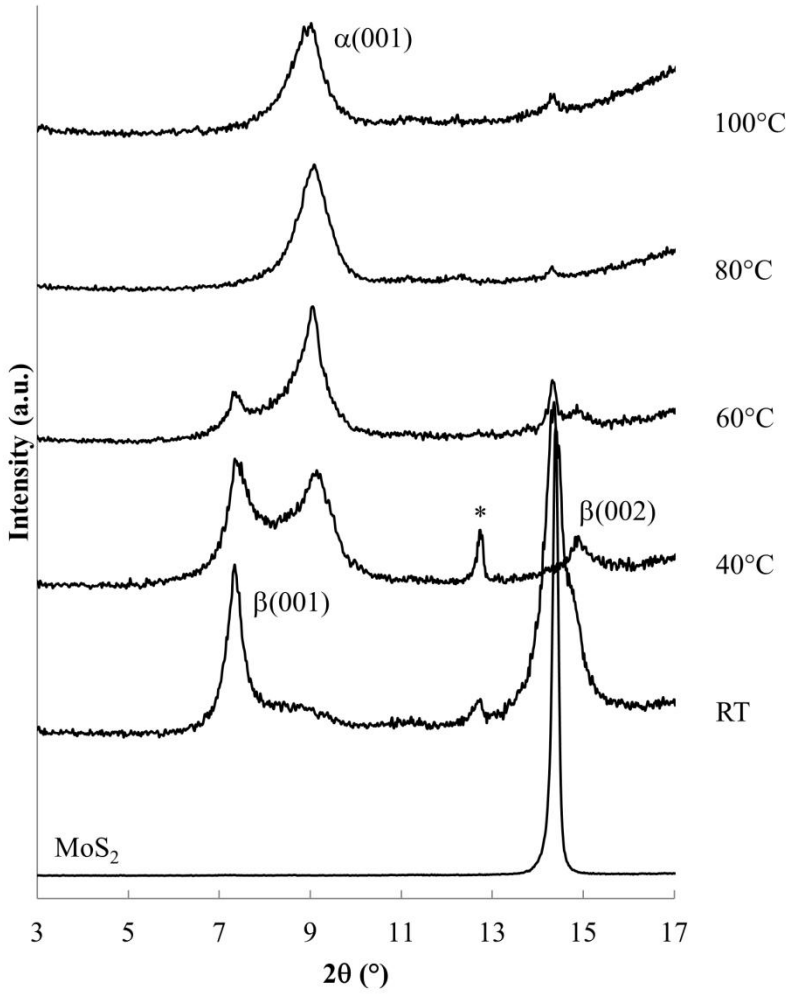

Figure 4.3 Powder XRD of MoS_2 and the intercalation compounds obtained after 24 h at reaction temperatures ambient to 100 °C.

Figure 4.3 shows XRD patterns obtained after 24 h reaction at ambient to 100 °C. Ambient temperature reaction produces a different new phase (with d = 1.19 nm, Δd = 0.57 nm), labelled the β phase, along with the unreacted host. Reaction products at 40 and 60 °C contain both the α and β phases along with unreacted MoS_2.

Higher temperature reactions, at 80 °C and 100 °C, produce mainly the α phase, with a very small residual of unreacted MoS_2.

Lower temperature reactions show an additional diffraction peak (tagged with an *) near d = 0.69 nm, attributed to Na_xMoS_2, i.e. the intercalation product without the en cointercalate. This phase has previously been reported, with d = 0.75 nm (ref. 28) or d=0.71 nm.[38] The small interlayer expansion observed for this phase ($\Delta d \approx 0.1$ nm) eliminates the possibility of en contained in that product.

Summarizing the changes observed with varied reaction temperature, (i) lower temperature reactions result in a relatively large amount of unreacted host (an incomplete reaction), and are relatively rich in the β phase, and (ii) higher temperatures generate nearly complete reactions to form mainly the α phase.

The incomplete reactions observed at lower temperature could arise from the slow kinetics of amine electride (reactant) formation, resulting in a low reductant concentration, or alternately they may be related to a slower rate of diffusion of the $Na(en)_x^+$ complex intercalate into the intercalation compound galleries.

In other experiments aimed at decreasing the electride reactant concentration, reactions for 48 h reaction at 60 °C were run using ½ the mass of Na or 5× the standard volume of en. Both changes results in products containing both the α and β phases and unreacted MoS_2. The association of β phase and incomplete reactions again provides some evidence that the β phase is a kinetic product. In one experiment using the decreased Na mass, the product obtained after 24 h reaction at 60 °C contained only the β phase (Figure 4.2. M½-60C-24h).

Products obtained at 60 °C with varied reaction times are shown in Figure 4.4. Shorter reaction times produce the β phase along with unreacted MoS_2; the α phase is first evident after reaction for 1 h. At longer reaction times, the β phase and MoS_2 are no longer observed. These data confirm that the β phase is formed more rapidly as a kinetic product, but ultimately disappears as the more stable α phase forms.

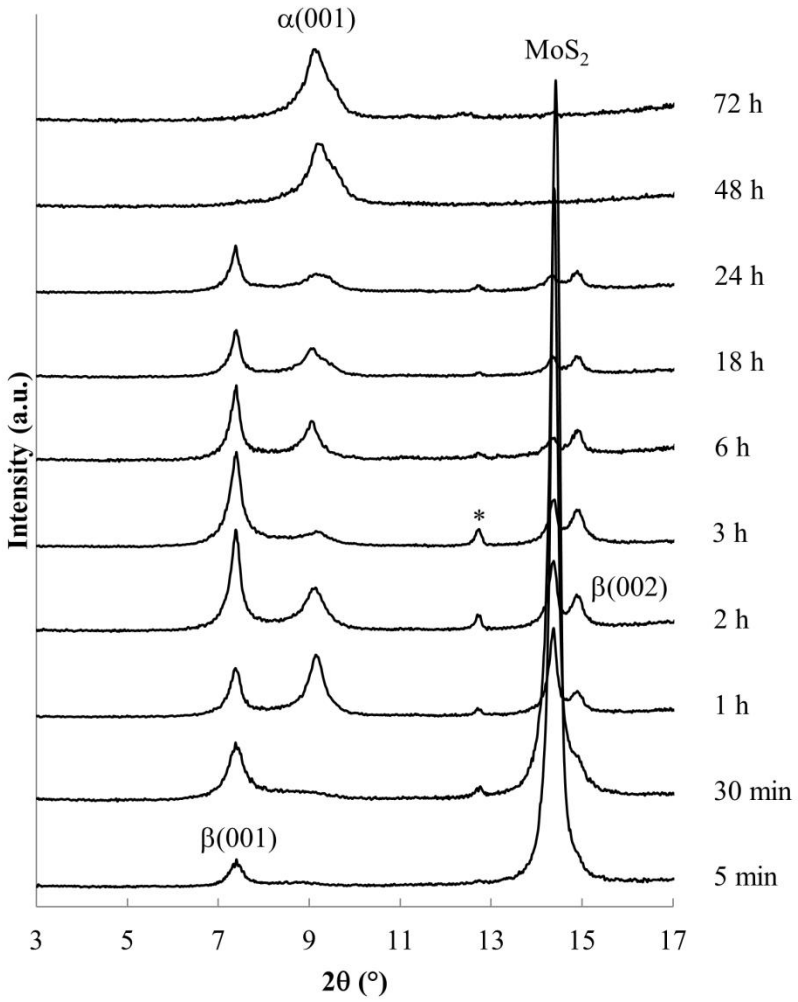

Figure 4.4 Powder XRD data obtained for reaction of MoS_2 with Na/en electride solution at 60 °C. Reaction times are indicated at the right.

Relative PXRD peak areas (A/A_t) were obtained by dividing the raw area of individual peak (A) by the total area of all observed peaks ($A_t = \Sigma A$), to normalize relative peak areas and more closely represent the volume fraction of the associated phases. Analysis of relative PXRD peak areas (A/A_t), shown in Figure 4.5, shows clearly the intermittent appearance of the β phase during the 60 °C reaction.

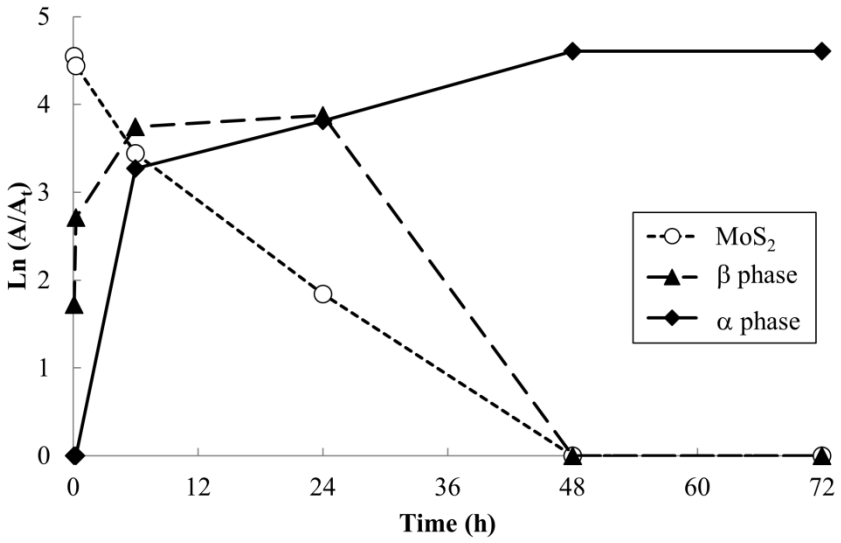

Figure 4.5 Ln(A/A_t) *vs*. reaction time at 60 °C.

Although lower electride concentrations, lower reaction temperatures and shorter reaction times are seen to favor formation of the β phase, this phase was difficult to obtain as a single-phase product. This indicates that the rates of conversion of MoS_2 to β phase, and β to α phase, i.e. rates k_1 and k_2 in Figure 4.6, were comparable under the range of reaction conditions studied.

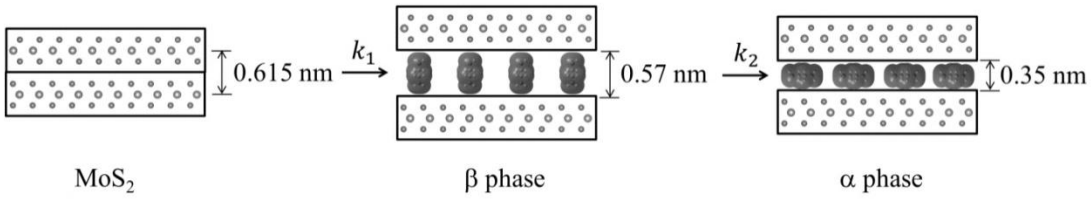

Figure 4.6 Proposed reaction mechanism; MoS_2 forms a metastable β phase, which converts to the more stable α phase.

We propose that the β phase appears due to the more rapid diffusion of the $Na(en)_x^+$ complex with a perpendicular orientation within intercalate galleries. Thermodynamic stabilities of these products depend on several factors, such as electrostatic and solvation enthalpies. Smaller galleries, as observed for the α phase, should generally have a more favorable lattice enthalpy, since $E \propto -1/d$.

The α and β phases obtained are both ascribed to the cointercalation of en with Na^+ to form an intercalate monolayer. The α phase expansion (Δd = 0.35 nm) corresponds to an en orientation with long axis parallel to host sheets, and the β phase expansion (Δd = 0.57 nm) to a perpendicular en orientation. Optimized molecular dimensions obtained by Gaussian (Figure 4.7) correlate well with the observed gallery dimensions. Amine intercalates have been previously reported with Δd = 0.37–0.40 nm for MS_2 hosts[13,26] but we are not aware of any reports on the observed β phase for any MX_2 intercalation products. Graphite intercalation compounds (GICs) containing en show both types of expansion, with the perpendicular orientation of Δd = ~0.5 nm for $LiC_x \cdot \delta en$ and a reported transition to parallel orientation observed upon

evacuation of the product.[33] That work also reported the formation of a GIC with composition NaC_{15}·1.0en with Δd = 0.36 nm, indicating a parallel en orientation.[33]

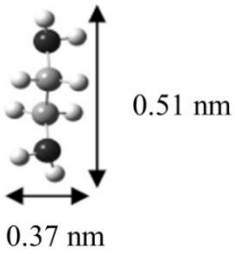

Figure 4.7 Gaussian-optimized molecular dimensions of ethylenediamine.

An alternate explanation for the appearance of α and β phases could be the formation of en monolayers and bilayers, respectively, as occurs in the hydration of A_xMS_2.[39] However, thermogravimetric data (*vide infra*) show that the obtained phases have similar en content, which does not support this model. Additionally, the observed d_{IC} for the α phase is 1.19 nm, which is significantly less than the 1.32 nm calculated to accommodate two en layers.

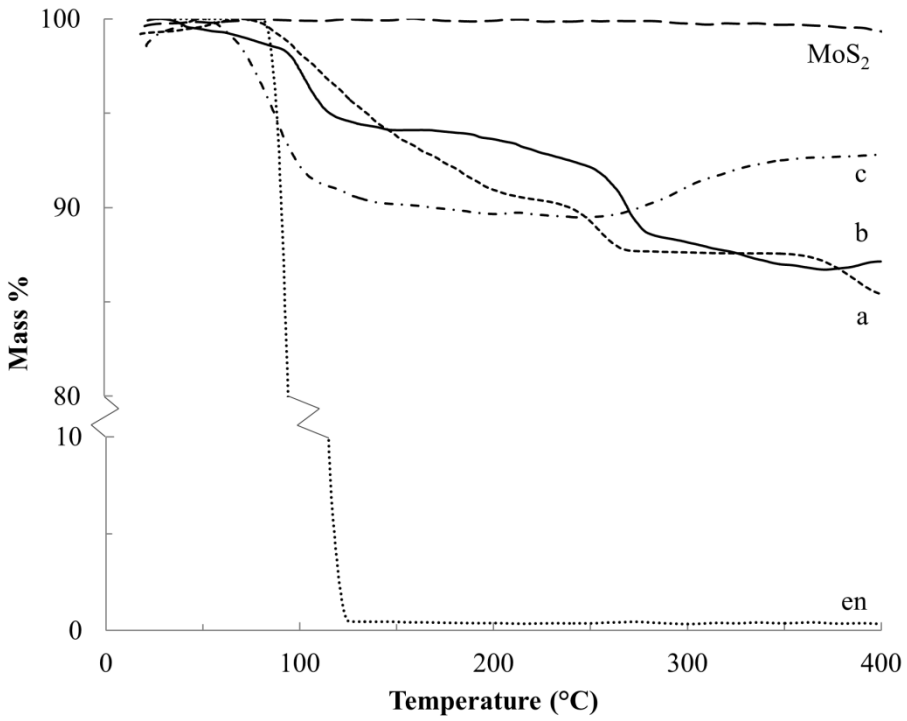

Figure 4.8 Thermograms of MoS_2, en, (a) the α phase Na-en-MoS_2 intercalation compound (S-60C-48h) and (b) a β phase predominant product (S-60C-3h) under Ar flow, and (c) β phase predominant product (S-60C-3h) analyzed under air flow.

Thermograms for the Na-en-MoS_2 intercalation compounds under Ar flow (Figure 4.8a, and b) show two mass loss events at 100–200 °C and 225–275 °C, which are attributed to volatilization (b.p. of en = 116 °C) and decomposition of the en cointercalate. Under air flow, a mass increase above 275 °C can be attributed to the formation of Na_2O (Figure 4.8c). From the mass loss and uptake, the composition for S-60C-48h (α-phase) and S-60C-3h (β-phase predominant) are found to be $Na_{0.3}MoS_2 \cdot 0.4en$ and $Na_{0.2}MoS_2 \cdot 0.3en$, respectively. Other studies of MS_2 (M = Ti, Ta and Nb) also give maximum en : MS_2 ratios in the 0.3-0.4 range.[24-26]

Where all graphene sheets are separated by intercalate galleries (i.e. in the stage 1 products), GIC have an en mass of 20–22%.[33] In comparison, the structurally-analogous MoS_2 intercalation compounds show en contents of ~12%. Calculated packing fractions (Table 4.1) correcting for the different host sheet surface areas and formula masses, indicate much denser intercalate packing for both α and β phases in MoS_2 than for the corresponding orientations in GICs. In part, this reflects a higher en : Na ratios in MoS_2 intercalation compounds (1.3-1.5 in MoS_2 compounds *vs.* 0.6-1.0 in stage 1 GICs[33]). Also, the packing fraction of β phases is lower due to the greater gallery expansion.

Table 4.1 Compositional data for en containing intercalation compounds

Composition	Stage	Phase	Packing fraction	Reference
LiC_{15}·0.8en	1	α	0.40	33
LiC_{26}·0.7en	2	β	0.28	
NaC_{15}·1.0en	1	α	0.51	
NaC_{25}·0.6en	2	α	0.40	
$Na_{0.3}MoS_2$·0.4en	1	α	0.88	This work
$Na_{0.2}MoS_2$·0.3en	1	β	0.43	

Less dense packing in the β-phase may facilitate $Na(en)_x^+$ complex diffusion, allowing more rapid formation of this phase. It may also be that the very high packing density in the α-phase MoS_2 compound prohibits reduction to the extent observed where no en cointercalate is present (such as in $Na_{0.6}MoS_2$).[4,5]

The calculated sheet charge densities for NaC_{15}·1.0en, $Na_{0.3}MoS_2$·0.4en and $Na_{0.2}MoS_2$·0.3en are 2.5, 3.5, and 2.3 e^- per nm^2, respectively. Again, we can propose that lower charge densities may allow for more rapid diffusion, but result in a less thermodynamically stable product.

SEM images (Figure 4.9) show that a layered microstructure is retained in all samples, with the reaction products displaying a somewhat delaminated appearance as compared to the starting MoS_2.

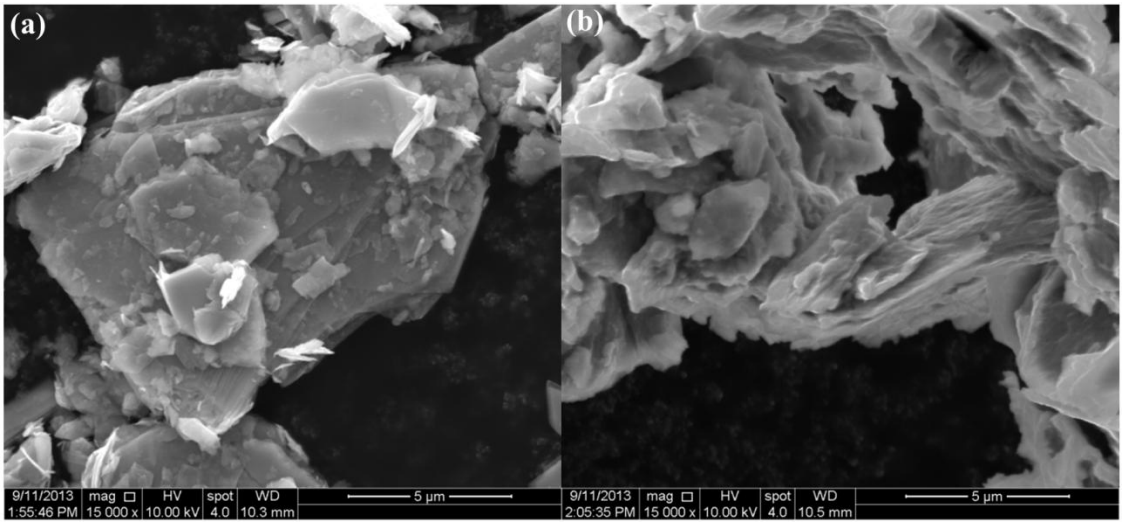

Figure 4.9 SEM images of (a) MoS_2 and (b) α phase intercalation compound $Na_{0.3}MoS_2$·0.4en

Raman spectra of MoS_2 and a representative Na-en-MoS_2 intercalation compound are shown in Figure 4.10. MoS_2 displays prominent sharp absorbance peaks at 390 cm^{-1} ($E_{2g}{}^1$ mode) and 418 cm^{-1} (A_{2g} mode) as has been reported previously.[40,41] After intercalation, the spectrum background increases significantly,

the two sharp peaks broaden and shift slightly to lower frequency, and two new strong broad peaks appear at ≈ 1350 and ≈ 1600 cm^{-1}. Very similar changes were previously observed following Li intercalation into MoS_2, with the new high frequency peaks ascribed to a disordered state arising from intercalate arrangement.[41] In the present case, en has molecular absorbances in this region, however, these should be relatively sharp and the other strong en absorbances expected at 3300 ($\upsilon(NH_2)$), 2900 ($\upsilon(CH_2)$) and 2850 ($\upsilon(CH_2)$) cm^{-1} were not detected.[42] Therefore the high frequency broad bands present in the intercalation compound samples more likely arise from a transition associated with disorder within the intercalate galleries.

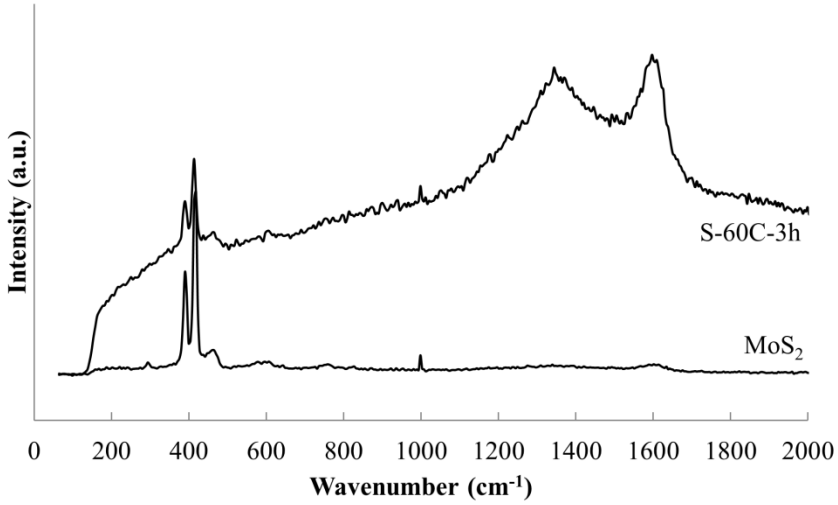

Figure 4.10 Raman spectra of MoS_2 and Na-en-MoS_2 intercalation compound (S-60C-3h) indicates the structural change upon intercalation.

In contrast to the chemical syntheses, galvanostatic reduction of MoS_2 in en/$NaPF_6$ did not generate predominant intercalation products. A very weak XRD

peak associated with the α phase is observed, but the principal change is a weakening and broadening of the MoS_2 host diffraction peaks (Figures 4.11 and 4.12).

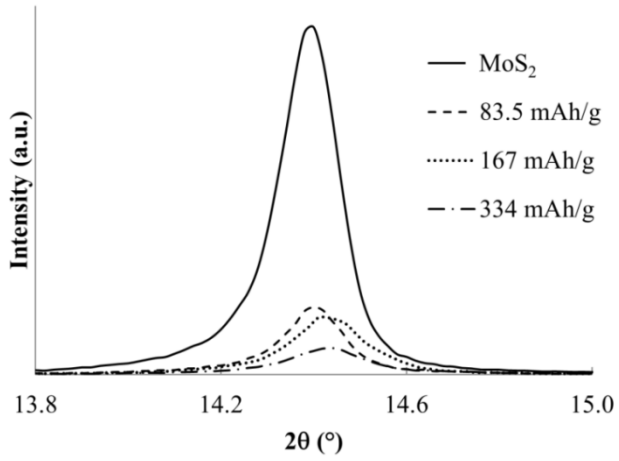

Figure 4.11 Powder XRD profiles for MoS_2 and products of electrochemical reduction in en/$NaPF_6$ with applied charges indicated.

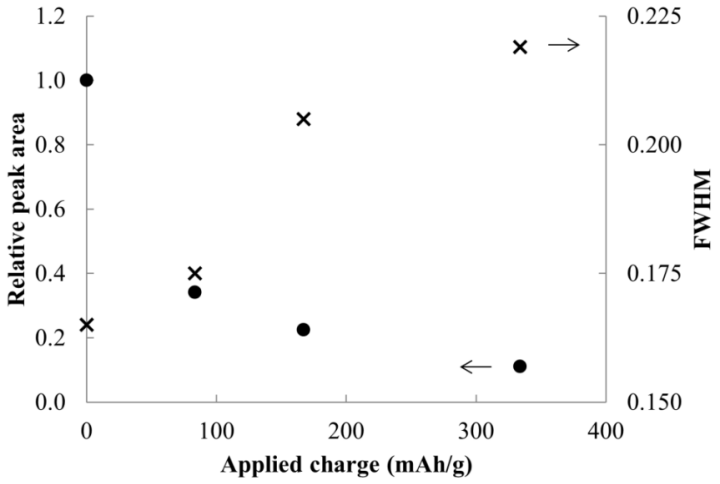

Figure 4.12 Relative peak areas and widths for MoS_2 and reduction products at different applied charges.

Lemmon *et al*. reported that reduction of MoS_2 in a 7 : 3 vv ethylene methyl carbonate : ethylene carbonate electrolyte with $LiPF_6$ resulted in formation of Li_2S and an amorphous form of Mo or Li_xMo.[15,16] The analogous reduction for Na reaction is in eqn (4):

$$MoS_2 + (4+x)Na^+ + (4+x)e^- \rightarrow 2\,Na_2S + Na_xMo \qquad (4)$$

Theoretically the capacity required for the above reduction is ≈ 840 mA h g^{-1} (if x = 1); each $1e^-$ reduction translates to 167 mA h g^{-1}. After applying from half to twice the latter charge, almost no intercalation products were evident. As can be seen, the ordered layered structure is destroyed even at much lower applied charges, suggesting an entirely different and non-intercalative mechanism for this electrochemical reduction.

4.5 CONCLUSIONS

MoS_2 reacts with electride solutions with amine to form intercalation compounds of composition $Na_{0.2\text{-}0.3}MoS_2 \cdot 0.3\text{-}0.4$en. A metastable product, identified as the β phase, shows a perpendicular en orientation with interlayer expansion of 0.57 nm, and the thermodynamic product, or α phase, shows a parallel orientation and interlayer expansion of 0.35 nm. Shorter reaction time, dilution and lower temperatures favor formation of the β phase. The intercalation products are not obtained by electrochemical reduction in en/$NaPF_6$.

4.6 ACKNOWLEDGEMENTS

We thank Professor Chih-Hung Chang and Changqing Pan (OSU Chemical Engineering) for assistance with Raman measurements. A.U.L. thanks the Whiteley Fellowship in Material Sciences for financial support.

4.7 REFERENCES

1. *Intercalation Chemistry*, ed. M. S. Whittingham and A. J. Jacobson, Academic Press, New York, NY, 1982.

2. *Intercalated layered materials*, ed., F. A. Lévy, D. Reidel Publishing, Dordrecht, Holland, 1979.

3. E. Benavente, M. A. Santa Ana, F. Mendizabal and G. Gonzalez, *Coord. Chem. Rev.*, 2002, 224, 87.

4. W. Rüdorff and H. H. Sick, *Angew. Chem.*, 1959, 71, 127.

5. W. Rüdorff, *Chimia*, 1965, 19, 489.

6. M. S. Whittingham and F. R. Gamble, *Mater. Res. Bull.*, 1975, 10, 363.

7. R. B. Somoano, V. Hadek, A. Rembaum, S. Samson and J. A. Woollam, *J. Chem. Phys.*, 1975, 62, 1068.

8. R. B. Somoano, V. Hadek and A. Rembaum, *J. Chem. Phys.*, 1973, 58, 697.

9. M. A. Santa Ana, V. Sanchez and G. Gonzalez, *Electrochim. Acta*, 1995, 40, 1773.

10. A. A. Stepanov, N. D. Lenenko, A. S. Golub and V. S. Pervov, *Russ. J. Electrochem.*, 2013, 49, 86.

11. M. S. Whittingham, *J. Electroanal. Chem.*, 1981, 118, 229.

12. G. Gonzalez, M. A. Santa Ana and E. Benavente, *Electrochim. Acta*, 1998, 43, 1327.

13. V. Sanchez, E. Benavente, M. A. Santa Ana and G. Gonzalez, *Chem. Mater.*, 1999, 11, 2296.

14. M. A. Lukowski, A. S. Daniel, F. Meng, A. Forticaux, L. S. Li and S. Jin, *J. Am. Chem. Soc.*, 2013, 135, 10274.

15. J. Xiao, D. W. Choi, L. Cosimbescu, P. Koech, J. Liu and J. P. Lemmon, *Chem. Mater.*, 2010, 22, 4522.

16. J. Xiao, X. J. Wang, X. Q. Yang, S. D. Xun, G. Liu, P. K. Koech, J. Liu and J. P. Lemmon, *Adv. Funct. Mater.*, 2011, 21, 2840.

17. L. David, R. Bhandavat and G. Singh, *ACS Nano*, 2014, 8, 1759.

18. G. S. Bang, K. W. Nam, J. Y. Kim, J. Shin, J. W. Choi and S.-Y. Choi, *ACS Appl. Mater. Interfaces*, 2014, 6, 7084.

19. J. Park, J.-S. Kim, J.-W. Park, T.-H. Nam, K.-W. Kim, J.-H. Ahn, G. Wang and H.-J. Ahn, *Electrochim. Acta*, 2013, 92, 427.

20. J. L. Dye, *Science*, 2003, 301, 607.

21. E. Wein, W. Mullerwarmuth and R. Schöllhorn, *Solid State Ionics*, 1987, 22, 231.

22. L. Bernard, M. McKelvy, W. Glaunsinger and P. Colombet, *Solid State Ionics*, 1985, 15, 301.

23. L. A. Brown, W. S. Glaunsinger and M. J. McKelvy, *J. Solid State Chem.*, 2000, 155, 326.

24. H. Ogata, H. Fujimori, S. Miyajima, K. Kobashi, T. Chiba, R. E. Taylor and K. Endo, *J. Phys. Chem. Solids*, 1997, 58, 701.

25. E. Figueroa, J. W. Brill and J. P. Selegue, *J. Phys. Chem. Solids*, 1996, 57, 1123.

26. H. Boller and H. Blaha, *J. Solid State Chem.*, 1982, 45, 119.

27. M. S. Whittingham, *Mater. Res. Bull.*, 1974, 9, 1681.

28. R. Schöllhorn and A. Weiss, *J. Less-Common Met*., 1974, 36, 229.

29. R. D. Shannon, *Acta Crystallogr. Sect. A: Cryst. Phys. Diffr. Theor. Gen. Crystallogr.*, 1976, 32, 751.

30. O. Matsumoto, E. Yamada, Y. Kanzaki and M. Konuma, *J. Phys. Chem. Solids*, 1978, 39, 191.

31. T. Maluangnont, K. Gotoh, K. Fujiwara and M. M. Lerner, *Carbon*, 2011, 49, 1040.

32. T. Maluangnont, G. T. Bui, B. A. Huntington and M. M. Lerner, *Chem. Mater.*, 2011, 23, 1091.

33. T. Maluangnont, M. M. Lerner and K. Gotoh, *Inorg. Chem.*, 2011, 50, 11676.

34. T. Maluangnont, W. Sirisaksoontorn and M. M. Lerner, *Carbon*, 2012, 50, 597.

35. Y. H. Zhao, M. H. Abraham and A. M. Zissimos, *J. Org. Chem.*, 2003, 68, 7368.

36. A. U. Liyanage and M. M. Lerner, *RSC Adv.*, 2012, 2, 474.

37. A. U. Liyanage, E. U. Ikhuoria, A. A. Adenuga, V. T. Remcho and M. M. Lerner, *Inorg. Chem.*, 2013, 52, 4603.

38. J. Zheng, H. Zhang, S. H. Dong, Y. P. Liu, C. T. Nai, H. S. Shin, H. Y. Jeong, B. Liu and K. P. Loh, *Nat. Commun.*, 2014, 5, 2995.

39. A. Lerf and R. Schöllhorn, *Inorg. Chem.*, 1977, 16, 2950.

40. C. N. R. Rao and A. Nag, *Eur. J. Inorg. Chem.*, 2010, 4244.

41. T. Sekine, C. Julien, I. Samaras, M. Jouanne and M. Balkanski, *Mater. Sci. Eng. B*, 1989, 3, 153.

42. M. G. Giorgini, M. R. Pelletti, G. Paliani and R. S. Cataliotti, *J. Raman Spectrosc.*, 1983, 14, 16.

CHAPTER 5

CONCLUSION

5.1 CONCLUSION

The development of novel synthetic methods, along with resulting new intercalation compounds and nanocomposites, and their structural and compositional analyses, are reported in this dissertation. Below are some conclusions and proposals for additional studies on new synthetic reactions.

A template synthesis method was developed to obtain $NiPS_3$/polymer nanocomposites. A summary of the resulting nanocomposites is shown in Table 5.1. The observed monolayer arrangement in intercalate galleries for $NiPS_3$/PEO is different from the previously-reported bilayers obtained by a topotactic route for MPS_3/PEO nanocomposites. Three other polymer/$NiPS_3$ nanocomposites ($NiPS_3$/PEI, $NiPS_3$/PVA and $NiPS_3$/PVP) are also reported for the first time using this new synthetic approach. The template method results in more densely packed galleries. More dilute conditions, a more polar solvent and longer aging times increases the crystallite size of the nanocomposites. The concentrations of $P_2S_6^{4-}$ and Ni^{2+} in the reaction solution govern the nanocomposite nucleation and growth, respectively.

Table 5.1 Summary of template synthesized $NiPS_3$/polymer nanocomposites reported in this dissertation

Nanocomposite	Composition	Δd (nm)	Polymer arrangement
$NiPS_3$/PEO	$NiPS_3(C_2H_4O)_1$	0.42	Parallel monolayer
$NiPS_3$/PEI	$NiPS_3(C_2H_5O)_1$	0.41	Parallel monolayer
$NiPS_3$/PVA	$NiPS_3(C_2H_4O)_{0.9}$	0.42	Parallel monolayer
$NiPS_3$/PVP	$NiPS_3(C_6H_9NO)_{0.5}$	1.56	Parallel monolayer

An exfoliation–adsorption method is used to prepare lower generation (G0.0−2.0) PAMAM/Na-montmorillonite nanocomposites. These are the first reports of the G0.0 and G1.0 PAMAM/Na-MMT nanocomposites and of a structurally ordered G2.0 PAMAM/Na-MMT nanocomposite. A summary of selected PAMAM/Na-MMT nanocomposites is shown in Table 5.2. G0.0 PAMAM always forms monolayers within intercalate galleries while G1.0 and G2.0 indicates formation of both monolayer and bilayer arrangements. G2.0 PAMAM/Na-MMT nanocomposites show monolayer to bilayer transition with increasing organic content in the reaction mixture. This is the first report of monolayer PAMAM arrangement in clays. Lower packing fractions are obtained with respect to the linear polymer/Na-MMT nanocomposites. Acidic conditions favor monolayer formation for all three of the dendrimer generations studied. The presence of Na^+ ions in the Na-MMT structure has a significant effect on nanocomposite formation. In basic conditions, PAMAMs show high mobility, ζ potential, and surface charge densities due to Na^+

complexation in solution. Both Na-MMT and PAMAM structural units are preserved in the nanocomposites obtained.

Table 5.2 Summary of exfoliation-adsorption synthesized selected PAMAM/Na-MMT nanocomposites reported in this dissertation

Sample [a]	Reaction condition temp.[b]/pH	Organic mass %	Δd (nm)	Polymer arrangement
0.6G(0.0)	RT/10-11	7.4	0.41	Monolayer
0.6G(1.0)	RT/10-11	10.2	0.45, 0.79	Mix of monolayer and bilayer
0.6G(2.0)	RT/10-11	14.1	0.84	Bilayer
0.6G(0.0)-2	RT/2-3	6.6	0.40	Monolayer
0.6G(1.0)-2	RT/2-3	6.6	0.40	Monolayer
0.6G(2.0)-80-2	80 °C/2-3	7.1	0.40	Monolayer

[a] For all the samples the reactant ratio (g/g PAMAM/Na-MMT) = 0.6, [b] RT = ambient temperature

An electride solution containing Na(m) and ethylenediamine (en) is used to synthesize intercalation compounds of MoS_2. Summary of obtained intercalation compounds is shown in Table 5.3. The β phase (perpendicular en arrangement) is not reported previously for any MS_2 intercalation compounds. The intercalation reaction proceeds *via* formation of a metastable kinetic product, the β phase, and subsequent generation of a stable thermodynamic product, the α phase. Lower electride concentrations, lower reaction temperatures and shorter reaction times favor formation of the β phase. These products have a greater packing fractions compared

to the structural analogous alkali metal-en-graphite intercalation compounds. Electrochemical reduction of MoS_2 in an en based electrolyte does not show the same intercalation behavior.

Table 5.3 Summary of synthesized MoS_2 intercalation compounds using electride chemistry in this dissertation

Intercalation compound	Composition	Δd (nm)	en arrangement
α-phase Na-en-MoS_2	$Na_{0.3}MoS_2 \cdot 0.4en$	0.35	Parallel monolayer
β-phase Na-en-MoS_2	$Na_{0.2}MoS_2 \cdot 0.3en$	0.57	Perpendicular monolayer

Overall, this dissertation introduces several new synthesis intercalation strategies to expand both intercalation chemistry and nanocomposite chemistry. During the process novel structures and reaction mechanisms were obtained.

The synthetic reactions discussed in this dissertation can be extended to other host structures. Template synthesis method could be utilized whenever the solution phase precursors are available to form the host. Sol-gel synthesis could be coupled with this method to form nanocomposites. As another example, the electride chemistry can be extended to synthesize possible intercalation compounds of other structurally similar MX_2 hosts. Other alkali metal, and amine combinations can be utilized to obtain electride solutions with complexes other than $[Na(en)_x^+]$. Since the redox chemistries of transition metal, chemistries of alkali metal and coordination and structures of amine are different; such exploration is likely to lead to new structures

and compositions, along with different materials properties. The application of electride chemistry in $NiPS_3$ is another possibility. Since electride solution can apply a greater reduction potential, this may allow new intercalation or nanocomposite chemistry.

Intercalation compounds may also act as precursors in the synthesis of other intercalation compounds and nanocomposites. For an example Na-en-MoS_2 could reacted with surfactants to obtain larger galleries, ultimately forming stable exfoliated nanosheets of $MoS_2^{\delta-}$, or can react with polymers or dendrimers to form Na-polymer-MoS_2 nanocomposites.

Previously there were reports on stabilization and/or higher capacity effected by PEO incorporation into Li_xMoS_2. Since Na-ion batteries are of interest currently, new path to obtain analogous nanocomposites are of interest. Since dendrimers have the capability to encapsulate other molecules, those are a very important topic in drug delivery. Future attempts can be directed to form nanocomposites with a dendrimer encapsulated compound. Nanocomposites containing dendrimers could act as a reservoir for the slow release of encapsulating drug or molecules.

BIBLIOGRAPHY

Alexandre, M.; Dubois, P., *Mater. Sci. Eng. R* **2000,** *28* (1-2), 1-63.

Alongi, J.; Monticelli, O.; Russo, S.; Camino, G., *J. Nanostruct. Polym. Nanocompos.* **2006,** *2* (4), 127-133.

Amin, A.; Taha, A. S.; El-Ghaffar, M. A. A., *J. Appl. Polym. Sci.* **2010,** *118* (1), 525-537.

Anthony, J. W.; Bideaux, R. A.; Bladh, K. W.; Nichols, M. C., *Handbook of Mineralogy*. Mineralogical Society of America: Chantilly, VA, **1990**.

Bai, J. F.; Zuo, J. L.; Tan, W. L.; Ji, W.; Shen, Z.; Fun, H. K.; Chinnakali, K.; Razak, I. A.; You, X. Z.; Che, C. M., *J. Mater. Chem.* **1999,** *9*, 2419.

Bang, G. S.; Nam, K. W.; Kim, J. Y.; Shin, J.; Choi, J. W.; Choi, S.-Y., *ACS Appl. Mater. Interfaces*, **2014**, *6*, 7084.

Benard, S.; Leaustic, A.; Riviere, E.; Yu, P.; Clement, R., *Chem. Mater.* **2001,** *13* (10), 3709-3716.

Benavente, E.; Santa Ana, M. A.; Mendizabal, F.; Gonzalez, G., *Coord. Chem. Rev.* **2002,** *224* (1-2), 87-109.

Bernard, L.; McKelvy, M.; Glaunsinger, W.; Colombet, P., *Solid State Ionics*, **1985**, *15*, 301.

Betley, T. A.; Holl, M. M. B.; Orr, B. G.; Swanson, D. R.; Tomalia, D. A.; Baker, J. R., *Langmuir* **2001,** *17* (9), 2768-2773.

Birtill, J. J.; Dickens, P. G., *Mater. Res. Bull.* **1978,** *13* (4), 311-316.

Boller, H.; Blaha, H., *J. Solid State Chem.* **1982,** *45* (1), 119-126.

Bonczek, J. L.; Harris, W. G.; Nkedi-Kizza, P., *Clays Clay Miner.* **2002,** *50* (1), 11-17.

Bosman, A. W.; Janssen, H. M.; Meijer, E. W., *Chem. Rev.* **1999,** *99* (7), 1665-1688.

Brec, R., *Solid State Ionics* **1986,** *22* (1), 3-30.

Brothers, H. M.; Piehler, L. T.; Tomalia, D. A., *J. Chromatogr. A* **1998,** *814* (1-2), 233-246.

Brown, L. A.; Glaunsinger, W. S.; McKelvy, M. J., *J. Solid State Chem.*, **2000**, *155*, 326.

Cakara, D.; Kleimann, J.; Borkovec, M., *Macromolecules* **2003,** *36* (11), 4201-4207.

Campanella, L.; Pistoia, G., *J. Electrochem. Soc.* **1971**, *118*, 1905-1908.

Carrado, K. A.; Thiyagarajan, P.; Elder, D. L., *Clays Clay Miner.* **1996,** *44* (4), 506-514.

Castagnola, M.; Zuppi, C.; Rossetti, D. V.; Vincenzoni, F.; Lupi, A.; Vitali, A.; Meucci, E.; Messana, I., *Electrophoresis* **2002,** *23* (12), 1769-1778.

Chen, F.; Xiong, H.; Yang, J. T.; Cai, W. W.; Zhong, M. Q., *e-Polym.* **2012,** No. 016.

Chen, X.; Li, Z.; Zhou, H.; Wang, T.; Qin, J.; Inokuchi, M., *Polymer* **2007,** *48* (11), 3256-3261.

Cheng, Y. Y.; Xu, Z. H.; Ma, M. L.; Xu, T. W., *J. Pharm. Sci.* **2008,** *97* (1), 123-143.

Clement, R.; Girerd, J. J.; Morgensternbadarau, I., *Inorg. Chem.* **1980,** *19* (9), 2852-2854.

Coradin, T.; Clement, R.; Lacroix, P. G.; Nakatani, K., *Chem. Mater.* **1996,** *8* (8), 2153-2158.

Costa, A. S.; Imae, T.; Takagi, K.; Kikuta, K., *Prog. Colloid Polym. Sci.* **2004,** *128*, 113-119.

David, L.; Bhandavat, R.; Singh, G., *ACS Nano*, **2014**, *8*, 1759.

Delgado, A.; Gonzalezcaballero, F.; Bruque, J. M., *J. Colloid Interface Sci.* **1986,** *113* (1), 203-211.

Dye, J. L., *Science*, **2003**, *301*, 607.

Ebber, A.; Vaher, M.; Peterson, J.; Lopp, M., *J. Chromatogr. A* **2002,** *949* (1-2), 351-358.

El-Sayed, M.; Kiani, M. F.; Naimark, M. D.; Hikal, A. H.; Ghandehari, H., *Pharm. Res.* **2001,** *18* (1), 23-28.

Esfand, R.; Tomalia, D. A., Laboratory Synthesis of Poly(amidoamine)(PAMAM) Dendrimers. in: Frechet, J. M. J.; Tomalia, D. A., eds. *Dendrimers and Other Dendritic Polymers*. John Wiley & Sons, Ltd.: Chichester, UK. **2002**, pp. 587-604.

Figueroa, E.; Brill, J. W.; Selegue, J. P., *J. Phys. Chem. Solids* **1996,** *57* (6-8), 1123-1127.

Foot, P. J. S.; Nevett, B. A., *Chem. Comm.* **1987,** (5), 380-381.

Fragnaud, P.; Prouzet, E.; Brec, R., *J. Mater. Res.* **1992,** *7* (7), 1839-1846.

Gamble, F. R.; Osiecki, J. H.; Cais, M.; Pisharod.R, *Science* **1971,** *174* (4008), 493-497.

Giannelis, E. P., *Adv. Mater.* **1996,** *8* (1), 29-35.

Gilman, J. W., *Appl. Clay Sci.* **1999,** *15* (1-2), 31-49.

Giorgini, M. G.; Pelletti, M. R.; Paliani, G.; Cataliotti, R. S., *J. Raman Spectrosc.*, **1983**, *14*, 16.

Glemser, O.; Lutz, G., *Z. Anorg. Allg. Chem.* **1951,** *264*, 17.

Glemser, O.; Lutz, G., *Z. Anorg. Allg. Chem.* **1952,** *269*, 93.

Glemser, O.; Lutz, G.; Meyer, G., *Z. Anorg. Allg. Chem.* **1956,** *285*, 173.

Gonzalez, G.; Santa Ana, M. A.; Benavente, E., *Electrochim. Acta*, **1998**, *43*, 1327.

Grabchev, I.; Petkov, C.; Bojinov, V., *Dyes Pigm.* **2004,** *62* (3), 229-234.

He, S.; Lin, J., *Appl. Mech. Mater.* **2012,** *108*, 91-94.

Hierlemann, A.; Campbell, J. K.; Baker, L. A.; Crooks, R. M.; Ricco, A. J., *J. Am. Chem. Soc.* **1998,** *120* (21), 5323-5324.

Hoffman, L. W.; Andersson, G. G.; Sharma, A.; Clarke, S. R.; Voelcker, N. H., *Langmuir* **2011,** *27*, 6759-6767.

Hu, Y.S.; Chen, W.; Xu, Q.; Yuan, R.Z., *J. Mater. Sci. Technol.* **2001**, *17*, S124-S126.

Huang, J. C.; Zhu, Z. K.; Yin, J.; Qian, X. F.; Sun, Y. Y., *Polymer* **2001,** *42* (3), 873-877.

Jacobson, A. J.; Nazar, L. F., Intercalation Chemistry. in *Encyclopedia of Inorganic and Bioinorganic Chemistry*, John Wiley & Sons, **2011**.

Jeevanandam, P.; Vasudevan, S., *Chem. Mater.* **1998,** *10* (5), 1276-1285.

Ji, Y.; Zuo, J. L.; Chen, L. X.; Tian, Y. Q.; Song, Y. L.; Li, Y. Z.; You, X. Z., *J. Phys. Chem. Solids* **2005,** *66* (1), 207-212.

Juang, T.-Y.; Chen, Y.-C.; Tsai, C.-C.; Dai, S. A.; Wu, T.-M.; Jeng, R.-J., *Appl. Clay Sci.* **2010,** *48* (1-2), 103-110.

Kanatzidis, M. G.; Bissessur, R.; Degroot, D. C.; Schindler, J. L.; Kannewurf, C. R., *Chem. Mater.* **1993,** *5* (5), 595-596.

Kerr, T.A.; Wu, H.; Nazar, L.F., *Chem. Mater.* **1996**, *8* (8), 2005-2015.

Kim, Y.; Klutz, A. M.; Jacobson, K. A., *Bioconjugate Chem.* **2008,** *19* (8), 1660-1672.

Kuzminskii, Y. V.; Voronin, B. M.; Petrushina, I. M.; Redin, N. N.; Prikhodko, G. P., *J. Power Sources* **1995,** *55* (1), 1-6.

Lagadic, I.; Lacroix, P. G.; Clement, R., *Chem. Mater.* **1997,** *9* (9), 2004-2012.

Lagadic, I.; Leaustic, A.; Clement, R., *Chem. Comm.* **1992,** (19), 1396-1397.

LeBaron, P. C.; Wang, Z.; Pinnavaia, T. J., *Appl. Clay Sci.* **1999,** *15* (1-2), 11-29.

Lee, D.; Char, K.; Lee, S. W.; Park, Y. W., *J. Mater. Chem.* **2003,** *13* (12), 2942-2947.

Lemehaute, A., *C. R. Acad. Sci.* **1978,** *287* (8), 309-311.

Lemmon, J. P.; Wu, J. H.; Oriakhi, C.; Lerner, M. M., *Electrochim. Acta* **1995,** *40* (13-14), 2245-2249.

Lerf, A., Intercalation compounds in layered host lattices: supramolecular chemistry in nanodimensions. in: Nalwa, H. S., ed. *Handbook of nanostructured materials and nanotechnology*, Academic Press: San Diego, **2000**; Vol. 5, Ch. 1, pp 1-166.

Lerf, A., *Dalton Trans.* **2014,** *43* (27), 10276-10291.

Lerf, A., Schollhorn, R., *Inorg. Chem.*, **1977**, *16*, 2950.

Lerner, M. M.; Oriakhi, C. O., Polymers in ordered nanocomposites. in: Goldstein, A. N., Ed. Handbook of nanophase materials, Marcel Dekker: New York, N.Y, **1997**, pp 199-219.

Lévy, F. A., *Intercalated layered materials*. D. Reidel Publishing: Dordrecht, Holland, **1979**.

Li, J.; Piehler, L. T.; Qin, D.; Baker, J. R.; Tomalia, D. A.; Meier, D. J., *Langmuir* **2000,** *16* (13), 5613-5616.

Liyanage, A. U.; Ikhuoria, E. U.; Adenuga, A. A.; Remcho, V. T.; Lerner, M. M., *Inorg. Chem.* **2013**, *52*, 4603.

Liyanage, A. U.; Lerner, M. M., *RSC Adv.* **2012,** *2* (2), 474-479.

Liu, L. M.; Qi, Z. N.; Zhu, X. G., *J. Appl. Polym. Sci.* **1999,** *71* (7), 1133-1138.

Loboue, H.; Guillot-Deudon, C.; Popa, A. F.; Lafond, A.; Rebours, B.; Pichon, C.; Cseri, T.; Berhault, G.; Geantet, C., *Catal. Today* **2008,** *130* (1), 63-68.

Loeb, A. L.; Overbeek, J. T. G.; Wiersema, P. H., *The electrical double layer around a spherical colloid particle*. MIT Press: Cambridge, MA, **1961**.

Lukowski, M. A.; Daniel, A. S.; Meng, F.; Forticaux, A.; Li, L. S.; Jin, S., *J. Am. Chem. Soc.*, **2013**, *135*, 10274.

Maluangnont, T.; Bui, G. T.; Huntington, B. A.; Lerner, M. M., *Chem. Mater.* **2011,** *23* (5), 1091-1095.

Maluangnont, T.; Gotoh, K.; Fujiwara, K.; Lerner, M. M., *Carbon* **2011,** *49* (3), 1040-1042.

Maluangnont, T.; Lerner, M. M.; Gotoh, K., *Inorg. Chem.* **2011,** *50* (22), 11676-11682.

Maluangnont, T.; Sirisaksoontorn, W.; Lerner, M. M., *Carbon* **2012,** *50* (2), 597-602.

Manias, E.; Polizos, G.; Nakajima, H.; Heidecker, M. J., in: Morgan, A. B.; Wilkie, C. A., eds., *Flame retardent polymer nanocomposites*, John Wiley & Sons, Inc.: Hoboken, New Jersey, NJ, **2007**, pp. 31-66.

Manova, E.; Severac, C.; Andreev, A.; Clement, R., *J. Catal.* **1997,** *169* (2), 503-509.

Manriquez, V.; Barahona, P.; Ruiz, D.; Avila, R. E., *Mater. Res. Bull.* **2005,** *40* (3), 475-483.

Matsumoto, O.; Yamada, E.; Kanzaki, Y.; Konuma, M., *J. Phys. Chem. Solids* **1978,** *39* (2), 191-192.

Mercier, R.; Malugani, J. P.; Fahys, B.; Douglade, J.; Robert, G., *J. Solid State Chem.* **1982,** *43* (2), 151-162.

Messersmith, P. B.; Giannelis, E. P., *Chem. Mater.* **1993,** *5* (8), 1064-1066.

Murugan, A.V.; Viswanath, A.K.; Gopinath, C.S.; Vijayamohanan, K., *J. Appl. Phys.* **2006**, *100* (7), 074319-1–074319-5.

Nanjwade, B. K.; Bechra, H. M.; Derkar, G. K.; Manvi, F. V.; Nanjwade, V. K., *Eur. J. Pharm. Sci.* **2009,** *38* (3), 185-196.

Nazar, L.F.; Wu, H.; Power, W.P., *J. Mater. Chem.* **1995**, *5* (11), 1985-93.

Ogata, H.; Fujimori, H.; Miyajima, S.; Kobashi, K.; Chiba, T.; Taylor, R. E.; Endo, K., *J. Phys. Chem. Solids* **1997,** *58* (5), 701-710.

Oriakhi, C. O.; Farr, I. V.; Lerner, M. M., *J. Mater. Chem.* **1996,** *6* (1), 103-107.

Oriakhi, C. O.; Nafshun, R. L.; Lerner, M. M., *Mater. Res. Bull.* **1996,** *31* (12), 1513-1520.

Oriakhi, C. O.; Zhang, X. R.; Lerner, M. M., *Appl. Clay Sci.* **1999**, *15* (1-2), 109-118.

Ouvrard, G.; Brec, R.; Rouxel, J., *Mater. Res. Bull.* **1985,** *20* (10), 1181-1189.

Park, J.; Kim, J.-S.; Park, J.-W.; Nam, T.-H.; Kim, K.-W.; Ahn, J.-H.; Wang, G.; Ahn, H.-J., *Electrochim. Acta*, **2013**, *92*, 427.

Pavlidou, S.; Papaspyrides, C. D., *Prog. Polym. Sci.* **2008,** *33* (12), 1119-1198.

Pereiraramos, J. P.; Kumagai, N., *J. Power Sources* **1995**, *56* (1), 87-90.

Posudievsky, O.Y.; Biskulova, S.A.; Pokhodenko, V.D., *J. Mater. Chem.* **2002**, *12* (5), 1446-1449.

Prouzet, E.; Ouvrard, G.; Brec, R.; Seguineau, P., *Solid State Ionics* **1988,** *31* (1), 79-90.

Punyacharoennon, P.; Charuchinda, S.; Srikulkit, K., *J. Appl. Polym. Sci.* **2008,** *110* (6), 3336-3347.

Rajesh, R.; Venkatesan, R., *J. Mol. Catal. A: Chem.* **2012**, *359*, 88-96.

Rao, C. N. R.; Nag, A., *Eur. J. Inorg. Chem.,* **2010**, 4244.

Ratanarat, K.; Nithitanakul, M.; Martin, D. C.; Magaraphan , R., *Rev. Adv. Mater. Sci.* **2003,** *5* (3), 187-192.

Ray, S. S.; Okamoto, M., *Prog. Polym. Sci.* **2003,** *28* (11), 1539-1641.

Rehim, M. H. A.; Youssef, A. M.; Essawy, H. A., *Mater. Chem. Phys.* **2010,** *119* (3), 546-552.

Rodlert, M.; Plummer, C. J. G.; Garamszegi, L.; Leterrier, Y.; Grunbauer, H. J. M.; Manson, J. A. E., *Polymer* **2004,** *45* (3), 949-960.

Rüdorff, W., *Chimia* **1965,** *19*.

Rüdorff, W.; Sick, H. H., *Angew. Chem.* **1959,** *71*, *127*.

Sadek, O. M.; Mekhemer, W. K., *Thermochim. Acta* **2001,** *370* (1-2), 57-63.

Sadekar, S.; Ghandehari, H., *Adv. Drug Deliv. Rev.* **2012**, *64*, 571-588.

Sanchez, V.; Benavente, E.; Santa Ana, M. A.; Gonzalez, G., *Chem. Mater.* **1999,** *11* (9), 2296-2298.

Santa Ana, M. A.; Sanchez, V.; Gonzalez, G., *Electrochim. Acta* **1995,** *40* (11), 1773-1775.

Schöllhorn, R.; Kuhlmann, R.; Besenhard, J. O., *Mater. Res. Bull.* **1976,** *11* (1), 83-90.

Schöllhorn, R.; Weiss, A., *J. Less-Common Met.* **1974,** *36* (1-2), 229-236.

Schöllhorn, R.; Zagefka, H. D., *Angew. Chem. Int. Ed.* **1977,** *16* (3), 199-200.

Sekine, T.; Julien, C.; Samaras, I.; Jouanne, M.; Balkanski, M., *Mater. Sci. Eng., B* **1989**, *3*, 153.

Shannon, R. D., *Acta Crystallogr., Sect. A: Cryst. Phys., Diffr., Theor. Gen. Crystallogr.*, **1976**, *32*, 751.

Shi, X. Y.; Banyai, I.; Lesniak, W. G.; Islam, M. T.; Orszagh, I.; Balogh, P.; Baker, J. R.; Balogh, L. P., *Electrophoresis* **2005,** *26* (15), 2949-2959.

Singh, P.; Moll, F.; Lin, S. H.; Ferzli, C.; Yu, K. S.; Koski, R. K.; Saul, R. G.; Cronin, P., *Clin. Chem.* **1994,** *40* (9), 1845-1849.

Somoano, R. B.; Hadek, V.; Rembaum, A., *J. Chem. Phys.* **1973,** *58* (2), 697-701.

Somoano, R. B.; Hadek, V.; Rembaum, A.; Samson, S.; Woollam, J. A., *J. Chem. Phys.* **1975,** *62* (3), 1068-1073.

Stepanov, A. A.; Lenenko, N. D.; Golub, A. S.; Pervov, V. S., *Russ. J. Electrochem.*, **2013**, *49*, 86.

Sukpirom, N.; Oriakhi, C. O.; Lerner, M. M., *Mater. Res. Bull.* **2000,** *35* (3), 325-331.

Takada, K.; Diaz, D. J.; Abruna, H. D.; Cuadrado, I.; Casado, C.; Alonso, B.; Moran, M.; Losada, J., *J. Am. Chem. Soc.* **1997,** *119* (44), 10763-10773.

Tan, N. C. B.; Balogh, L.; Trevino, S. F.; Tomalia, D. A.; Lin, J. S., *Polymer* **1999,** *40* (10), 2537-2545.

Tang, M. X.; Redemann, C. T.; Szoka, F. C., *Bioconjugate Chem.* **1996,** *7* (6), 703-714.

Thomas, D. M.; McCarron, E. M., *Mater. Res. Bull.*. **1986**, *21* (8), 945-960.

Tomalia, D. A., *Prog. Polym. Sci.* **2005**, *30* (3-4), 294-324.

Tomalia, D. A.; Naylor, A. M.; Goddard, W. A., *Angew. Chem. Int. Ed. Engl.* **1990,** *29* (2), 138-175.

Vaia, R. A.; Giannelis, E. P., *Macromolecules* **1997,** *30* (25), 8000-8009.

Wang, L.; Schindler, J.; Kannewurf, C.R.; Kanatzidis, M.G., *J. Mater. Chem.* **1997**, *7* (7), 1277-83.

Wein, E.; Mullerwarmuth, W.; Schollhorn, R., *Solid State Ionics*, **1987**, *22*, 231.

Whittingham, M. S., *J. Electroanal. Chem.* **1981,** *118*, 229-239.

Whittingham, M. S., *Mater. Res. Bull.* **1974,** *9* (12), 1681-1690.

Whittingham, M. S.; Gamble, F. R., *Mater. Res. Bull.*, **1975**, *10*, 363.

Whittingham, M. S.; Jacobson, A. J., *Intercalation Chemistry*. Academic Press: New York, NY., **1982**.

Wiersema, P. H.; Loeb, A. L.; Overbeek, J. T., *J. Colloid Interface Sci.* **1966,** *22* (1), 79-99.

Wilson, S. T.; Lok, B. M.; Messina, C. A.; Cannan, T. R.; Flanigen, E. M., *J. Am. Chem. Soc.* **1982,** *104* (4), 1146-1147.

Wu, J. H.; Lerner, M. M., *Chem. Mater.* **1993,** *5* (6), 835-838.

Xiao, J.; Choi, D.; Cosimbescu, L.; Koech, P.; Liu, J.; Lemmon, J. P., *Chem. Mater.* **2010,** *22* (16), 4522-4524.

Xiao, J.; Wang, X. J.; Yang, X. Q.; Xun, S. D.; Liu, G.; Koech, P. K.; Liu, J.; Lemmon, J. P., *Adv. Funct. Mater.*, **2011**, *21*, 2840.

Xie, W.; Gao, Z. M.; Pan, W. P.; Hunter, D.; Singh, A.; Vaia, R., *Chem. Mater.* **2001,** *13* (9), 2979-2990.

Yamanaka, S.; Kobayashi, H.; Tanaka, M., *Chem. Lett.* **1976,** (4), 329-332.

Yang, D.; Frindt, R. F., *J. Mater. Res.* **2000,** *15* (11), 2408-2413.

Zhao, M. Q.; Crooks, R. M., *Adv. Mater.* **1999,** *11* (3), 217-220.

Zhao, Y. H.; Abraham, M. H.; Zissimos, A. M., *J. Org. Chem.* **2003,** *68* (19), 7368-7373.

Zheng, J.; Zhang, H.; Dong, S. H.; Liu, Y. P.; Nai, C. T.; Shin, H. S.; Jeong, H. Y.; Liu, B.; Loh, K. P., *Nat. Commun.*, **2014**, *5*, 2995.

APPENDIX A

PREPARATION AND CHARACTERIZATION OF NANOCOMPOSITES OF POLYAMIDOAMINE (PAMAM) DENDRIMERS WITH MOLYBDENUM(VI) OXIDE (MoO_3)

Esther U. Ikhuoria,[a] Amila U. Liyanage, and Michael M. Lerner

Department of Chemistry

Oregon State University

Corvallis, OR 97331-4003, USA

[a] Fulbright visiting scholar, Oregon State University, 2011/2012.
Department of Chemistry, University of Benin, Benin City, Nigeria.

Mat. Chem. Phys., 2013, 139 (2-3), 911-916.

A.1 ABSTRACT

The preparation and characterization of polymer nanocomposites is an important research area because of the significant changes in materials properties relative to the component phases or to conventional microscale or macroscale composites. Polyamidoamine (PAMAM)/molybdenum(VI) oxide (MoO_3) nanocomposites were synthesized using an exfoliation/adsorption method and characterized by powder X-ray diffraction, thermogravimetric analyses, scanning electron microscopy and infrared spectroscopy. Generation 0 (G0) and generation 2 (G2) PAMAM forms nanocomposites with MoO_3 with either intercalate monolayers or bilayers, with resulting gallery expansions (Δd) of ~ 0.5 and ~ 0.7-0.8 nm, respectively. G0 only forms monolayers whereas G2 forms mono and bilayers. The spherical PAMAM conformation in aqueous medium changes dramatically to a highly-flattened conformation within the intercalate galleries. Reaction temperature also affects the structure of the obtained G2 PAMAM nanocomposites. Bilayer nanocomposites obtained at 40 and 120 °C show Δd = 1.4 nm and 0.7 nm, respectively. Mixed phases were obtained at 60 °C. The obtained nanocomposite compositions and structures are compared with previously-reported polymer/MoO_3 nanocomposites.

A.2 INTRODUCTION

Nanocomposites are materials derived from two or more phases where at least one dimension of the combination is in the nanometer scale. Polymer nanocomposites are a new class of advanced polymer composites that often display enhanced physical properties such as strength, hardness, thermal and viscoelasticity. Nanocomposite properties depend not only on those of their parent phases, but also on the structural complexity, morphology and interfacial interactions of these constituents. With an eye towards new and improved devices, nanocomposites often display dramatically improved performance relative to those currently available.[1] For example, a material's stiffness can be improved without sacrificing mechanical toughness, or its barrier properties enhanced without sacrifice of desirable properties such as transparency, flame retardancy and biodegradability.[2] The ability to avoid the trade-off in functional materials which is typical of conventional composites illustrates the potential importance of nanocomposites.

Two dimensional (2D) layered structures have been investigated intensively as host lattices for preparing nanocomposites. These host lattices may exfoliate into a polymer matrix or incorporate polymer guests within well-defined interlayer galleries.[3] Many two dimensional compounds which involve intercalation of molecules or ions between inorganic layered sheets have been reported.[4,5] Again, the preparation and detailed characterization of polymer nanocomposites is an active area of research because of the possibility of a remarkable improvement in materials properties when compared with purely organic or inorganic phases or conventional micro and macro composites.

Dendrimers are synthetic, mono-disperse macromolecules with a regular and highly-branched three-dimensional architecture.[6] In contrast to traditional polymers, dendrimers have core-shell structures consisting of three basic architectural components: a core, interior shells (generations) with repeating branch-cell units, and terminal functional groups.[7] They are produced by an interactive sequence of reaction steps, in which each added step leads to a higher-generation material.[6] This approach provides unprecedented control over composition and architecture, as well as the ability to add numerous different terminal groups that affect their surface chemistry.[8] Polyamidoamine (PAMAM) dendrimers are one of the most well investigated families and have been evaluated for diverse applications ranging from drug delivery to molecular encapsulation and gene therapy, as well as for building blocks for nanostructures.[9-12]

Molybdenum trioxide (MoO_3) is an example of 2D layered structure that has been examined as a potentially useful electrode because of it rich redox chemistry.[13,14] It exhibits a unique layered structure in which Mo atom is surrounded by distorted octahedron of oxygen atoms with two layers of corner-sharing MoO_6 units.[15] As an electrode material for rechargeable battery application, MoO_3 is limited by slow kinetics for Li-ion transport, an electronically-insulating state upon full oxidation, and poor cycling behavior when compared to other metal oxides/chalcogenides.[15] One approach to modify the properties of the layered MoO_3 has been intercalation of electronically-conducting guests.[4] Previous studies have also reported on the intercalation of polyethylene oxide (PEO),[16,17] linear polyethylenimine (LPEI),[18] polyaniline (PANI),[19] polyvinylpyrrolidone (PVP) and

polyacrylamide (PAM).[20] Polymer/MoO_3 nanocomposites have also been studied as a cathode for secondary lithium ion batteries, where monolayer and bilayer nanocomposites of PEO/MoO_3 have indicated significant differences from each other in both lithium ion transport and cell capacity in cycling.[14] Unlike polymers, dendrimers have a confined shape and a size which is possibly useful for a controlled intercalation and electrode behavior. However, there has been no report on the intercalation of dendrimers into MoO_3. Here we report on the synthesis and characterization of layered nanocomposites derived from PAMAM dendrimers and MoO_3.

A.3 EXPERIMENTAL

A.3.1 MATERIALS

MoO_3 (99.5%, Sigma-Aldrich), $Na_2MoO_4{\cdot}2H_2O$ (99%, Strem Chemicals) and $Na_2S_2O_4$ (Laboratory grade, Fisher) were used as received. $[Na(H_2O)_2]_{0.25}MoO_3$ was prepared by reacting MoO_3 with an aqueous solution of $Na_2S_2O_4$ according to a literature method.[21] Distilled water (DI) was used in all experiments. Aqueous suspensions of amine terminated polyamidoamine (PAMAM) dendrimers of different generations (G0, G1, G2) were obtained from Dendritech (Midland, M.I) and used as supplied. Some of the physical properties of the generations of PAMAM dendrimer used are presented in Table A1.[22]

Table A1. Physical properties of amine surface functional PAMAM dendrimers.

Generation	Surface groups	Molar mass	Diameter (nm)
0	4	517	1.4
1	8	1430	1.9
2	16	3256	2.6

A.3.2 SYNTHESES

$[Na(H_2O)_2]_{0.25}MoO_3$ was reacted with PAMAM to form PAMAM/MoO_3 nanocomposites using the exfoliation/adsorption method described previously[18] for polymer/MoO_3 nanocomposites with slight modifications indicated below. The ratio of reactants PAMAM to $[Na(H_2O)_2]_{0.25}MoO_3$ was varied from 0.10/1.0 to 0.80/1.0 (g/g). In a typical experiment, $[Na(H_2O)_2]_{0.25}MoO_3$ (80 mg) was exfoliated by ultrasonication (GE 600W) at ambient temperature in 20 mL of DI. An aqueous solution of PAMAM (8-64 mg in 20 mL) was slowly added to the resulting suspension and stirred for 6 h on a hotplate with surface temperature 60 °C. The suspension temperatures were 0-15° less than the heating surface but were not directly measured. The flocculate was separated by centrifugation, washed with a copious amount of DI, and dried under vacuum at 80 °C for 24 h. Experimental variables evaluated included the PAMAM generation selected, the reactant ratios employed, and the temperature of the aqueous suspension during the 6 h reaction. The nanocomposites obtained are designated by the PAMAM generation and reactant ratio, thus G2-0.1 indicates the product obtained by reacting generation 2 PAMAM with $[Na(H_2O)_2]_{0.25}MoO_3$ in a 0.10/1.0 g/g ratio. For reactions carried out on a heating

surface other than at 60 °C, the heating surface temperature (in °C) is also indicated in the label, for example G2-0.1-80.

A.3.3 CHARACTERIZATION

Products were characterized by powder X-ray diffraction (PXRD) using a Rigaku Miniflex II X-Ray diffractometer with Ni-filtered Cu Kα radiation (λ = 0.15418 nm) at a scan rate of 1° min^{-1} between 3° and 30° 2θ. Thermogravimetric analyses were collected on a Shimadzu TGA-50 at 5 °C min^{-1} under flowing Ar. Scanning electron micrographs (SEMs) were obtained using an FEI Quanta 600F FEG instrument. IR spectra were recorded using a Nicolet iS10 FT-IR spectrometer with Smart iTR ATR sampling accessory and Ge crystal from 4000-700 cm^{-1}.

A.4 RESULTS AND DISCUSSION

When PAMAM/MoO_3 nanocomposites were synthesized at room temperature, only multiple phase products were obtained. However, after reactions on the 60 °C heating surface, PXRD single phase products could also be obtained. Figure A1 shows the PXRD patterns of the nanocomposites prepared at 60 °C from different reactant ratios of G0 or G2 PAMAM and $[Na(H_2O)_2]_{0.25}MoO_3$. The MoO_3 sheet thickness is 0.69 nm, and the repeat distance (d) increases to 0.97 nm in $[Na(H_2O)_2]_{0.25}MoO_3$, so that the interlayer expansion (Δd) is 0.28 nm. This expansion is consistent with a Na^+ plus water monolayer intercalate.[14,21] The repeat distance, d, further increases to approximately 1.2 nm for all nanocomposites derived from G0 PAMAM and $[Na(H_2O)_2]_{0.25}MoO_3$. This interlayer expansion (Δd) of ~ 0.5 nm relative to MoO_3 is much less than the diameter of solution-phase G0 PAMAM

(Table A1), and therefore indicates the formation of an intercalate gallery containing PAMAM in a highly flattened conformation. In the case of G2 PAMAM, G2-0.1 shows unreacted $[Na(H_2O)_2]_{0.25}MoO_3$ along with a phase similar to that described above ($\Delta d = 0.51$ nm). For other compositions, one or more of three phases with interlayer expansions of ≈ 0.5, 0.7-0.8, or 1.4-1.5 nm are obtained. Table A2 shows the observed PXRD repeat distance and derived interlayer expansions at different reactant ratios of the nanocomposites. Samples G2-0.2, G2-0.3, and G2-0.4 show two of the expanded phases; at higher reactant ratios only a single phase with $\Delta d \approx 0.8$ nm is observed. The (010) reflection is observed in all PXRD patterns, along with higher-order reflections in some patterns, indicating that the MoO_3 sheets themselves remain intact and largely unchanged from the host structure. The phases with $\Delta d = 0.5$ and 0.7-0.8 nm are ascribed to PAMAM monolayers and bilayers between MoO_3 galleries, respectively (Figure A2), and these assignments are consistent with compositional data presented below and with previous reports (Table A3). PEO/MoO_3 shows a single phases with expansions of about 0.6 or 0.8 nm, corresponding to the formation of monolayers and bilayers, respectively.[14] LPEI/MoO_3 (ref. 18) and PANI/MoO_3 (ref. 19) both show a single phase with $\Delta d \approx$ 0.5 nm, corresponding to monolayer formation.

Table A2. PXRD repeat distances (d) and derived interlayer expansions (Δd) of PAMAM/MoO_3 nanocomposites at different reactant ratios.

Reactant ratio	G0		G2	
	d (nm)	Δd (nm)	d (nm)	Δd (nm)
0.1	1.20	0.51	0.96; 1.20	0.24; 0.51
0.2	1.21	0.52	1.41; 2.23	0.72; 1.54
0.3	1.20	0.51	1.34; 2.12	0.65; 1.43
0.4	1.20	0.51	1.41; 2.13	0.72; 1.44
0.5	1.20	0.51	1.48	0.79
0.6	1.19	0.50	1.46	0.77
0.7	1.20	0.51	1.47	0.78
0.8	1.18	0.49	1.51	0.82

Table A3. Comparison of PAMAM/MoO_3 with other polymer/MoO_3 nanocomposites.

Intercalate	Organic mass %	Δd (nm)	Type	Packing fraction	Reference
PEO	10*	0.60	Monolayer	0.46*	14
	21*	0.83	Bilayer	0.74*	
LPEI	16	0.47	Monolayer	0.96*	18
PANI	17*	0.54	Monolayer	0.71*	19
G0 PAMAM	12-14	0.51	Monolayer	0.55-0.69	This work
G2 PAMAM	22-25	0.79	Bilayer	0.77-0.95	

* Calculated from the compositional and structural data provided in the reference indicated.

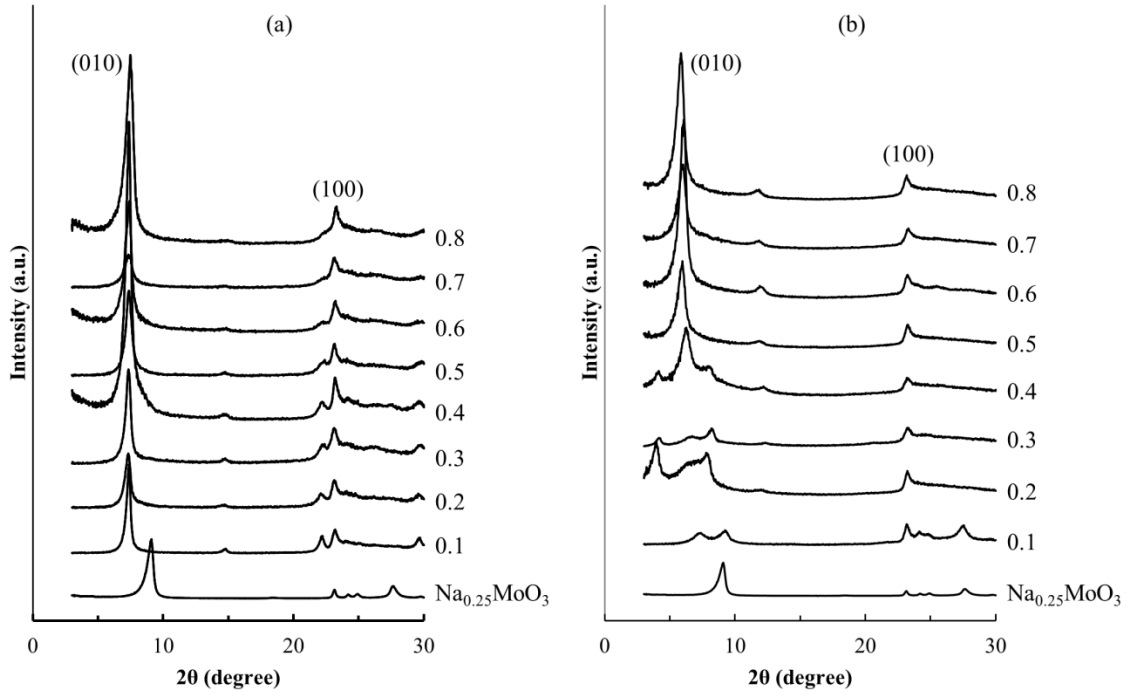

Figure A1. PXRD patterns of $[Na(H_2O)_2]_{0.25}MoO_3$ and PAMAM/MoO_3 nanocomposites with G0 (a) or G2 (b) PAMAM at different reactant ratios.

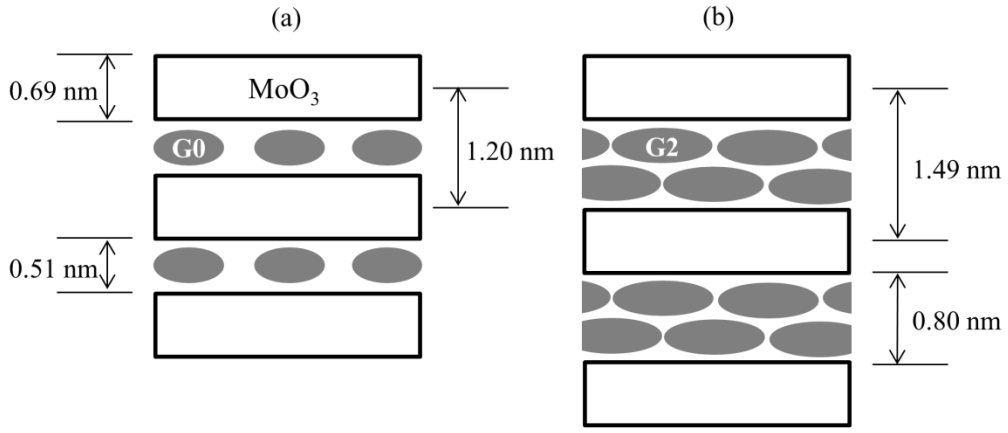

Figure A2. Proposed schematic structure of obtained nanocomposites. (a) G0/MoO_3 monolayer and (b) G2/MoO_3 bilayer.

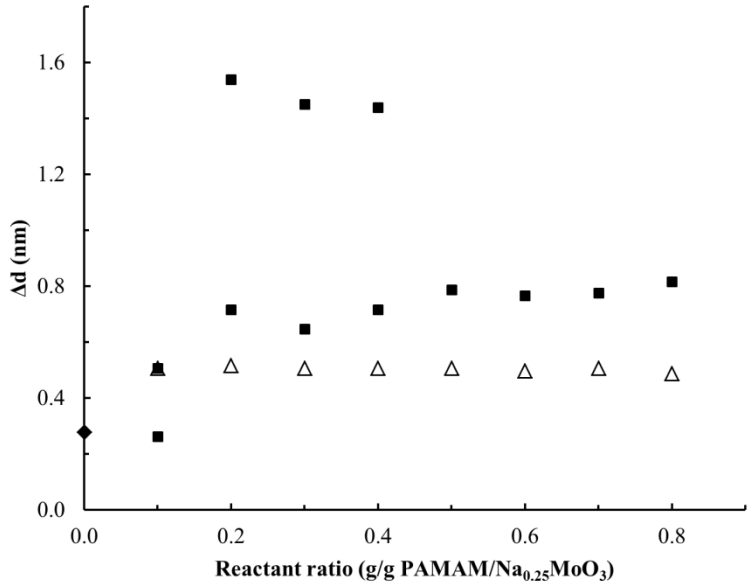

Figure A3. Interlayer expansions (Δd) obtained at different reactant ratios for PAMAM/MoO_3 nanocomposites using PAMAM G0 (Δ) and G2 (■).

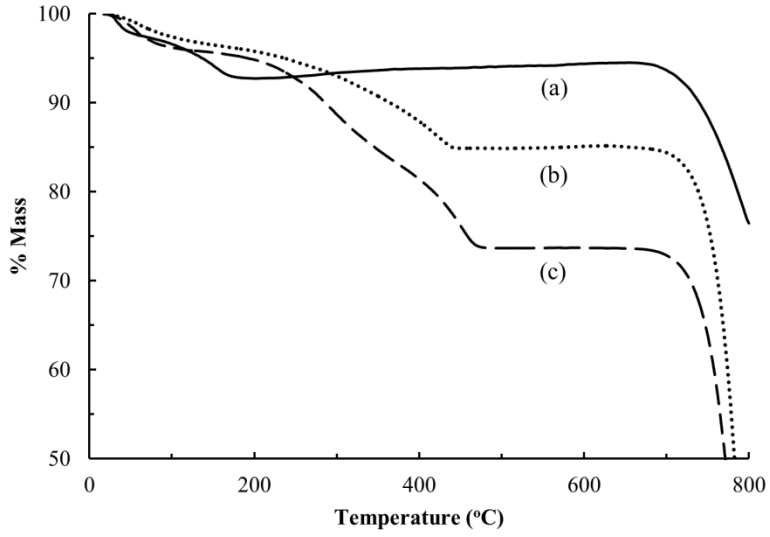

Figure A4. Thermographs of $[Na(H_2O)_2]_{0.25}MoO_3$ (a), and the nanocomposites G0-0.5 (b) and G2-0.5 (c).

Figure A4 shows the thermographs of $[Na(H_2O)_2]_{0.25}MoO_3$ and two representative nanocomposites. $[Na(H_2O)_2]_{0.25}MoO_3$ shows a dehydration mass loss of about 5% below 150 °C, and is then thermally stable up to about 700 °C. Both nanocomposites also show a mass loss attributed to dehydration at low temperatures, and a larger mass loss from 200 to 400 °C attributed to the decomposition and volatilization of PAMAM. From these mass loss events, the compositions of PAMAM, H_2O, and $Na_{0.25}MoO_3$ in each material were obtained. These compositions are reported in Table A4.

As can be seen in Figure A3 and Table A4, the nanocomposites where PXRD data indicate a single bilayer phase, G2-0.5 to G2-0.8, contain 22-25 mass % PAMAM. The G0 PAMAM nancomposites, which all show a single monolayer phase, contain a PAMAM content of 12-14 mass %. This approximate 2:1 ratio of PAMAM content for the two phases supports their assignments as bilayer and monlayer intercalate structures as described above, and agrees with the organic content observed previously for polymer/MoO_3 nanocomposites (10-17% for monolayer and 21% for bilayer structures) as shown in Table A3. Compositions G2-0.2 to 0.4 are mixed phase products containing about 22-28 mass % PAMAM.

Table A4**.** Compositional data for different reactant ratios using PAMAM G0 and G2.

Reactant ratio	Mass %			Mole ratio, r_i	Packing fraction
	H_2O	PAMAM	$Na_{0.25}MoO_3$		
G0-0.1	3.0	11.5	85.1	0.039	0.55
G0-0.2	3.6	13.0	83.4	0.045	0.62
G0-0.4	3.6	12.1	84.3	0.042	0.59
G0-0.5	3.5	11.6	84.9	0.040	0.56
G0-0.6	2.7	12.3	84.9	0.042	0.60
G0-0.7	3.6	13.5	80.0	0.049	0.69
G0-0.8	2.9	12.6	84.5	0.043	0.63
G2-0.1	3.9	11.5	84.6	0.006	n.a.
G2-0.2	4.5	21.8	73.7	0.014	n.a.
G2-0.3	4.2	26.8	69.0	0.018	n.a.
G2-0.4	5.1	28.0	66.9	0.019	n.a.
G2-0.5	4.3	22.0	73.7	0.014	0.77
G2-0.6	3.4	24.2	72.4	0.015	0.90
G2-0.7	6.2	24.8	69.0	0.016	0.95
G2-0.8	4.3	22.6	73.1	0.014	0.78

Where interlayer expansions and phase compositions are known, the packing fraction of PAMAM in the interlayer galleries can be determined as follows (equation (1)):[23]

$$Packing\ fraction = \frac{Z.r_i.V_{vdw}}{a.c.\Delta d} \qquad (1)$$

where Z = 2 (the number of MoO_3 units per half unit cell), r_i = mole ratio of PAMAM to $Na_{0.25}MoO_3$, V_{vdw} is the van der Waals volume of PAMAM according to Ref. 24, and a and c are MoO_3 unit cell parameters: a = 0.396 nm, c = 0.370 nm.[21] Packing fractions therefore represent the relative filling by guest intercalate of available volume in the expanded galleries. For comparison, V_{vdw} and packing fractions of PEO, LPEI and PANI in MoO_3 were also estimated by a literature method.[23] As shown in Table A3, packing fractions obtained for PEO/MoO_3, LPEI/MoO_3, PANI/MoO_3 monolayers and the PEO/MoO_3 bilayer are 0.46, 0.96, 0.71 and 0.74 respectively. The packing fraction calculated for all the compositions studied was in the range of 0.77-0.95 for G2 and 0.55-0.69 for G0. The present results demonstrate that starting compositions have little or no effect on the product packing fraction, and that G2 PAMAM packs more densely in the intercalate galleries than does G0 PAMAM.

The effect of reaction temperature was examined by preparing a series of G2-0.3 nanocomposites under different heating conditions. At 20 °C, a mix of $[Na(H_2O)_2]_{0.25}MoO_3$ and a bilayer phase are obtained with Δd = 0.72 nm (Figure A5). At 40 °C, a single-phase product with Δd = 1.44 nm was obtained. This phase is also obtained as part of the mixed-phase product at 60 °C with G2-0.2, G2-0.3, and G2-0.4. Above 40 °C, there is a gradual decrease in the Δd = 1.44 nm phase and increase in a bilayer PAMAM phase (Δd = 0.72 nm) similar to that obtained for G2-0.3 at 60 °C. At the highest temperatures, the packing fractions (Table A5) are greater than 1, indicating that non-intercalated PAMAM is present in the samples.

Calculations of packing fractions indicate that the very highly expanded phase must be stage 1 (with all galleries occupied). Unusually higher expansion (d = 3.8 nm, Δd = 3.1 nm) has been reported previously for PVP/$Li_{0.25}MoO_3$ and PAM/$Li_{0.25}MoO_3$ nanocomposites.[20] The actual PAMAM arrangement or conformational changes to form these very large galleries has yet to be established.

Table A5**.** Effect of temperature on the structure of G2-0.3 nanocomposites.

Temp (^oC)	Mass %			Mole ratio, r_i	d (nm)	Δd (nm)	Packing Fraction
	H_2O	PAMAM	$Na_{0.25}MoO_3$				
20	3.6	14.1	82.3	0.008	0.97; 1.43	0.28; 0.74	n.a.
40	3.7	24.2	72.1	0.015	2.13	1.44	0.48
60	4.1	26.8	69.1	0.018	1.32; 2.12	0.63; 1.43	n.a.
80	5.5	30.0	64.5	0.021	1.12; 1.40	0.43; 0.71	n.a.
100	4.9	30.6	64.5	0.022	1.42	0.73	1.34
120	5.0	26.4	68.6	0.018	1.44	0.75	1.06

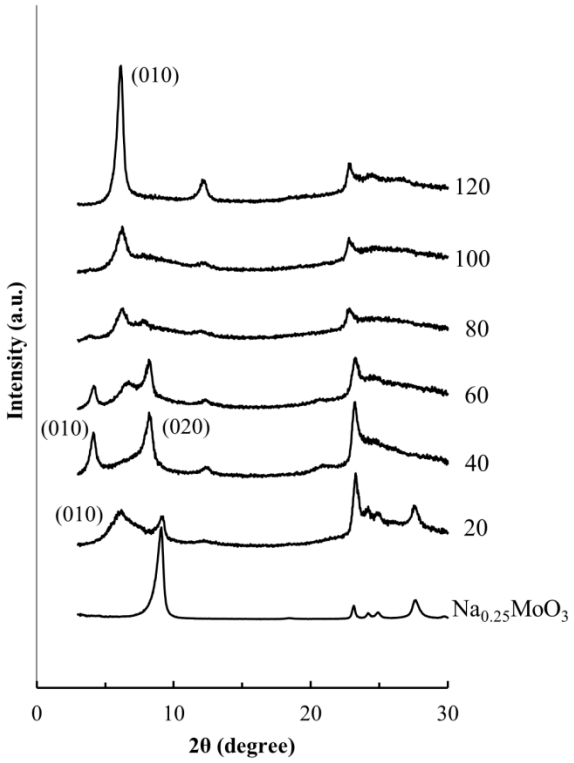

Figure A5. PXRD patterns showing the effect of temperature on G2 PAMAM/MoO_3 nanocomposites.

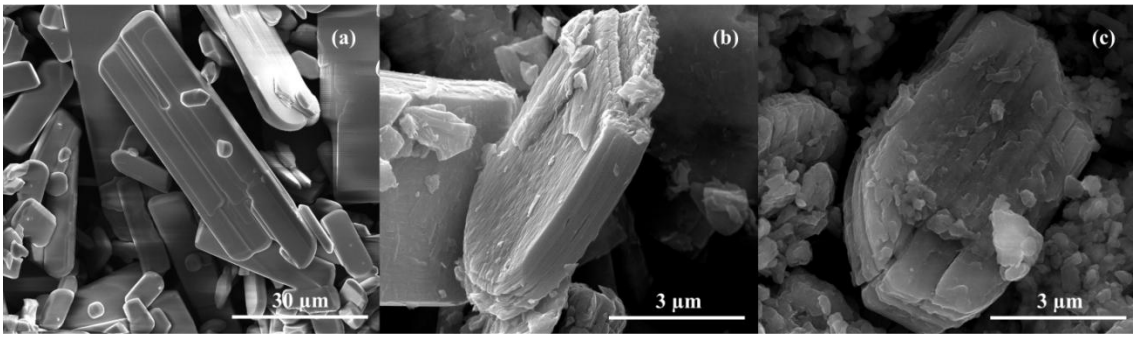

Figure A6**.** SEM micrographs of (a) MoO_3, (b) Na_xMoO_3 and (c) the nanocomposite G2-0.8.

SEM images of the starting materials, MoO_3, $[Na(H_2O)_2]_{0.25}MoO_3$ and the PAMAM/MoO_3 nanocomposite (G2-0.8) are presented in Figure A6. Particles clearly retain their macroscopic features but show exfoliation and fragmentation during the nanocomposite formation.

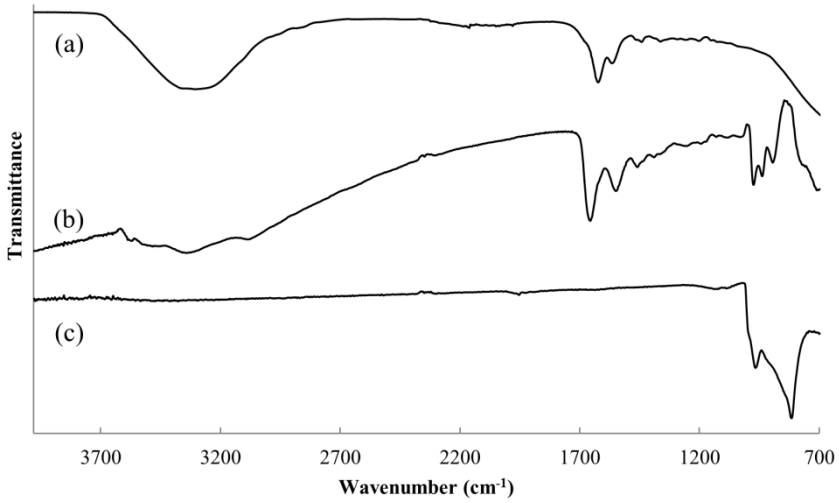

Figure A7. IR spectra of G2 PAMAM (a), nanocomposite G2-0.7 (b) and MoO_3 (c).

The IR spectra of PAMAM and its nanocomposites are presented in Figure A7. The amidic groups (HNC=O) groups present on the dendrimer give absorption bands at 1623-35 cm^{-1} (amide I, mainly C=O stretching) and 1551-67 cm^{-1} (amide II, combination of N-H in-plane bending and C-N stretching).[25] In the G2-0.7 nanocomposite, which is representative, the amide I band has shifted to a slightly higher value of 1655 cm^{-1} while the amide II band shifted to a lower value of 1548 cm^{-1}. The positions of the amide bands arising from the intercalate are close to those of native PAMAM as has been observed previously for a PVP/MoO_3 nanocomposite.[20] A band at 3086 cm^{-1} corresponding to N-H amide stretching mode was also present for the nanocomposites.[26] The spectrum for MoO_3 shows bands at

966 and 816 cm^{-1}, corresponding to M=O and M-O stretching vibrations, respectively,[17] which shift to 974, 938 and 894 cm^{-1} in the nanocomposites. The shift to higher wavenumber absorbances suggests that the anionic MoO_3 layers in the nanocomposite are less reduced than in $Na_{0.25}MoO_3$.[20]

A.5 CONCLUSION

This study indicates that PAMAM dendrimers can be intercalated into MoO_3 as monolayers or bilayers. The intercalate arrangement is strongly dependent on the PAMAM generation. Bilayers of G2 PAMAM can be formed in MoO_3 gallery even at low PAMAM composition. This is a new observation, which is contrary to the observation with other polymer guests that bilayers are formed only at higher compositions.

Reaction temperature was observed to affect the structure of the obtained nanocomposites. Pure bilayers with different levels of expansion were obtained at 40 and 120 °C, whereas mixed phases were obtained at 60 °C.

A.6 REFERENCES

1. S. S. Ray, M. Okamoto, *Progress in Polymer Science.* 28 (2003) 1539-1641.

2. E. Manias, G. Polizos, H. Nakajima, M. J. Heidecker, in: A. B. Morgan and C. A. Wilkie (Eds.), *Flame retardant polymer nanocomposites*, John Wiley & Sons, Inc. Hoboken, New Jersey, 2007, pp. 31-66.

3. T. A. Kerr, H. Wu, L. F. Nazar, *Chemistry of Materials.* 8 (1996) 2005-2015.

4. A. V. Murugan, A. K. Viswanath, C. S. Gopinath, K. Vijayamohanan, *Journal of Applied Physics*. 100 (2006).

5. C. O. Oriakhi, X. R. Zhang, M. M. Lerner, *Applied Clay Science*. 15 (1999) 109-118.

6. A. W. Bosman, H. M. Janssen, E. W. Meijer, *Chemical Reviews*. 99 (1999) 1665-1688.

7. D. A. Tomalia, *Progress in Polymer Science*, 30 (2005) 294-324.

8. N. C. B. Tan, L. Balogh, S. F. Trevino, D. A. Tomalia, J. S. Lin, *Polymer*. 40 (1999) 2537-2545.

9. D. A. Tomalia, A. M. Naylor, W. A. Goddard, *Angewandte Chemie-International Edition in English*, 29 (1990) 138-175.

10. S. Sadekar, H. Ghandehari, *Advanced Drug Delivery Reviews*, 64 (2012) 571-588.

11. R. Rajesh, R. Venkatesan, *Journal of Molecular Catalysis A:Chemical*, 359 (2012) 88-96.

12. L. W. Hoffman, G. G. Andersson, A. Sharma, S. R. Clarke, N. H. Voelcker, *Langmuir*, 27 (2011) 6759-6767.

13. L. Campanella, G. Pistoia, *Journal of the Electrochemical Society*, 118 (1971) 1905-1908.

14. L. F. Nazar, H. Wu, W. P. Power, *Journal of Materials Chemistry*. 5 (1995) 1985-1993.

15. J. P. Pereiraramos, N. Kumagai, *Journal of Power Sources*. 56 (1995) 87-90.

16. N. Sukpirom, C. O. Oriakhi, M. M. Lerner, *Materials Research Bulletin*. 35 (2000) 325-331.

17. Y. S. Hu, W. Chen, Q. Xu, R. Z. Yuan, *Journal of Materials Science & Technology*. 17 (2001) S124-S126.

18. C. O. Oriakhi, R. L. Nafshun, M. M. Lerner, *Materials Research Bulletin*. 31 (1996) 1513-1520.

19. O. Y. Posudievsky, S. A. Biskulova, V. D. Pokhodenko, *Journal of Materials Chemistry*. 12 (2002) 1446-1449.

20. L. Wang, J. Schindler, C. R. Kannewurf, M. G. Kanatzidis, *Journal of Materials Chemistry*. 7 (1997) 1277-1283.

21. D. M. Thomas, E. M. McCarron, *Materials Research Bulletin*. 21 (1986) 945-960.

22. R. Esfand, D. A. Tomalia, in: J. M. J. Fréchet, D. A. Tomalia (Eds.), *Dendrimers and Other Dendritic Polymers*, John Wiley & Sons, Ltd. Chichester, UK, 2002, pp. 587-604.

23. A. U. Liyanage, M. M. Lerner, *RSC Advances*. 2 (2012) 474-479.

24. Y. H. Zhao, M. H. Abraham, A. M. Zissimos, *Journal of Organic Chemistry*. 68 (2003) 7368-7373.

25. I. Grabchev, C. Petkov, V. Bojinov, *Dyes and Pigments*. 62 (2004) 229-234.

26. A. S. Costa, T. Imae, K. Takagi, K. Kikuta, *Progress in Colloid & Polymer Science*. 128 (2004) 113-119.

APPENDIX B

SUPPLEMENTARY DATA: SYNTHESIS AND CHARACTERIZATION OF LOW-GENERATION POLYAMIDOAMINE (PAMAM) DENDRIMER – SODIUM MONTMORILLONITE (Na-MMT) CLAY NANOCOMPOSITES

Amila U. Liyanage, Esther U. Ikhuoria,[a] Adeniyi A. Adenuga,

Vincent T. Remcho, and Michael M. Lerner

Department of Chemistry

Oregon State University

Corvallis, OR 97331-4003, USA

[a] Fulbright visiting scholar, Oregon State University, 2011/2012. Permanent address: Department of Chemistry, University of Benin, Benin City, Nigeria.

Inorg. Chem., 2013, 52 (8), 4603–4610.

B.1 SUPPLEMENTARY DATA

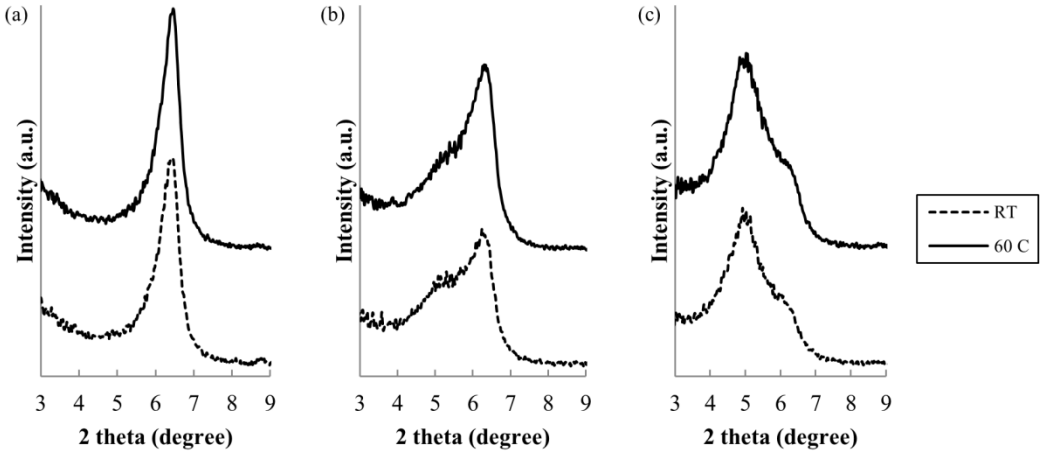

Figure B1. PXRD data for (a) G(0.0), (b) G(1.0), and (c) G(2.0)/Na-MMT nanocomposites synthesized at room temperature and 60 ^{o}C. Reactant ratios were 0.3 g/g PAMAM/Na-MMT.

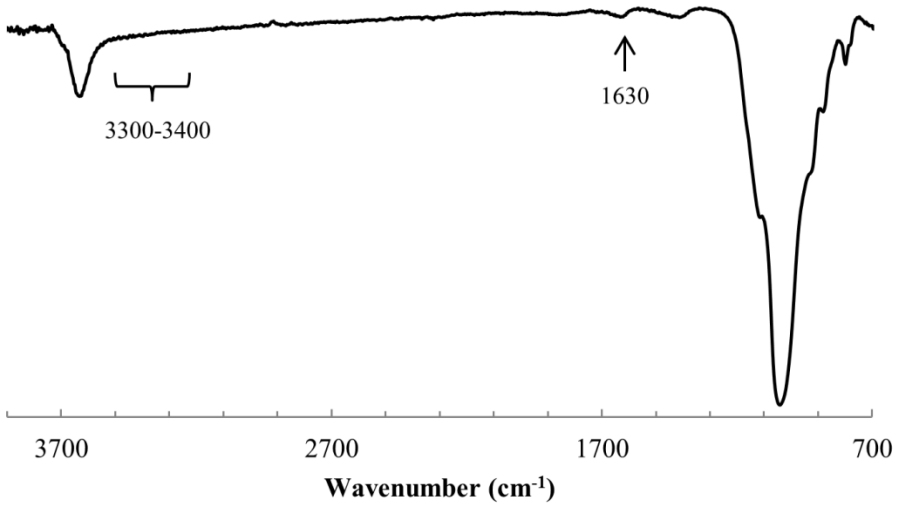

Figure B2. FTIR spectrum of dehydrated Na-MMT.

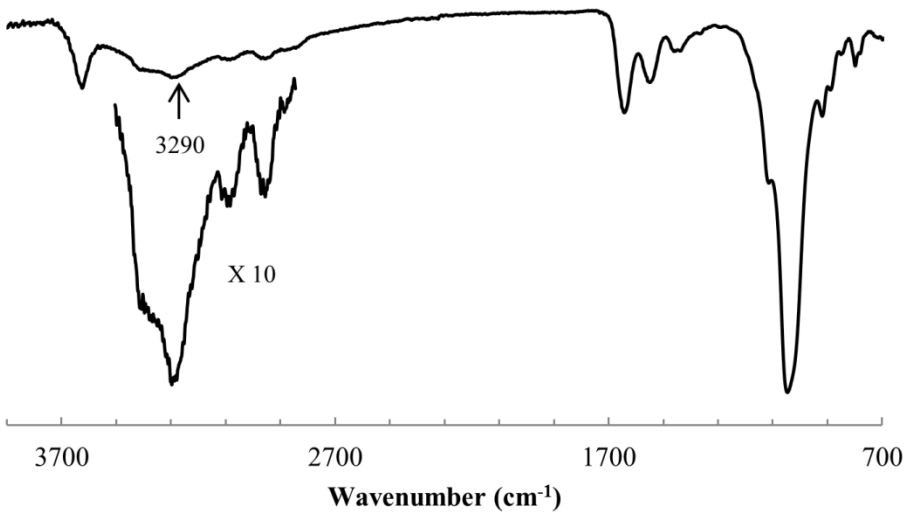

Figure B3. FTIR spectrum of a 0.4 PAMAM G(2.0)/Na-MMT nanocomposite. The 2850-3500 cm^{-1} region is intensified x10 for clarity.